Violation of an augmented set of Leggett-Garg inequalities and the implementation of a continuous in time velocity measurement

by

Shayan-Shawn Majidy

A thesis
presented to the University of Waterloo
in fulfillment of the
thesis requirement for the degree of
Masters of Science
in
Physics (Quantum Information)

Waterloo, Ontario, Canada, 2019

I hereby declare that I am the sole author of this thesis. This is a true copy of the thesis, including any required final revisions, as accepted by my examiners.

I understand that my thesis may be made electronically available to the public.

Abstract

Macroscopic realism (MR) is the view that a system may possess definite properties at any time independent of past or future measurements, and may be tested experimentally using the Leggett-Garg inequalities (LGIs). In this work we advance the study of LGIs in two ways using experiments carried out on a nuclear magnetic resonance spectrometer. Firstly, we addresses the fact that the LGIs are only necessary conditions for MR but not sufficient ones. We implement a recently-proposed test of necessary and sufficient conditions for MR which consists of a combination of the original four three-time LGIs augmented with a set of twelve two-time LGIs. We explore different regimes in which the two- and three-time LGIs may each be satisfied or violated. Secondly, we implement a recent proposal for a measurement protocol which determines the temporal correlation functions in an approximately non-invasive manner. It employs a measurement of the velocity of a dichotomic variable Q, continuous in time, from which a possible sign change of Q may be determined in a single measurement of an ancilla coupled to the velocity. This protocol involves a significantly different set of assumptions to the traditional ideal negative measurement protocol and a comparison with the latter is carried out.

Acknowledgements

First and foremost, I would like to thank my supervisor Prof. Raymond Laflamme. Ray's insistent curiosity has been contagious and the way he conducts himself on a daily basis has been inspiring. I feel very fortunate to have him as a role model, as a scientist and as a person. Secondly, I would like to express my deep gratitude to Prof. Jonathan Halliwell. Had I known that the initial email I sent him would lead to the relationship I have with him today, I would of sent it much sooner. His wisdom and encouragement have been crucial to navigating through the different stages of my research. Lastly, I would like to thank my examination committee for their time reading my thesis, the Department of Physics and Astronomy and the Institute for Quantum Computing for funding my research and my peers for creating a warm and supportive environment.

Lastly, I would like to thank my family and in particular my uncle Payam. If there is anything I accomplish in this life, it's because of him.

Table of Contents

List of Tables

List of Figures

Chapter 0

Introduction

Quantum technologies have shown their potential to impact a range of sectors, including communications, finance, health and security [1]. Harnessing the power of quantum mechanics into practical quantum technologies will be aided by deeper understandings of the foundations of quantum mechanics. Were it not for an understanding of the concepts of *quantum entanglement* and *quantum superposition*, famous breakthroughs such as the BB84 protocol [2] and Shor's factoring algorithm [3] would not have been possible. A propitious question left to explore in quantum foundations is that– If reality is described by quantum mechanics, can these laws be scaled to commonplace objects? This idea of systems composed of countless atoms existing in quantum superposition of macroscopically distinct states is known as *macroscopic coherence.*

Anthony Leggett and Anupam Garg drew attention to the study of this subject in the 1980's by codifying how physicist expect macroscopic objects to behave into a set of assumptions that they defined as *macroscopic realism* (MR) [4, 5]. Leggett and Garg then used these assumption to derive a set of inequalities that any macroscopic system should obey. These are the Leggett-Garg inequalities (LGIs). If measurements on a system should violate the LGIs then a macroscopic understanding of the system must be abandoned. In this way the LGIs serve as a test of macroscopic coherence.

In this work we aim to advance the study of the LGIs by addressing two contemporary challenges in the field. The first concerns the question of conditions for MR that are both necessary and sufficient, which was first addressed by Refs. [6, 7] and subsequently in Refs. [8, 9]. We follow the latter papers, which concern a set of augmented LGIs in which the original three-time LGIs (LG3s) are amended with a set of twelve two-time LGIs (LG2s) and form a set of necessary and sufficient conditions for MR.

The second challenge we look to address arises from the need of LGI experiments to adopt a macroscopically non-invasive measurement protocol. If the measurement was deemed to be invasive it could then be argued then that it was the effect of the measurement, and not a failure of MR, which caused the violation of the inequality [10, 11, 12]. The best one can hope to achieve in addressing this argument is to implement a measurement protocol whose argument for invasiveness would need to be so contrived that the alternative explanation of a violation of MR would be more likely. One strategy to treat this argument is to implement different measurement protocols that are constructed from different sets of assumptions. The agreement of the results from these different protocols will further strengthen either protocols argument for being non-invasive. To advance this strategy we perform in this work the first experimental implementation of the continuous in time velocity measurement (CTVM) protocol [13]. The CTVM protocol is methodologically different from the more commonly implemented [14, 15, 16] technique of ideal negative measurements (INM). We implement both the CTVM and INM protocols in this work and verify that they do provide similar results under the parameters in which the CTVM can be faithfully implemented.

The contents of this thesis are organized into four chapters. In Chapter 1 we provide a brief overview of the study of realism. This begins with a simple review of local realism and the Bell inequalities before introducing the subject of macroscopic realism and the LGIs. Then, In Chapter 2, we review how a nuclear magnetic resonance spectrometer can be used for performing quantum information processing tasks. This will complete the review portion of the thesis and we will then move into the two chapters containing novel work. In Chapter 3 we conduct two sets of experiments which explore different regimes of the augmented LG framework. In the first set of experiments the LG3s are satisfied and the LG2s are not. This experimentally demonstrates that the original LGI framework was not a sufficient test of MR. Then, in the second set of experiments the LG3s will be violated and the LG2s will be satisfied. This provides a natural parallel to the Bell model in which the situation "looks classical" for partial snapshots, but the violation of MR is only apparent when one looks for an underlying probability. Finally in Chapter 4 we perform the first experimental implementation of the CTVM protocol. This entails first finding a set of suitable parameters in which the CTVM can be faithfully implemented before performing a violation of the LGIs with this protocol. This will be the third set of experiments done in this thesis. We will then compare the results of the second and third set of experiments to verify that INM and CTVM protocols do provide similar results.

Chapter 1

Violating realism
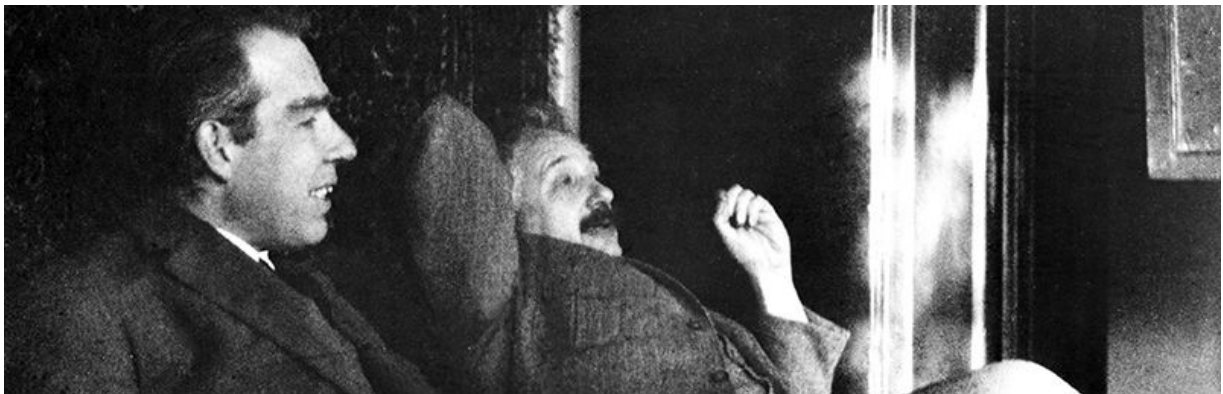
"*Quantum mechanics is very impressive. But an inner voice tells me that it is not yet the real thing. The theory produces a good deal but hardly brings us closer to the secret of the Old One. I am at all events convinced that He does not play dice.*"

- Albert Einstein in response to a letter from Max Born

1.1 The Bell framework

1.1.1 Local realism

The idea that the universe continues to exist when no one is looking at it is a self-evident assumption in classical physics. The notion that the existence of the universe is independent of the mind of the observer is known as *realism*. Remarkably, even this seemingly basic premise of reality was called into question with the introduction of quantum mechanics and lead to one of the greatest debates in physics history [17].

On one side of this debate was Niels Bohr, who believed that the idea of reality without observation was meaningless. Bohr believed that since quantum systems will exist in superpositions of states between measurements, then reality will not exist in a definite state until it is observed [18]. Thus, from Bohr's view the wave functions, which describe the superpositions that exist in quantum mechanics, also provide a complete description of the universe. This view is known as the Copenhagen interpretation of quantum mechanics. On the other side of this debate was Albert Einstein, who believed that reality must exist independent of us observing it. This would mean that the wavefunction, which does not make definite predictions of states between measurements, must be an incomplete description of reality. To rectify this, Einstein proposed the existence of hidden variables which can not be observed but, if they could, would provide a definite description of reality [19].

Einstein, along with Boris Podolsky and Nathan Rosen, proposed a thought experiment known as the Einstein-Podolsky-Rosen (EPR) paradox [20] to demonstrate how ridiculous they felt the Copenhagen interpretation was. The EPR paradox proposed that in order to abandon realism one would also need to abandon the fundamental concept of *locality*. Locality, in this context, is the idea that an action at one point in space can only influence one at another if there is something, such as a field or a particle, carrying that influence. Additionally, since relativity limits the speed at which such influences can travel to a maximum of the speed of light, then locality implies that an action at one point in space can not have an instantaneous effect elsewhere. Einstein went on to define *local realism* as the combination of these seemingly inseparable postulates. Necessarily, induction (that causality propagates only forward in time) was later added as a third postulate of local realism. Ultimately what Einstein *et al.* demonstrated was that if the Copenhagen interpretation of quantum physics is true then it must violate local realism.

The EPR paradox itself is fairly straightforward. Consider a pair of spin $\frac{1}{2}$ particles that are formed in the triplet spin state (i.e. the spins are in the same direction) and that are
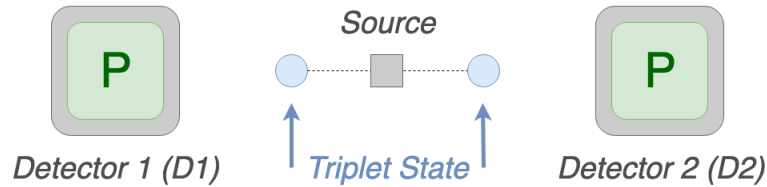
Figure 1.1: The general design of the EPR paradox. A pair of spin $\frac{1}{2}$ particles are formed in the triplet state and move in opposite directions in space. The spin of the particles is measured along some axis by detectors $D1$ and $D2$. The detectors both return either the $+1$ (P) or -1 (N) result.

moving in opposite directions in space.[1] The spin of the particles can be measured along some axis by detectors $D1$ and $D2$. The detectors will both measure either the $+1$ (P) or -1 (N) result (see Fig. 1.1). The authors then argued that if the spins are not in a definite state until being measured, then they must somehow communicate instantaneously with one another when being measured to always maintain the same result. Einstein perceived this as a violation of locality and so he argued that the result of this measurement must have been predetermined. Furthermore, since the wave function does not contain this predetermined information then their must exist some more complete specification of the systems state.

Since both models predict the same experimental result for the EPR paradox, the confrontation between the Copenhagen interpretation of quantum mechanics and local realism would initially remain at a standstill. The expectation of both of these models was that the two detectors would return the same results on each run and that the P and N results would occur with equal probabilities. The local hidden variable theory would argue that this was a result of the state of the particles, whether P or N, having been determined at the particles inception and being revealed when the particles states was measured. On the other hand, the Copenhagen interpretation would argue that the particles had existed in a superposition of the P and N states and it was at the moment of measurement that the particles took on a definite state. This standstill would endure beyond Einsteins life, until John Bell proposed a test which could experimentally distinguish between these two models [21].

---

[1]In their original argument the spins are formed in the singlet spin state (i.e. the spin are in opposite directions). The EPR paradox follows exactly the same for the triplet and singlet states.
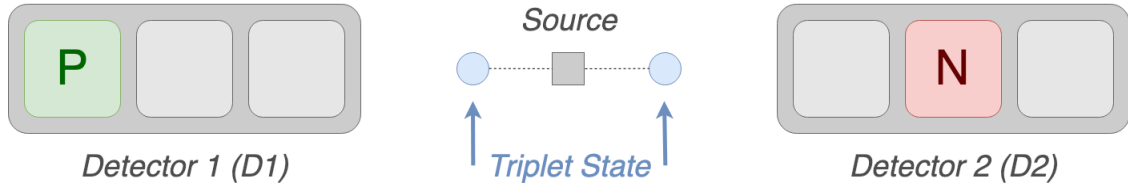
Figure 1.2: A modification of the general design of EPR paradox given in Fig. 1.1. In this design the particles spin is measured along one of three coplanar axes, separated by 120°, on detectors $D1$ and on $D2$. The detectors each have three screens corresponding to the choice of axis. Each screen will again return either the P or N result.

1.1.2 Bell's theorem

In 1964, John Bell demonstrated that Bohr and Einstein's models could be distinguished with a slightly more detailed measurement scheme [21]. An example of such a scheme is given, schematically, in Fig. 1.2. In this set up each detector can now measure one of three different properties of the spin. These three properties correspond to the particles spin being measured along one of three different coplanar axis that are separated by 120°. The detectors can now be thought of as having three screens, with each screen corresponding to one of the chosen axes of measurement. As before, each screen can give a P or N result. This scheme can distinguish the two models by comparing the probability of measuring the same result on both $D1$ and $D2$, given that the axis of measurement (or a screen) is chosen at random.

As before, the local hidden variable model would argue that the results of the measurements are determined when the particles are generated. This implies that the particles can be generated in one of $2^3 = 8$ possible states which correspond to the eight possible measurement outcomes. Six of these eight states will have two outcomes which are the same and two of these states will have all three measurement outcomes which are the same:

$$2 \text{ same: } (P,P,N),(P,N,P),(N,P,P),(N,N,P),(N,P,N),(P,N,N)$$
$$3 \text{ same: } (P,P,P),(N,N,N)$$

As shown in Table 1.1, if the particles were generated in any of the "2 same" states then their will exist a probability of $\frac{5}{9}$ of measuring the same state on each detector. Furthermore, if the particles were generated in any of the "3 same" states then their will exist a probability of 1 of measuring the same state on each detector. Thus, given that the particles are randomly generated in any one of these states, the probability of measuring

6

	(D2) Screen A	(D2) Screen B	(D2) Screen C
(D1) Screen A	Same	Same	Different
(D1) Screen B	Same	Same	Different
(D1) Screen C	Different	Different	Same

Table 1.1: The possible measurement outcomes for a triplet state that was generated in the (P, P, N) state. This table shows that, of the nine possible pairs of measurements , five will return the same result. Thus there is a $\frac{5}{9}$ probability of measuring the same result. It is easy to check that this holds true for any of the "2 same" states $((P, N, P), (N, P, P), (N, N, P), (N, P, N), (P, N, N))$.

the same result on both screens is, according to the local hidden variable model, equal to:

$$p(\text{same}) = \left(\frac{6}{8} \times \frac{5}{9}\right) + \left(\frac{2}{8} \times 1\right) = \frac{2}{3} \approx 0.667 \tag{1.1}$$

This probability can be compared with the predictions of the Copenhagen model. Again, pairs of measurements performed along the same axis will return the same result. However, if pairs of measurements are performed along different axis then we must use vector projections to measure the probability of returning the same result. As shown in Fig. 1.3, the probability of measuring the same result on two different axis of measurement is equal to $\frac{1}{4}$. Thus, given that axis of measurement are chosen at random, the probability of measuring the same result on both screens is, according to the Copenhagen model, equal to:

$$p(\text{same}) = \left(1 \times \frac{3}{9}\right) + \left(\frac{1}{4} \times \frac{6}{9}\right) = \frac{15}{36} \approx 0.416 \tag{1.2}$$

This difference in the expected probabilities provides a means of experimentally testing the existence of local realism.

1.1.3 The Bell and CHSH inequalities

In practise, experimental tests of local realism are most commonly done by using the Bell or CHSH inequalities. A simple derivation of the Bell inequalities can be constructed from the content of the preceding section. Consider any *one* of the eight possible initial states predicted by a local realistic model. The "probability" that two of the measured results
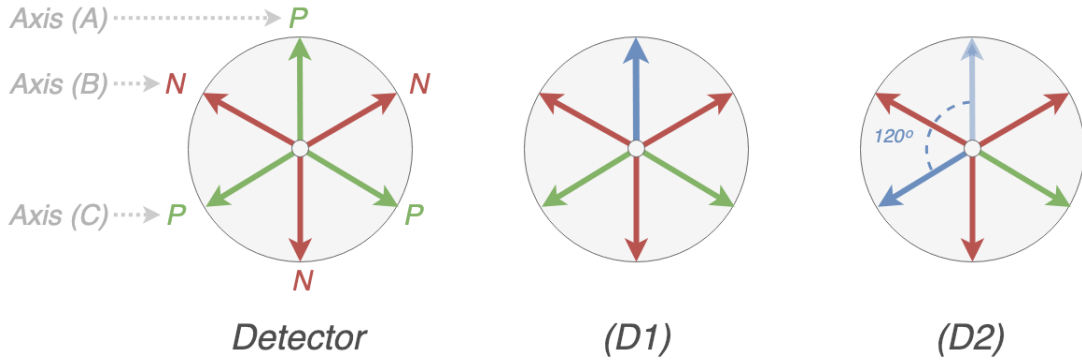
Figure 1.3: A depiction of a particles spin being measured along one of three co-planar axis. The *Detector* shows the possible axis of measurement and their possible results (either P or N). Both detectors $D1$ and $D2$ perform such measurements. Once $D1$ returns a certain result (highlighted in blue), then the probability that $D2$ will return the same measurement on a different axis is equal to the projection of the result of $D1$ onto the chosen axis of $D2$. The probability of this projection is $\cos(\frac{120}{2})^2 = \frac{1}{4}$.

are the same for a single pair of measurements will be either 1 or 0, *e.g.* given the state (P, P, N) the $p(A = B) = 1$, the $p(B = C) = 0$ and the $p(A = C) = 0$ (where $A = B$ means the result of screen A is the same as the result on screen B). As shown in Table 1.2, the sum of these "probabilities" will always equal either 1 or 3 for any of the eight possible states. This is a simplified formulation of the Bell inequality:

$$p(A = B) + p(B = C) + p(A = C) \geq 1 \tag{1.3}$$

The Bell inequalities were later generalized by John Clauser, Michael Horne, Abner Shimony and Richard Holt (CHSH) for cases where there is not only perfect correlations (or anticorrelations) between measurements [22]. These CHSH inequalities are most commonly presented in terms of expectation values (since they are not dealing with definite outcomes) and with the measurements being conducted along two different axis instead of three. Different equivalent derivations exist for the CHSH inequalities. In this work we present one constructed by John Preskill [23]. For this derivation we adopt the notation that the first particle can be measured by observables $\hat{a}$ or $\hat{a}'$ (previously called screens A or B on $D1$) and the second particle can be measured by either $\hat{b}$ or $\hat{b}'$ (previously called screens A or B on $D2$). The outcome of these measurement are $(a, a', b, b') \in \{\pm 1\}$. Thus, either $a + a' = 0$ and so $a - a' = \pm 2$ or that $a - a' = 0$ and so $a + a' = \pm 2$. We can use

	p(A=B)	+ p(B=C)	+ p(A=C)	=
(P,P,P)	(1)	+ (1)	+ (1)	= 3
(N,N,N)	(1)	+ (1)	+ (1)	= 3
(P,P,N)	(1)	+ (0)	+ (0)	= 1
(N,N,P)	(1)	+ (0)	+ (0)	= 1
(P,N,P)	(0)	+ (0)	+ (1)	= 1
(N,P,N)	(0)	+ (0)	+ (1)	= 1
(N,P,P)	(0)	+ (1)	+ (0)	= 1
(P,N,N)	(0)	+ (1)	+ (0)	= 1

Table 1.2: The sum of the "probabilities" that pairs of measurements made on a triplet state will return the same result. The eight possible initial states are considered here. The sum of the three probabilities are either 1 or 3.

these result to define the function C as

$$C \equiv (a + a')b + (a - a')b' = \pm 2 \tag{1.4}$$

which is bounded by ± 2. Thus the following bound holds:

$$|\langle C \rangle| \leq \langle |C| \rangle = 2 \tag{1.5}$$

Substituting back in the definition of C gives us the CHSH inequalities

$$|\langle ab \rangle + \langle a'b \rangle + \langle ab' \rangle - \langle a'b' \rangle| \leq 2 \tag{1.6}$$

It follows that these inequalities can be violated by a quantum system. Consider the operators $\hat{a}, \hat{a}', \hat{b}$ and $\hat{b}'$ written now in terms of the dot product of the Pauli vector ($\vec{\sigma}$) and a corresponding unit three-vector ($\vec{a}, \vec{a}', \vec{b}$ and $\vec{b}'$).

$$a = \vec{\sigma}^{(A)} \cdot \vec{a}, \qquad a' = \vec{\sigma}^{(A)} \cdot \vec{a}', \qquad b = \vec{\sigma}^{(B)} \cdot \vec{b}, \qquad b' = \vec{\sigma}^{(B)} \cdot \vec{b}'$$

The superscripts (A) and (B) are to be clear of the different spaces being considered. For the Bell state $|\psi^-\rangle = (|01\rangle - |10\rangle)/\sqrt{2}$

$$\langle \psi^- | (\vec{\sigma}^{(A)} \cdot \vec{a})(\vec{\sigma}^{(B)} \cdot \vec{b}) | \psi^- \rangle = -\vec{a} \cdot \vec{b} = -\cos\theta \tag{1.7}$$
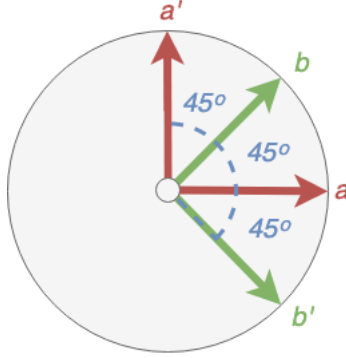
Figure 1.4: The four co-planar axes separated by successive 45° angles which are used in the CHSH violation proof.

where θ is the angle between $\vec{a}$ and $\vec{b}$. For the case of the four axes being coplanar and separated by successive 45° angles (as shown in Figure 1.4) the CHSH inequalities are violated since

$$|-\cos(\frac{\pi}{4}) - \cos(\frac{\pi}{4}) - \cos(\frac{\pi}{4}) + \cos(\frac{3\pi}{4})| \leq 2 \tag{1.8}$$

$$2\sqrt{2} \leq 2 \tag{1.9}$$

The first experimental violations of the Bell or CHSH inequalities was performed by Alain Aspect [24] using entangled photon pairs. Furthermore, in that same year Arthur Fine proved that the Bell and CHSH inequalities are not only necessary but sufficient conditions for local realism, a result known as *Fine's theorem* [25]. Thus, together these works demonstrated a sufficient violation of Einstein's local realism. Since then experimental violations of the Bell and CHSH inequalities have been performed on different quantum systems.

Finally, some closing remarks are in order to avoid common misconceptions that arise when studying the violations of local realism. Firstly, the results of the Bell and CHSH experiments demonstrate a violation of local realism as a whole, but whether the violation is due to a violation of locality, or of realism or even of both is not determined. When considering these possible options it is easy to confuse a violation of locality with one of relativity. But in fact, non-locality and relativity can be perfectly consistent with one another since relativity only requires that causality is preserved, *i.e.* that the flow of information is not superluminal. Causality is preserved in Bell and CHSH experiments because the influence between the two particles can only be seen after the measurements

have been made. Thus, the Bell and CHSH experiments do not permit any information to be transmitted between the particles. Secondly, it is also important to note that the Bell and CHSH tests are not a proof of the Copenhagen interpretation of quantum mechanics but are only a no-go theorem for local hidden-variable theories. There does exist other theories which, like the Copenhagen interpretation, are consistent with all quantum experimental results. Some of these other theories do not violate realism at all, like the de Broglie–Bohm theory of quantum mechanics [26] or theories which are constructed using Einstein-Rosen bridges [27]. Furthermore, it has even been proposed that both locality and realism could be maintained by adopting the many-worlds interpretation of quantum mechanics, which was first alluded to by Erwin Schrödinger [28] in 1952, later formulated by Hugh Everett in 1957 [29, 30] and finally popularized by Bryce Seligman DeWitt [31] in the 1970s. Ultimately, what the Bell and CHSH tests provided are not a conclusive interpretation of the underlying nature of quantum mechanics but a stepping stone to new questions in the field.

1.2 Fine's theorem

1.2.1 Marginal probabilities

Given the significance of Fine's theorem in creating sufficient and testable conditions for local realism, we will include a brief introduction to this theorem. Before doing so, it will be helpful to review the notion of a marginal probability distribution and to present a means for visualizing a marginals relationship with its underlying probably distribution.

First, we will consider a simple system which is described by two variables, s_1 and s_2, that can each take values of ± 1. Each combination of possible measurements of (s_1, s_2) will have some probability of occurring, we denote these pairwise probabilities as $p_{12}(s_1, s_2)$. This notation could also be extended to systems with more variables, *i.e.* $p_{123...n}(s_1, s_2, s_3, \ldots s_n)$.

Since this system is completely described by two variables, then the four pairwise probabilities ($p_{12}(s_1, s_2)$) will describe the system in its entirety and so we call these the systems *underlying probability distribution*, or sometimes more simply just its probability distribution. By summing over one of the systems variables (s_1 or s_2) we can find the systems different *marginal probabilities* or simply its different *marginals*. The marginals give the probability distribution of measuring some variables without taking into consideration the values of the others. For example, if we sum our two variables underlying probability

Probability table for $p_{12}(s_1,s_2)$ with marginals

	$s_1 = +$	$s_1 = -$	Total
$s_2 = +$	$p_{12}(+,+)$	$p_{12}(-,+)$	$p_2(+)$
$s_2 = -$	$p_{12}(+,-)$	$p_{12}(-,-)$	$p_2(-)$
Total	$p_1(+)$	$p_1(-)$	

Probability table for $p_{12}(s_1,s_2)$ written as marginals $p_1(s_1)$

	$s_1 = +$	$s_1 = -$
$s_2 = +$	$p_1(+)$	$p_1(-)$
$s_2 = -$		

Probability table for $p_{12}(s_1,s_2)$ written as marginals $p_2(s_2)$

	$s_1 = +$	$s_1 = -$
$s_2 = +$	$p_2(+)$	
$s_2 = -$	$p_2(-)$	
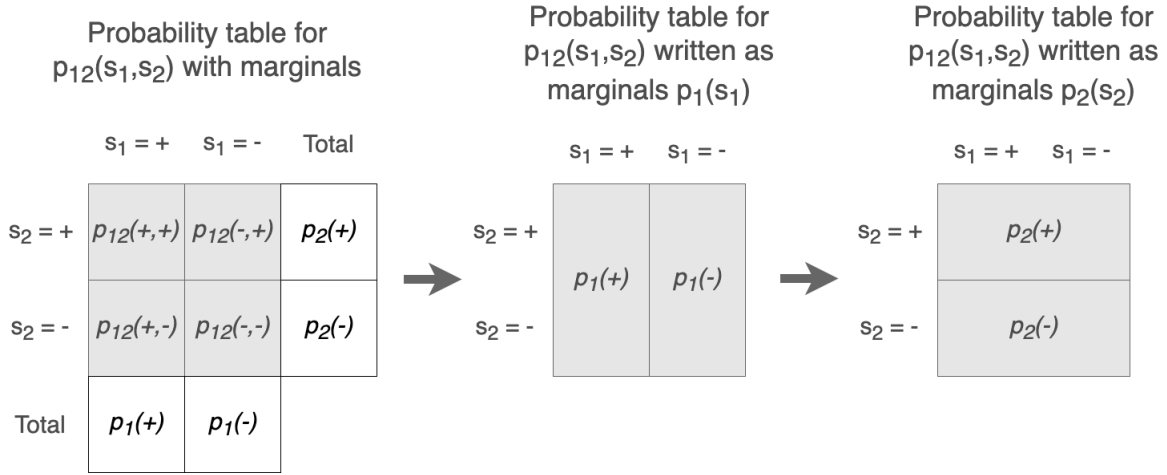
Figure 1.5: Different ways of denoting the marginals of a probably distribution. The first table depicts the values of the underlying probability distribution with the marginals written along the end column and end row. In the second and third tables the marginals are given as their own tables where the elements of the marginals are given as the merging of elements from the original table. This notation highlights the relationship between the marginals and their underlying distribution and can be used for systems with any number of variables.

distribution over s_1 then we will get the marginal probabilities of measuring s_2, which are denoted as $p_2(s_2)$. The first table in Figure 1.5 provides the underlying probability distribution and the marginal probabilities for this simple system.

The format used in the first table of Figure 1.5 is fairly standard for representing probabilities of two variable systems. In this format the individual marginals are given at the end of each row and column. While this notation is convenient for two variable tables it becomes difficult to use for higher variable systems. Instead we can use a different notation for writing marginals which emphasizes their relationship with the underlying probably distribution and can be used for any number of variables. This notation comes with the cost of only being able to consider one marginal distribution at a time. The method consists of writing each marginal distribution as an additional table where the elements of the marginals are given as the merging of elements from the original table. Two examples of this are given in Figure 1.5, one for the $p_1(s_1)$ marginal distribution and one for the $p_2(s_2)$ marginal distribution.

Returning to the CHSH inequalities, under the assumptions of local realism, the CHSH

inequalities are constructed for a system with four variables, s_1, s_2, s_3, s_4, (two spins, each being measured along one of two axis) where each variable can, again, take values of ± 1. Such a system will have an underlying probability distribution of sixteen elements, $p_{1234}(s_1, s_2, s_3, s_4)$. The first table in Figure 1.6 gives the underlying probability distribution for this system and provides four examples of the notation for depicting marginals which was introduced earlier.

Now imagine that you are given the probability distributions given in red in Figure 1.6 and are asked if these distributions could be the marginal distribution of some more fundamental underlying probability distribution - how could you determine this? This is an important question in Bell and CHSH tests and is one of the questions that is addressed by Fine's theorem.

In experimental tests of the CHSH inequalities, a combination of pairwise probability distributions ($p(s_1, s_3)$, $p(s_1, s_4)$,$p(s_2, s_3)$ and $p(s_2, s_4)$) are measured and the assumption is made that they are in fact the marginals of an underlying probability distribution. This assumption is necessary for then constructing bounds on the relationships which can exist between these pairwise probabilities and to in turn constructing bounds on the correlations which can exist between measurements. What a violation of the CHSH inequalities then shows is that the assumption of the existence of such an underlying distribution was faulty and this result can be interpreted as a violation of a form of realism. In this way the CHSH inequalities are a necessary test for local realism, in that a violation of the CHSH inequalities implies that no underlying probability distribution exists. However, the formulation of the CHSH inequalities does not prove the converse – that a satisfaction of the CHSH inequalities implies the existence of underlying probability distribution of all variables. This is where Fine's theorem comes in to effect. One of the results of Fine's theorem is that the CHSH and Bell inequalities are not just necessary conditions, but are also sufficient ones.

1.2.2   Statement of the theorem, definitions and notation

We were careful in the last subsection to say "one result" of Fine's theorem, since Fine's original paper showed the equivalence of five different statements regarding the results of a quantum correlation experiment. Often when papers regarding Bell, CHSH or (as we will see) Leggett-Garg experiments refer to Fine's theorem they usually are referring to one of these five results which equates a satisfaction of the Bell inequalities with the existence of an underlying probability distribution. The five equivalent statements, as originally presented by Fine are:

13

Probability table for $p_{1234}(s_1, s_2, s_3, s_4)$

		$s_1 = +$		$s_1 = -$	
		$s_3 = +$	$s_3 = -$	$s_3 = +$	$s_3 = -$
$s_2 = +$	$s_4 = +$	$(+,+,+,+)$	$(+,+,-,+)$	$(-,+,+,+)$	$(-,+,-,+)$
	$s_4 = -$	$(+,+,+,-)$	$(+,+,-,-)$	$(-,+,+,-)$	$(-,+,-,-)$
$s_2 = -$	$s_4 = +$	$(+,-,+,+)$	$(+,-,-,+)$	$(-,-,+,+)$	$(-,-,-,+)$
	$s_4 = -$	$(+,-,+,-)$	$(+,-,-,-)$	$(-,-,+,-)$	$(-,-,-,-)$

Marginal $p_{123}(s_1, s_2, s_3)$

$(+,+,+)$	$(+,+,-)$	$(-,+,+)$	$(-,+,-)$
$(+,-,+)$	$(+,-,-)$	$(-,-,+)$	$(-,-,-)$

Marginal $p_{124}(s_1, s_2, s_4)$

$(+,+,+)$	$(-,+,+)$
$(+,+,-)$	$(-,+,-)$
$(+,-,+)$	$(-,-,+)$
$(+,-,-)$	$(-,-,-)$

Marginal $p_{12}(s_1, s_2)$

$(+,+)$	$(-,+)$
$(+,-)$	$(-,-)$

Marginal $p_{13}(s_1, s_3)$

$(+,+)$	$(+,-)$	$(-,+)$	$(-,-)$
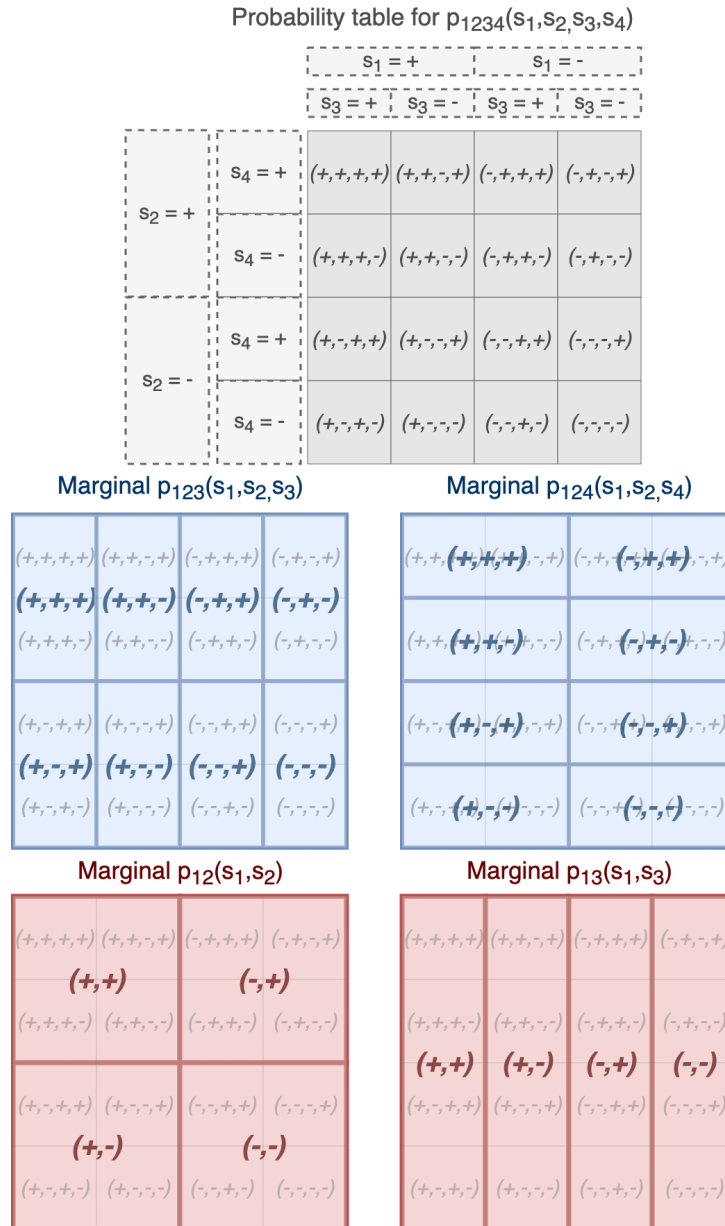
Figure 1.6: An example of a simple method for visualizing the marginals of a probability distribution. The first table gives the underlying probability distribution for a four variable system. The later tables give the marginal probabilities. In blue are the marginal probabilities over three variables and in red are the marginal probabilities over two variables.

1. There is a deterministic hidden-variables model for the experiment.

2. There is a factorizable, stochastic model for the experiment.

3. There is one joint distribution for all observables of the experiment, whose marginals return the probabilities of the experiment.

4. There are well-defined, compatible joint distributions for all pairs and triples of commuting and noncommuting observables.

5. The Bell/CHSH inequalities hold.

Fine's paper considers correlation experiments that involve distinct measurements in two space-time regions, that he denotes as R_1 and R_2. In these experiments, measurements are made on non-commuting observables A and A' in R_1 and B and B' in R_2, where each observable may take values of ± 1. These observables could be, for example, the measurements of the spin along two distinct axis made on a spin triplet, such as in the EPR experiments. Additionally, it is assumed that the observables from the separate space-time regions will commute with one another.

In these correlation experiments there are eight different probabilities which are experimentally measured - those of the four observables (A, A', B, B') and those of the four compatible pairs of observables $(AB, AB', A'B, A'B')$. These will be referred to as the *probabilities of the experiment*. $P(S)$ is defined to be the probability that the observable S takes the value $+1$ and $P(\bar{S})$ is the probably that the compliment of S, $\bar{S}$, takes the value of $+1$, or equivalently that S takes the value of -1. Additionally, $P(ST)$ is the probability of the observables S and T both taking the value of $+1$ (again, the bar notation is used when considering operators that take values of -1). To be clear, these probabilities are not the same probabilities that we discussed earlier in this subsection. Before we were discussing the probability of a system being in a particular state, *e.g.* $p_{12}(s_1, s_2)$, here we are describing the probability of returning a particular measurement out come given a certain state. Determining $P(S)$ requires knowledge of both the probability distribution of possible states and the outcome of the measurement S for each of those states.

Lastly, Fine defines a *deterministic hidden-variable model* to consist of three components:

1. **A set of hidden variables: Λ.** These variables are the complete set for specifying a state, they do necessarily need to be "hidden" (*e.g.* for our two spin system this would be the set of four doubles $\{s_1, s_2\} = \{(+, +), (+, -), (-, +), (-, -)\}$).

2. **A normalized probability density:** $\rho(\lambda)$**.** Where λ is an element of Λ (*e.g.* for our two spin system this would be equivalent to saying that $\sum_{s_1, s_2} p_{12}(s_1, s_2) = 1$).

3. **Response functions:** $A(\lambda), A'(\lambda), B(\lambda), B'(\lambda)$**.** These functions give the λ determined responses for the measurements, which means that they must be defined over all of Λ. The response functions have outcomes of ± 1 which depend deterministically on the state λ they are acting on. These response functions must also satisfy the following integrands.

$$P(S) = \int_\Lambda \tilde{S}(\lambda)\rho(\lambda)d\lambda \tag{1.10}$$

where $S \in \{A, A', B, B', \bar{A}, \bar{A}', \bar{B}, \bar{B}'\}$ and the tilde maps the observables with outcomes $\{-1, +1\}$ to an equivalent set of observables with outcomes $\{0, 1\}$. To be precise, $\tilde{S}(\lambda) = 1$ if $S(\lambda) = 1$ and $\tilde{S}(\lambda) = 0$ if $S(\lambda) = -1$. Equivalently, Eqn. (1.10) says that the probability that the observable S takes the value of $+1$ is equal to the weighted sum of states λ in which $S(\lambda)$ takes the value $+1$.

Fine uses the notation that when $P(\bar{S})$ is on the left hand side of the equation then the $\tilde{S}$ is to be replaced with $1 - \tilde{S}$ on the right hand side of the equation. This maintains the notation that $P(\bar{S})$ is the probability of $\bar{S}$ returning the $+1$ value. The response functions must also satisfy

$$P(ST) = \int_\Lambda \tilde{S}(\lambda)\tilde{T}(\lambda)\rho(\lambda)d\lambda \tag{1.11}$$

for S and T ranging over all compatible pairs of observables and their complements (*i.e.* they do not include combinations of A with A' or B with B'). The same convention is used for the bars and tildes.

The response functions may be a foreign notation, but they are easy to interpret after considering an example. Consider the two spin system from before, this system will have $\Lambda = \{s_1, s_2\} = \{(+, +), (+, -), (-, +), (-, -)\}$. Each of these doubles will have some probability of occurring, for example

$$p(+, +) = 0.3, \quad p(+, -) = 0.1$$

$$p(-, +) = 0.4, \quad p(-, -) = 0.2$$

We have that A and A' depend only on the state of the first spin and B and B' depend only on the state of the second spin. Then for each λ then operator A will return either ± 1, for example

$$A(+, s_2) = 1, \quad A(-, s_2) = -1$$

We can then use these values to calculate $P(A)$ and $P(\bar{A})$,

$$P(A) = (1)0.3 + (1)0.1 + (0)0.4 + (0)0.2 = 0.4$$

$$P(\bar{A}) = (1-1)0.3 + (1-1)0.1 + (1-0)0.4 + (1-0)0.2 = 0.6$$

1.2.3   The arguments of Fine's theorem

In this subsection we present a review of the arguments from Fine's paper. We have expanded on the arguments that Fine made and added some additional examples for clarity.

Statement 1 $\leftrightarrow$ Statement 3

1. There is a deterministic hidden-variables model for the experiment.

3. There is one joint distribution (denoted as $P(AA'BB')$) for all observables of the experiment, whose marginals return the probabilities of the experiment.

$\mathbf{1 \rightarrow 3}$: Statement one immediately implies the first half of statement three. That is, by its definition a deterministic hidden-variable model deterministically provides a description of a system for all observables over all possible states. This means that the equation

$$P(AA'BB') = \int \tilde{A}(\lambda)\tilde{A}'(\lambda)\tilde{B}(\lambda)\tilde{B}'(\lambda)\rho(\lambda)d\lambda \qquad (1.12)$$

defines a joint distribution for the four observables. In other words, the exact outcome of every measurement is known for each state of the system.

It then follows from Eqn. (1.10) and (1.11) that the marginals of the probability distribution in Eqn. (1.12) do provide the exact experimental probabilities. For example, the marginal distributions of $P(AS_1BS_2)$ over S_1 and S_2 are equal to the experimental probability $P(AB)$:

$$= P(AA'BB') + P(A\bar{A}'BB') + P(AA'B\bar{B}') + P(A\bar{A}'B\bar{B}')$$

$$= \int \tilde{A}(\lambda)\tilde{A}'(\lambda)\tilde{B}(\lambda)\tilde{B}'(\lambda)\rho(\lambda) + \tilde{A}(\lambda)(1-\tilde{A}'(\lambda))\tilde{B}(\lambda)\tilde{B}'(\lambda)\rho(\lambda)d\lambda + \ldots$$

$$\tilde{A}(\lambda)\tilde{A}'(\lambda)\tilde{B}(\lambda)(1-\tilde{B}'(\lambda))\rho(\lambda) + \tilde{A}(\lambda)(1-\tilde{A}'(\lambda))\tilde{B}(\lambda)(1-\tilde{B}'(\lambda))\rho(\lambda)d\lambda$$

$$= \int \tilde{A}(\lambda)\tilde{B}(\lambda)\Big(\tilde{A}'(\lambda)\tilde{B}'(\lambda) + (1-\tilde{A}'(\lambda))\tilde{B}'(\lambda) + \tilde{A}'(\lambda)(1-\tilde{B}'(\lambda)) + \ldots$$

$$(1 - \tilde{A}'(\lambda))(1 - \tilde{B}'(\lambda)) \Big)$$

$$= \int \tilde{A}(\lambda)\tilde{B}(\lambda) \Big(1\Big)\rho(\lambda)d\lambda$$

$$= P(AB)$$

This can equivalently be shown for any of the experimentally measured single and pairwise probabilities.

3 → 1: If we are given a distribution $P(AA'BB')$ whose marginals return the single and double observable experimental probabilities then there exists a simple way to define a deterministic hidden-variable model. Such a model will consist of

1. **Set of hidden variables:** Λ will consist of the sixteen quadruples $\lambda = (s_1, s_2, s_3, s_4)$, where $s_i = \pm 1$.

2. **Response functions:** $A(\lambda) = s_1$, $A'(\lambda) = s_2$, $B(\lambda) = s_3$, $B'(\lambda) = s_4$. They each depend on a separate variable. Eqn. (1.10) and (1.11) also hold since the marginals of the four observable probabilities were assumed to yield the probability of the experiment.

3. **Normalized probability density:** Define $\rho(\lambda)$ as $\rho(s_1, s_2, s_3, s_4) = P(AA'BB')$. $\rho(\lambda)$ is normalized since $P(AA'BB')$ is normalized.

Statement 1 ↔ Statement 4

1. There is a deterministic hidden-variables model for the experiment.

4. There are well-defined, compatible joint distributions for all pairs and triples of commuting and non-commuting observables.

1 → 3 → 4: In the equivalence argument for 1 → 3, we showed that statement one implies the existence of a $P(AA'BB')$ whose marginals return the eight probabilities of the experiment. We now extend this to include the existence of pairs and triples of commuting and *non-commuting* observables.

The existence of triples of operators follows the same argument as was used for pairs, but including the triples also highlights the existence of well defined probabilities for non-commuting observables. For example, one the marginals of

$$P(ABB') = \int \tilde{A}(\lambda)\tilde{B}(\lambda)\tilde{B}'(\lambda)\rho(\lambda)d\lambda \tag{1.13}$$

would be $P(BB')$ and one of the marginals of

$$P(A'BB') = \int \tilde{A}'(\lambda)\tilde{B}(\lambda)\tilde{B}'(\lambda)\rho(\lambda)d\lambda \tag{1.14}$$

would also be the same value of $P(BB')$. B and B' are not necessarily commuting observables, and yet their joint distribution is well defined. (Note that this means that the existence of deterministic hidden variables is contrary to the notion in quantum mechanics that joint distributions are only well defined for commuting observables.)

4 → 1: To prove the converse we show that if one has a well-defined distributions of non-commuting observables, in particular $P(ABB')$, $P(A'BB')$ and their common marginal $P(BB')$, then one can construct a distribution $P(AA'BB')$ whose marginals will again return back the measured probabilities. An example of such a construction is:

$$P(AA'BB') = \frac{P(ABB')P(A'BB')}{P(BB')} \tag{1.15}$$

$$= \frac{(\int_\Lambda \tilde{A}(\lambda)\tilde{B}(\lambda)\tilde{B}'(\lambda)\rho(\lambda)d\lambda)(\int_\Lambda \tilde{A}'(\lambda)\tilde{B}(\lambda)\tilde{B}'(\lambda)\rho(\lambda)d\lambda)}{\int_\Lambda \tilde{B}(\lambda)\tilde{B}'(\lambda)\rho(\lambda)d\lambda} \tag{1.16}$$

$$= \int_\Lambda \tilde{A}(\lambda)\tilde{A}'(\lambda)\tilde{B}(\lambda)\tilde{B}'(\lambda)\rho(\lambda)d\lambda) \tag{1.17}$$

Where Eqn. (1.17) is the probability distribution whose marginal, we showed earlier, would return the measured probabilities.

Statement 1 ↔ Statement 5

1. There is a deterministic hidden-variables model for the experiment.

5. The Bell/CHSH inequalities hold.

1 → 4 → 5: As proven earlier, the existence of a deterministic hidden-variable model implies the existence of well-defined compatible joint distributions for all pairs and triples of commuting and non-commuting observables. These joint distributions can then be used to create restrictions on the probabilities of a correlation experiment. We first write $P(ABB')$ as a sum of marginals:

$$P(ABB') = P(AA'BB') + P(A\bar{A}'BB') \tag{1.18}$$

19

Since $P(AA'BB') \leq P(A'B)$ and $P(A\bar{A}'BB') \leq P(\bar{A}'B)$ (this inequality and the others we present in this argument can be more easily visualized using the depiction of marginals introduced earlier) we have that

$$P(AA'BB') + P(A\bar{A}'BB') \leq P(A'B) + P(\bar{A}'B') \tag{1.19}$$

Since $P(\bar{A}'B') = P(B') - P(A'B')$ (this is is true from rearranging the marginal equation) we have that

$$P(ABB') \leq P(A'B) + P(B') - P(A'B') \tag{1.20}$$

Following the same logic as the previous three equations but starting with $P(\bar{A}BB')$ we also find that,

$$P(\bar{A}BB') = P(\bar{A}A'BB') + P(\bar{A}\bar{A}'BB') \tag{1.21}$$
$$\leq P(A'B') + P(\bar{A}'B) \tag{1.22}$$
$$= P(A'B') + P(B) - P(A'B) \tag{1.23}$$

Then using similar marginal probability relationships we find that,

$$P(A) = P(AB) + P(A\bar{B}) \tag{1.24}$$
$$P(A) = P(AB) + P(A\bar{B}B') + P(A\bar{B}\bar{B}') \tag{1.25}$$
$$P(A) = P(AB) + (P(AB') - P(ABB')) + P(A\bar{B}\bar{B}') \tag{1.26}$$
$$P(A\bar{B}\bar{B}') = P(A) - P(AB) - P(AB') + P(ABB') \tag{1.27}$$
$$0 \leq P(A\bar{B}\bar{B}') = P(A) - P(AB) - P(AB') + P(ABB') \tag{1.28}$$

and again a similar calculation will find that,

$$0 \leq P(\bar{A}\bar{B}\bar{B}') = 1 - P(A) - P(B) - P(B') + P(AB') + P(\bar{A}BB') \tag{1.29}$$

The bound from Eqn. (1.28) can be rewritten as,

$$- P(A) + P(AB) + P(AB') - P(ABB') \leq 0 \tag{1.30}$$

and together with Eqn. (1.20) will form the bound,

$$P(AB) + P(AB') + P(A'B') - P(A'B) - P(A) - P(B') \leq 0 \tag{1.31}$$

A similar calculation shows that the bound for $P(\bar{A}BB')$ in Eqn. 1.23 can be used in Eqn. 1.29 to fine,

$$-1 \leq P(AB) + P(AB') + P(A'B') - P(A'B) - P(A) - P(B') \tag{1.32}$$

Together Eqn. (1.31) and (1.32) give the bound,

$$-1 \leq P(AB) + P(AB') + P(A'B') - P(A'B) - P(A) - P(B') \leq 0 \qquad (1.33)$$

Which is equivalent to one of the four CHSH inequalities. Similar calculations for the other three observable terms will provide three more pairs of inequalities which can be used to construct the other three CHSH inequalities, which together are,

$$-1 \leq P(AB) + P(AB') + P(A'B') - P(A'B) - P(A) - P(B') \leq 0 \qquad (1.34)$$
$$-1 \leq P(A'B) + P(A'B') + P(AB') - P(AB) - P(A') - P(B') \leq 0 \qquad (1.35)$$
$$-1 \leq P(AB') + P(AB) + P(A'B) - P(A'B') - P(A) - P(B) \leq 0 \qquad (1.36)$$
$$-1 \leq P(A'B') + P(A'B) + P(AB) - P(AB') - P(A') - P(B) \leq 0 \qquad (1.37)$$

5 → 4 → 1: As proven earlier, the existence of the three observable distributions $P(ABB')$ and $P(A'BB')$ which yield the same distribution $P(BB')$ and also yield the probabilities of the experiment implies the existence of a deterministic hidden variable model (4 → 1). Thus to prove that 5 → 1 we will show that the CHSH inequalities being satisfied implies the existence of such distributions, $P(ABB')$ and $P(A'BB')$. First let β be the minimum of the following non-negative terms

1. $P(B)$

2. $P(B')$

3. $P(AB) + P(B') - P(AB')$

4. $P(AB') + P(B) - P(AB)$

5. $P(A'B) + P(B') - P(A'B')$

6. $P(A'B') + P(B) - P(A'B)$

This is true for $P(BB') = \beta$. We then use this definition of β to define the additional terms,

1. $P(B\bar{B}') = P(B) - \beta$

2. $P(\bar{B}B') = P(B') - \beta$

3. $P(\bar{B}\bar{B}') = 1 - P(B) - P(B') + \beta$

21

We then let α be the minimum of

1. β

2. $\beta - (P(A) + P(B) + P(B') - P(AB') - P(AB) - 1)$

3. $P(AB)$

4. $P(AB')$

and let α' be the minimum of

1. β

2. $\beta - (P(A') + P(B) + P(B') - P(A'B') - P(A'B) - 1)$

3. $P(A'B)$

4. $P(A'B')$

Furthermore, the CHSH inequalities, given in Eqn. (1.34 - 1.37), guarantee that α and α' are both non-negative and that,

$$0 \leq \alpha \leq \beta \leq 1, \qquad 0 \leq \alpha' \leq \beta \leq 1$$

We now set $P(ABB') = \alpha$ and $P(A'BB') = \alpha'$ and then write the remaining distributions as

1. $P(AB\bar{B}') = P(AB) - \alpha$

2. $P(A\bar{B}B') = P(AB') - \alpha$

3. $P(A\bar{B}\bar{B}') = P(A) - P(AB) - P(AB') + \alpha$

4. $P(\bar{A}BB') = \beta - \alpha$

5. $P(\bar{A}B\bar{B}') = P(B) - P(AB) - \beta + \alpha$

6. $P(\bar{A}\bar{B}B') = P(B') - P(AB') - \beta + \alpha$

7. $P(\bar{A}\bar{B}\bar{B}') = 1 - P(A) - P(B) - P(B') + P(AB) + P(AB') + \beta - \alpha$

8. $P(A'B\bar{B}') = P(A'B) - \alpha'$

9. $P(A'\bar{B}B') = P(A'B') - \alpha'$

10. $P(A'\bar{B}\bar{B}') = P(A') - P(AB) - P(A'B') + \alpha'$

11. $P(\bar{A}'BB') = \beta - \alpha'$

12. $P(\bar{A}'B\bar{B}') = P(B) - P(A'B) - \beta + \alpha'$

13. $P(\bar{A}'\bar{B}B') = P(B') - P(A'B') - \beta + \alpha'$

14. $P(\bar{A}'\bar{B}\bar{B}') = 1 - P(A') - P(B) - P(B') + P(A'B) + P(A'B') + \beta - \alpha'$

We now finally need to verify that each right-hand term defined (of the fourteen listed above) is both non-negative and not larger than the already defined joint probability for any two of the three observables on the left-hand side of it. These can all be verified from the definitions of α, α', β, from the assumption that the CHSH inequalities hold and the use of probabilistic relationships (*e.g.* $P(AB) \leq \min[P(A), P(B)]$). Thus the satisfaction of the CHSH inequalities verifies the existence of a $P(ABB')$ and $P(A'BB')$ with the desired properties.

Statement 1 ↔ Statement 2

1. There is a deterministic hidden-variables model for the experiment.

2. There is a factorizable, stochastic model for the experiment.

1 → 2: First we demonstrate that every stochastic model can be interpreted as a factorizable stochastic model. To do so we first need to define such a model. We will first relax the requirement that the outcome of each response function is deterministic. We instead use the probabiltiy function $P(S, \lambda)$ and $P(ST, \lambda)$ where $P(S, \lambda)$ is the *probability* that the observable S takes the value $+1$ when measuring the state λ. Likewise, $P(ST, \lambda)$ gives the probability that both S and T return the values $+1$ for the state λ. We then define the new restrictions on these response function to be

$$P(S) = \int_\Lambda P(S, \lambda)\rho(\lambda)d\lambda \tag{1.38}$$

$$P(ST) = \int_\Lambda P(ST, \lambda)\rho(\lambda)d\lambda \tag{1.39}$$

Again adopting the same bar notation, $(P(\bar{S}, \lambda) = 1 - P(S, \lambda))$. Finally this stochastic hidden-variable model is said to be factorizable if

$$P(ST, \lambda) = P(S, \lambda)P(T, \lambda) \tag{1.40}$$

With the model defined, it is easy to show that ever deterministic hidden-variables model is a factorizable stochastic model, one where all the probabilities are either 0 or 1. We set $P(S, \lambda) = 1$ if $S(\lambda) = 1$, $P(S, \lambda) = 0$ if $S(\lambda) = -1$ and let $P(ST, \lambda) = P(S, \lambda)P(T, \lambda)$. Then Eqns (1.38) and (1.39) reduce to the defined integrands for the response functions for the deterministic model, Eqns (1.10) and (1.10).

$\mathbf{2 \to 5 \to 1:}$ Fine does not prove this in his own work but references a paper by Clauser and Horne which proves that statement 2 implies statement 5 [32] which completes the proof since it was already shown that statements 5 and 1 are equivalent.

1.3 The Leggett-Garg framework

1.3.1 Macroscopic realism

The experimental violations of the Bell inequalities opened the door to new questions in the field of quantum foundations. One such question being that – If reality is described by quantum mechanics, then can these laws be scaled to commonplace objects? This idea of systems composed of countless atoms existing in quantum superpositions of macroscopically distinct states is a type of macroscopic quantum phenomena known as *macroscopic coherence* (see Fig. 1.7 for examples of other macroscopic quantum phenomena which have been experimentally realized). Anthony Leggett and Anupam Garg drew attention to the study of this subject by first codifying how physicist expect macroscopic objects to behave into a set of assumptions that they defined as *macroscopic realism* (MR) [4, 5]. As defined by Leggett and Garg these assumptions are

1. Macroscopic realism per se (MRps): A macroscopic system with two or more macroscopically distinct states available to it will at all times be in one or the other of these states.

2. Noninvasive measurability (NIM): It is possible, in principle, to determine the state of the system with arbitrarily small perturbation on its subsequent dynamics.

Leggett and Garg later added the condition that future measurements should not affect the present state (a condition they named induction), but this assumption is rarely contested. Leggett and Garg used these assumptions to derive a set of inequalities that any macroscopic system should obey. These are the Leggett-Garg inequalities (LGIs) and are the topic of the succeeding section. Before proceeding to use these assumptions in our discussion, it is worthwhile to pause and briefly reflect on the first two.

The foremost assumption of MR is MRps. On the outset, the interpretation of this assumption seems clear – that macroscopic objects do not exist in superpositions of states. However, the exact interpretation of this assumption has been debated by different authors [33]. Maroney and Timpson have presented at least three different interpretations of MRps [34]. Of these, the one which they refer to as "operational eigenstate mixture macrorealism" is the notion of MRps that Leggett and Garg seem to allude to in their original work. As defined by the authors operational eigenstate mixture macrorealism is the view that:

The only possible preparation states of a system are operational eigenstates of [some macroscopic definite observable] and statistical mixtures thereof.

This view suggests that, despite what is occurring at the microscopic level, the macroscopic properties of a system will behave in the same way whether they are being observed or not. This is also the only interpretation of MRps which can be tested by the LGIs [34] and as such is the interpretation that we consider in this work.

Furthermore, the NIM assumptions also carries with it nuances which are worth accentuating. The first of these is that the NIM assumption defines a non-invasive measurement from a macroscopically real understanding of the system. This means that when one is testing for MR, the argument they adopt for the non-invasiveness of their measurement technique only needs to hold at macroscopic level. Thus, a measurement on a quantum system can still satisfy the NIM postulate even is it collapses the wave function [35], since the concept of a wave function does not exist in a macrorealistic understanding of the world. Secondly, as was the case when considering locality with realism, the assumptions of NIM and MRps are not readily separable. Leggett has stated on many occasions that he sees NIM as such a natural corollary of MRps that it is hard to imagine how NIM could fail but MRps not [36]. However, there is nothing in the derivation of the LGIs themselves which excludes the failure of NIM and not MRps [6, 34, 37]. As was the case when testing local realism, tests of macroscopic realism must consider both MRps and NIM as a whole and not as individual assumptions.
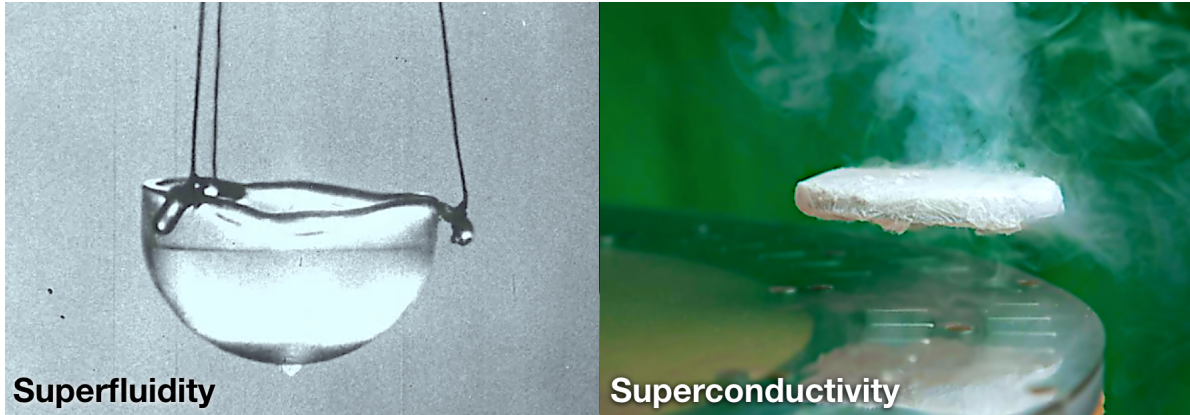
Figure 1.7: Examples of macroscopic quantum phenomena which have been experimentally realised. *Superfluid*: An image of liquid Helium-4 cooled to below 3° K where it enters the superfluid phase. Once a superfluid, the helium atoms will all exists in their lowest energy state. This is made possible since Helium-4 atoms, unlike common Helium atoms, behaves as bosons and can thus occupy the same energy level. As a result the atoms are mathematically indistinguishable, which in turns results in the atoms moving in unison. This unified motion results in the atoms having no internal friction and thus zero viscosity. The lack of viscosity then allows the helium to drip through a solid container which was previous able to hold the helium when it was in a liquid state. The drops forming on the bottom of the container demonstrate this effect. For a more detailed review on the quantum mechanical nature of this effect see [38]. *Superconductor:* An image of a high temperature super conductor levitating above a magnet, an effect known as quantum locking. This is a result of the property of a superconductor where the superconductor expels nearly all internal magnetic fields. Only quantized strands of the magnetic field are able to travel through the superconductor. These strands are locked in place and in turn trap the superconductor in space. Superconductors are commonly used for producing strong magnetic fields (as in NMR or in a particle accelerator) or for storing energy. For a detailed introduction to superconductivity see [39].

1.3.2 The Leggett-Garg inequalities

Leggett and Garg would go on to use the assumptions of macroscopic realism to derive a set of inequalities that any macroscopic system should obey. These are the Leggett-Garg inequalities (LGIs). If measurements on a system are to violate the LGIs then a macroscopic understanding of the system must be abandoned. In this way the LGIs serve as a test of macroscopic coherence.

To date, experimental violation of the LGIs have predominately been performed on microscopic systems (see [40] for an exception). These experiments remain a topic of interest for different reasons. For one, violations on microscopic systems are a necessary stepping stone towards achieving macroscopic coherence. Even at the level of microscopic systems the study of the LGIs have been riddled with challenges which will need to be addressed before one can feasibly move to larger systems. A second motivation for the study of the LGIs is that they serve as a test of whether a system is behaving quantum-mechanically. The use of the LGIs in this manner has been adopted in different fields including quantum transport [41], quantum biology [42] and quantum computing [43].

The formalism of the LGIs is fairly straightforward. First consider a dichotomic observable [2], Q, with outcomes $s_i \in \{\pm 1\}$ measured at time t_i. When measuring this observable Q at two different times t_i, t_j ($Q(t_i) \equiv Q_i$), the outcomes will either be correlated ($s_i s_j = 1$) or anti-correlated ($s_i s_j = -1$). The *correlation function*, C_{ij},

$$C_{ij} = \langle Q_i Q_j \rangle = \sum_{i,j} s_i s_j p_{ij}(s_i, s_j) \tag{1.41}$$

assigns a value to this correlation. C_{ij} is bounded by ± 1 corresponding to the cases of perfect correlation and anti-correlation respectively, and $p_{ij}(s_i, s_j)$, the *two-time probability*, is the probability of obtaining the results s_i and s_j when measurements are made at times t_i, t_j, respectively. By performing three experiments that measure the observable Q at pairs of times (t_1, t_2), (t_2, t_3) and (t_1, t_3) the correlation functions C_{12}, C_{23}, and C_{13} can be obtained. For a system which obeys the assumptions of MRps and NIM it can be proven that these correlations are bounded by the four three-time LGIs (LG3s) [4, 5].

$$1 + C_{12} + C_{23} + C_{13} \geq 0 \tag{1.42}$$
$$1 - C_{12} - C_{23} + C_{13} \geq 0 \tag{1.43}$$
$$1 + C_{12} - C_{23} - C_{13} \geq 0 \tag{1.44}$$

---

[2]These inequalities can be derived even if Q is not dichotomous so long as it is bounded by $|Q| \leq 1$ [44, 45].

$$1 - C_{12} + C_{23} - C_{13} \geq 0 \tag{1.45}$$

Proof: The assumption of MRps implies that Q will take definite values at all times. This implies the existence of an underlying probability $p_{ij}(s_i, s_j, s_k)$, which the two-time probabilities are the marginals of.

$$p_{ij}(s_i, s_j) = \sum_{s_k} p_{ij}(s_i, s_j, s_k) \tag{1.46}$$

Secondly, the NIM assumption implies that the probability of the measured results should be independent of whether earlier measurements are made, mathematically this is written as:

$$p_{12}(s_i, s_j, s_k) = p_{13}(s_i, s_j, s_k) = p_{23}(s_i, s_j, s_k) \equiv p(s_i, s_j, s_k) \tag{1.47}$$

With these two assumptions the correlation functions defined in Eq. 1.41 are equivalent to $(p(\pm 1, \pm 1, \pm 1) \equiv p_{\pm\pm\pm})$:

$$C_{12} = p_{+++} + p_{++-} - p_{+-+} - p_{-++} + p_{--+} - p_{-+-} - p_{+--} + p_{---} \tag{1.48}$$

$$C_{23} = p_{+++} - p_{++-} - p_{+-+} + p_{-++} - p_{--+} - p_{-+-} + p_{+--} + p_{---} \tag{1.49}$$

$$C_{13} = p_{+++} - p_{++-} + p_{+-+} - p_{-++} - p_{--+} + p_{-+-} - p_{+--} + p_{---} \tag{1.50}$$

Using the unit measure axiom of probability, namely that the probability of the entire sample space is equal to one, these correlations can be combined to give:

$$C_{12} + C_{23} + C_{13} = -1 + 4(p_{+++} + p_{---}) \tag{1.51}$$

$$-C_{12} - C_{23} + C_{13} = -1 + 4(p_{+-+} + p_{-+-}) \tag{1.52}$$

$$C_{12} - C_{23} - C_{13} = -1 + 4(p_{++-} + p_{--+}) \tag{1.53}$$

$$-C_{12} + C_{23} - C_{13} = -1 + 4(p_{-++} + p_{+--}) \tag{1.54}$$

Since the sum of any two probabilities is necessarily bounded by 0 and 1 these equations will have the lower bound of

$$1 + C_{12} + C_{23} + C_{13} \geq 0 \tag{1.55}$$

$$1 - C_{12} - C_{23} + C_{13} \geq 0 \tag{1.56}$$

$$1 + C_{12} - C_{23} - C_{13} \geq 0 \tag{1.57}$$

$$1 - C_{12} + C_{23} - C_{13} \geq 0 \tag{1.58}$$
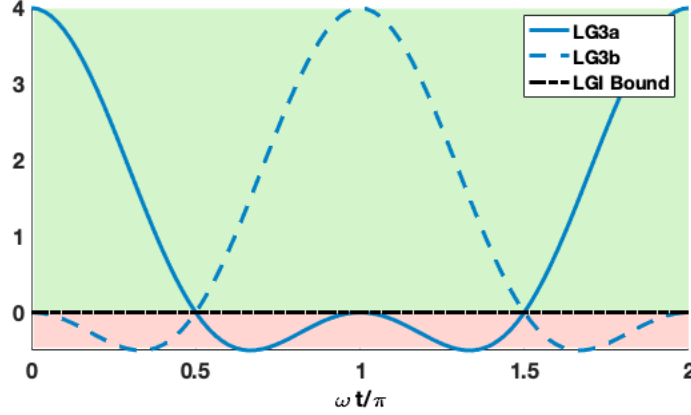
Figure 1.8: Two of the LG3s as functions of $\omega t/\pi$ for measurements made at equidistant time intervals. The red and green regions indicate where the LG3s, respectively, are and are not violated.

These inequalities can, however, be violated by quantum systems. For example, consider a spin-$\frac{1}{2}$ particle evolving under a Hamiltonian $\hat{H} = \omega \hat{X}/2$ and measured by $\hat{Q} = \hat{Z}$, where $\hat{X}$ and $\hat{Z}$ are the Pauli-x and Pauli-z matrices. For such a model it is readily shown that for any initial state the quantum mechanical correlation function is [35]:

$$C_{ij} = \frac{1}{2}\langle \hat{Q}_1\hat{Q}_2 - \hat{Q}_2\hat{Q}_1 \rangle \tag{1.59}$$

$$= \cos(\omega(t_j - t_i)) \tag{1.60}$$

By using Eq.(1.60) and considering the case of equidistant time intervals, *i.e.*, $t_j - t_i = t$, the four LG3s reduce to three inequalities

$$(\text{LG3a}) \quad 1 + 2\cos(\omega t) + \cos(2\omega t) \geq 0 \tag{1.61}$$

$$(\text{LG3b}) \quad 1 - 2\cos(\omega t) + \cos(2\omega t) \geq 0 \tag{1.62}$$

$$1 - \cos(2\omega t) \geq 0 \tag{1.63}$$

the third of which is always satisfied. As shown in Fig. 1.8, one of the other two inequalities, Eq.(1.61) or (1.62), will be violated for all but discrete choices of ωt. Thus, the LGIs can be violated by a quantum system.

29
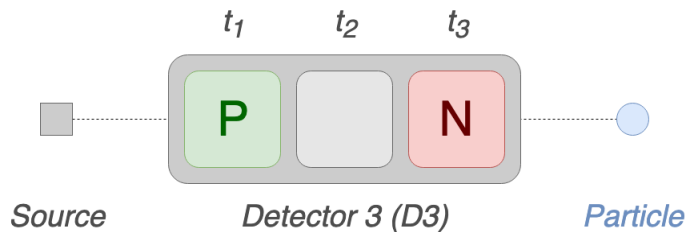
Figure 1.9: A particle moving through the detector $D3$. $D3$ measures the spin of the particle along one chosen axis for each of the three different times, t_1, t_2 and t_3. The result of each measurement is either positive P or negative N.

The first experimental violations of the Leggett-Garg inequalities was performed by Palacious-Laloy *et al* in 2010 [46] and this work was shortly followed by violations performed on a host of different quantum systems.

Alternative derivation

We will close this section with a simple alternative derivation of the LGIs which highlights their similarities with the Bell model.

Consider the experimental design depicted in Fig. 1.9. This design consists of a spin-$\frac{1}{2}$ particle whose spin is measured by a detector $D3$ at different pairs of times $((t_1, t_2), (t_2, t_3)$ or $(t_1, t_3))$. The outcome of each measurement will be either $+1$ (P) or -1 (N). The measured outcomes at pairs of times, (t_i, t_j), will either be correlated or anti-correlated. The correlation function, C_{ij}, will assign a value of $+1$ for a positive correlation and a value of -1 for an anti-correlation. As shown in Table 1.3, the sum of the different correlation functions is bounded by -1 and $+3$ for any possible state. This provides a simplified derivation of the Leggett-Garg inequalities:

$$-1 \leq C_{12} + C_{23} + C_{13} \leq 3 \tag{1.64}$$

Similar to the derivation of the Bell inequalities presented in this work, this alternative derivation does not require any algebra using probability theory. Instead it considers all possible measurement outcomes for pairs of correlations of the simple dichotomic observable to be able to create upper and lower bounds on the sums of the correlations functions.

	C12	+ C23	+ C13	=
(P,P,P)	(+1)	+ (+1)	+ (+1)	= 3
(N,N,N)	(+1)	+ (+1)	+ (+1)	= 3
(P,P,N)	(+1)	+ (-1)	+ (-1)	= -1
(N,N,P)	(+1)	+ (-1)	+ (-1)	= -1
(P,N,P)	(-1)	+ (-1)	+ (+1)	= -1
(N,P,N)	(-1)	+ (-1)	+ (+1)	= -1
(N,P,P)	(-1)	+ (+1)	+ (-1)	= -1
(P,N,N)	(-1)	+ (+1)	+ (-1)	= -1

Table 1.3: The possible correlation functions for a spin-$\frac{1}{2}$ system measured at pairs of times. The eight possible initial states are considered here. The sum of the three possible correlation functions, C_{ij}, are bounded by $-1 \leq C_{12} + C_{23} + C_{13} \leq 3$.

Chapter 2

Nuclear magnetic resonance quantum information processing

2.1 Fundamentals of NMR

Nuclear magnetic resonance (NMR) was discovered long before the advent of quantum computing. This allowed the machinery and techniques of NMR to be refined for nearly fifty years before being adapted to serve as a quantum information processor (QIP). To date, many quantum algorithms and benchmarks have been performed on NMR spectrometers [47]. As such, NMR QIPs have played a critical role in the development of quantum technologies. We will begin this chapter with a basic review of the physics of an NMR spectrometer insomuch as to understand its functionality as QIP. A summary of this review is provided in Fig. 2.1.

A liquid state NMR experiment begins with a sample consisting of an ensemble of 10^{23} molecules dissolved in some solution. The spin of the nuclei in this sample will be randomly orientated in space, since no particular orientation will provide a favourable energy. Thus, the individual spin of the nuclei will cancel and the sample will have an overall magnetic moment of $\vec{\mu} = 0$.

Once this sample is placed in a spectrometer it will experience an (ideally) uniform magnetic field, $\vec{B} = B_0 \hat{z}$. Since the nuclei have an electric charge and a magnetic moment they will necessarily interact with this magnetic field [1]. The presence of this magnetic field

---

[1]In most quantum computing experiments we are concerned with only spin $\frac{1}{2}$ nuclei which means that the electric component of this interaction is zero
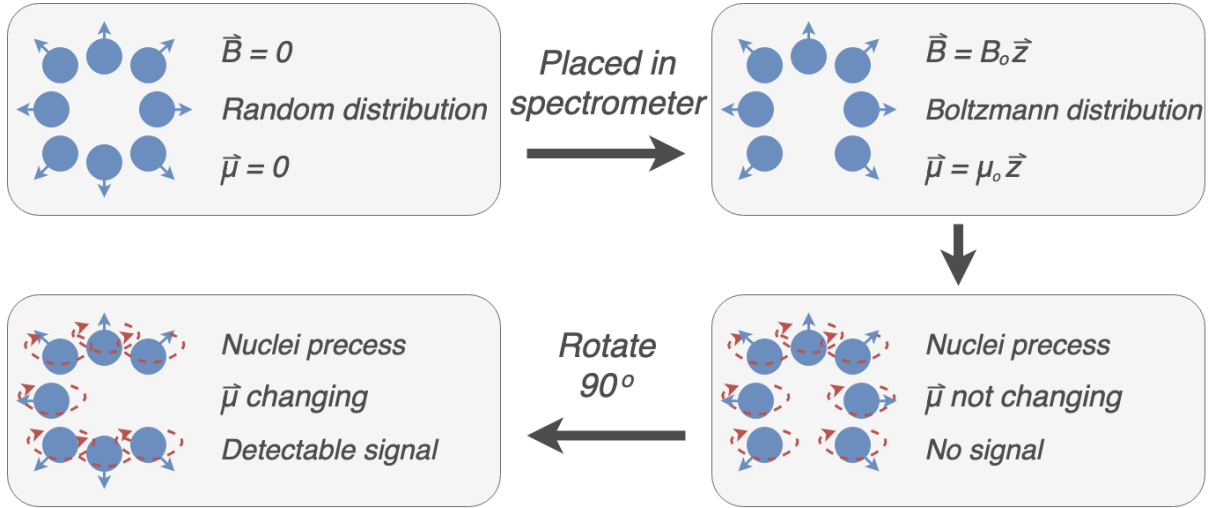
Figure 2.1: An overview of the fundamentals of an NMR experiment as outlined in section 2.1.

will create two effects of interest in the sample. The first is that since the nuclei have a magnetic moment, they will either slightly align or slightly anti-align with the magnetic field. Those spins who align with the field will have less potential energy than those who anti-align. This splitting of the energy levels is known as *Zeeman splitting*. The nuclei will only slightly align or anti-align since the thermal energy in the lab will be much greater than the energy difference from the Zeeman splitting. The distribution of states between these two energy levels is given by the Boltzmann distribution:

$$\rho_n = \frac{e^{-E_n/k_BT}}{\sum_m e^{-E_m/k_BT}} = \frac{\exp(-\hbar\omega_n/k_BT)}{\sum_m \exp(-\hbar\omega_m/k_BT)} \tag{2.1}$$

Here ω_n and E_n are the precession frequency and the energy of the state ρ_n respectively and T is the temperature. As well, $\hbar$ is the reduced Plank's constant and k_B is the Boltzmann constant. The existence of slightly more states in the lower energy level (the alligned state) will result in a small net magnetic moment along $\hat{z}$, $\hat{\mu} = \mu_0\hat{z}$. The second effect of interest caused by the external field, is that the individual nuclei will begin to precess around the axis of the external field $\vec{z}$. The overall magnetic moment of the sample though will not be precessing since it is aligned with the field $\vec{B}$.

At this point a radio frequency pulse is applied to the sample which causes the ensemble of spins to rotate along the x-y axis. This causes a rotation of the overall net magnetic

moment $\hat{\mu}$ into a direction which is transverse to the external field $\vec{B}$. Now that the net magnetic moment $\hat{\mu}$ is transverse to $\vec{B}$ it will begin to process around $\hat{z}$. This rotating magnetic moment will create a changing magnetic field which will, as a consequence of Faraday's law, induce a current. This current is detected by coils which wrap around the NMR sample. This current is ultimately what communicates what the state of the ensemble system is. After the pulse is applied the precessing nuclei will gradually move out of phase with one another and the net magnetization will gradually realign with the overall magnetic field $\vec{B}$. These two forms of relaxation gradually eliminate the signal and end the experiment.

2.2 Implementation as a quantum computer

It can be shown that an NMR spectrometer can be harnessed as a quantum computer by demonstrating that it will satisfy the five criteria for quantum computation outlined by David DiVincenzo [48]. This section outlines how liquid state NMR spectrometers can be used to satisfy each of these DiVincenzo criteria and thus serve as a quantum computer. An overview of the contents of this section are provided in Table 2.1.

2.2.1 The qubit

The first criteria for a quantum computer is the existence of two-level quantum system to encode the qubit. A natural choice for an NMR QIP are the two Zeeman levels of a spin-$\frac{1}{2}$ nuclei. The state $|0\rangle$ is encoded as the lower energy state (spin up) and the state $|1\rangle$ is encoded as the higher energy state (spin down). Different spin $\frac{1}{2}$ nuclei such as ^{1}H, ^{13}C, ^{15}N, ^{19}F and ^{31}P have been used as qubits in this way.

Recall from section 2.1, that the nuclei's state is determined by the current induced by the nuclei's precessing magnetic field. There are two reasons why this is relevant for defining our qubit. The first, is that due to technological limits, the current induced by an individual nuclei is too weak to be detected. Thus, what we consider as "one qubit" is about 10^{23} nuclei who precess with the same frequency. The second reason that this is relevant, is that since the nuclei can only be distinguished by their precession frequencies, then the number of qubits an NMR sample has is equal to the number of nuclei it has with distinct precession frequencies. To understand how many distinct precession frequencies a NMR sample will have, we must consider the samples Hamiltonian.

	Criteria	NMR Realization
1.	**A scalable physical system with well characterized qubits**	**Qubit:** Ensemble of chemically distinct nuclear spins. **Scalability:** Limited by molecules and low polarization
2.	**The ability to initialize the state of the qubits to a simple fiducial state, such as** $\|00\ldots\rangle$	Pseudopure state
3.	**A universal set of quantum gates.**	**1-Qubit gates**: Single qubit rotations with RF pulses. **CNOT**: Depends on the coupling of spins.
4.	**A qubit-specific measurement capability.**	Ensemble weak measurement
5.	**Long relevant decoherence times, much longer than the gate operation time**	**Decoherence:** T1 >1 sec, T2 >1 sec **Gate time:** Microseconds

Table 2.1: An overview of how an NMR spectrometer satisfies each of the DiVincenzo criteria for quantum computation.

The Hamiltonian of a liquid state NMR sample consists of two terms. The first is the Zeeman term, which describes the precession of the nuclei around $\hat{z}$. For a molecule with n distinct precession frequencies the Zeeman Hamiltonian is (in units of $\hbar$)

$$H_z = \sum_l -\frac{\omega_l}{2} Z^l \qquad (2.2)$$

Z^l is the Pauli matrix Z on the lth nuclei[2] and ω_l is the angular frequency of the lth nuclei. This frequency is equal to

$$\omega_l = \gamma_l \tilde{B}_l = \gamma_l (1 - \delta_l) B_0 \qquad (2.3)$$

where γ_l is the nuclei's gyromagnetic ratio and $\tilde{B}_l$ is the *effective* magnetic field that the nuclei experiences. Thus, an NMR can have distinct ω_l, and thus multiple qubits, for two reasons. The first, is that the heteronuclear spins will naturally have different values of γ_l. The second, is that the homonuclear spins may experience different effective magnetic fields, $\tilde{B}_l$. $\tilde{B}_l$ deviates slightly from the overall magnetic field due to the magnetic environment of the different nuclei. Quantitatively the amount of this deviation is given by the nucleis *chemical shift*, denoted as δ_l. It is for these reasons that trichloroethylene (TCE) for example is a three qubit sample (see Fig. 2.2).

The second term in the sample's Hamiltonian arises from the interactions between the nuclei. These interactions are dominated by two effects, the interactions between the dipoles and the interactions between the spins. The dipole-dipole interactions are averaged out due to the tumbling of the liquid solution, leaving only the spin-spin interactions. The effect of this interaction is given by the J-coupling term

$$H_J = \sum_{l,m} \frac{\pi J_{lm}}{2} Z^l Z^m \qquad (2.4)$$

where J_{lm} is the coupling between the lth and mth nuclei. Since the nuclei do not interact strongly with the environment these two components of the Hamiltonian completely describe the evolution of the qubits in an NMR QIP. The three qubit sample TCE from Fig. 2.2, for example, has the following Hamiltonian

$$H_{tce} = -\frac{\omega_1}{2} ZII - \frac{\omega_2}{2} IZI - \frac{\omega_3}{2} IIZ + \frac{\pi J_{12}}{2} ZZI + \frac{\pi J_{23}}{2} IZZ + \frac{\pi J_{13}}{2} ZIZ \qquad (2.5)$$

[2](e.g. $Z^1 = Z \otimes I \otimes ... \otimes I$ or $Z^3 = I \otimes I \otimes Z \otimes I \otimes ... \otimes I$)
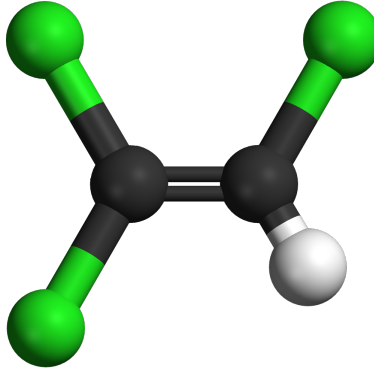
Figure 2.2: The molecular structure of trichloroethylene. Trichloroethylene can be used as a three qubit sample. The three qubits are the two ^{13}C and the one ^{1}H. The Hydrogen provides a different ω_l since it has a different γ from the ^{13}C. The two ^{13}C are distinguishable since they have different chemical environments. One ^{13}C is bounded to two ^{17}Cl while the other is bounded to a ^{17}Cl and a ^{1}H.

Density matrix description

Some of the the topics in this chapter can be explained in more depth by describing the qubits using the density matrix formalism. Similar to how a single qubit is described by the ensemble average of a collection individual nuclei, the density matrix of a single qubit is also described by the average of the individual nuclei's density matrices. If each individual nuclei n_i is in the general state $|\psi_i\rangle = \alpha_i |0\rangle + \beta_i |1\rangle$, then the state of the ensemble system is given by

$$\rho = \frac{1}{N} \sum_i |\psi_i\rangle \langle\psi_i| = \overline{|\psi\rangle \langle\psi|} \tag{2.6}$$

The density matrix for an individual qubit will have four elements. The diagonal elements are the *populations* (ρ_0, ρ_1) and the off-diagonal elements are the *coherences* (ρ_+, ρ_-).

$$\rho = \begin{bmatrix} \rho_0 & \rho_+ \\ \rho_- & \rho_1 \end{bmatrix} \tag{2.7}$$

The populations are real and positive numbers which sum to 1. Despite the seemingly obvious connection, the populations do not represent the percentage of spins in the system that are in the states $|0\rangle \langle0|$ or $|1\rangle \langle1|$. In fact essentially no nuclei will be in exactly one of the two states, but will exist in a superposition of the two. What the populations

represent is how much of the ensemble would be in one of those states if ρ was projected onto $|0\rangle\langle 0|$ or $|1\rangle\langle 1|$. On the other hand, the coherences are complex numbers which are complex conjugates of one another. Experimentally the coherences describe the transverse magnetization. Since they are complex numbers they have an amplitude and a phase. The amplitude is related to magnitude of the magnetization in the $x-y$ plane and the phase with the direction of that magnetization. This formalism will be drawn on through out the chapter.

2.2.2 Initialization

The second criteria for a QIP is the ability to initialize the system of qubits to a simple fiducial state. All models of computation are based on performing a set of operations on an initial state and measuring the final result. Since the final result will depend on the initial state, the initialization of the system is essential and a natural choice for such a state is $|0\rangle^{\otimes n}$. This means that an NMR QIP requires some process to map the thermal state of a sample to $|0\rangle^{\otimes n}$. The initial challenge in achieving this can be seen by considering the one qubit case.

The populations of ρ_0 and ρ_1 for the thermal state are given by the Boltzmann distribution (Eq. 2.1). The energies for the two states are

$$E_0 = \omega_0/2 = -\gamma B_0/2 \tag{2.8}$$
$$E_1 = -\omega_0/2 = \gamma B_0/2 \tag{2.9}$$

We define $\mathcal{B} \equiv \hbar\gamma B_0/k_B T$. Since $\mathcal{B}$ at room temperature is small ($\mathcal{O}(10^{-8})$ in SI units) we can approximate the Taylor series expansion of $\exp(\pm\mathcal{B}) \approx 1 \pm \mathcal{B}/2$. Thus the populations at thermal equilibrium are:

$$\rho_0 = (1 + \mathcal{B}/2)/2 \tag{2.10}$$
$$\rho_1 = (1 - \mathcal{B}/2)/2 \tag{2.11}$$

which gives the thermal state:

$$\rho_{thermal} = \frac{1}{2}\begin{bmatrix} 1 + \frac{\mathcal{B}}{2} & 0 \\ 0 & 1 - \frac{\mathcal{B}}{2} \end{bmatrix} = \frac{1}{2}I + \frac{\mathcal{B}}{4}Z \tag{2.12}$$

Again, since $\mathcal{B}/4$ is small, then the thermal state will be approximately equal to the identity, *i.e.* the maximally mixed state. For this system to be in the pure state $|0\rangle^{\otimes n}$ it would require $\mathcal{B}/2 = 1$ which would require temperatures of the order of $10mK$, which
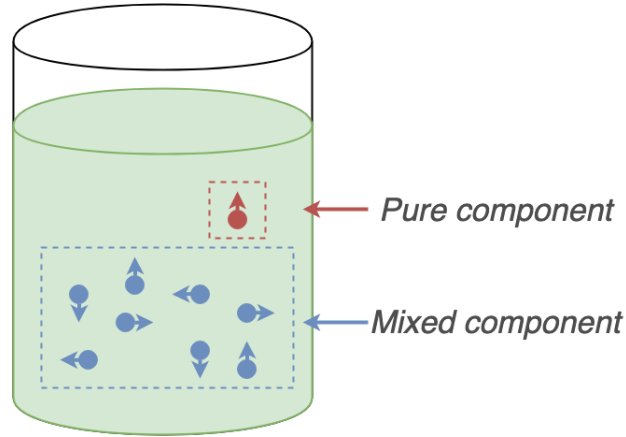
Figure 2.3: A schematic depiction of, one interpretation of, the pseudo-pure state (pps). The pps (Eq. 2.13) has a maximally mixed component and a pure component. For a pps state the sample is prepared such that a fraction of the nuclei are in the pure state while the rest of the nuclei form a maximally mixed state. Since the mixed state is not effected by unitary evolutions and does not produce any signal it effectively can be ignored.

is experimentally impractical. Instead what is used in NMR QIP is a pseudo-pure state (pps) [49, 50]. This pps has the general form:

$$\rho_{pps} = \frac{1-\epsilon}{2^n} I + \epsilon \left|00\ldots0\right\rangle \left\langle00\ldots0\right| \tag{2.13}$$

The ρ_{pps} state effectively behaves as a pure state since the identity term is invariant under unitary operations and produces no detectable signal when being measured. This leaves only the pure term being effected by the pulses and producing signals which are measured (see Fig. 2.3 for a schematic depiction). The preparation of a pps state requires the use of non-unitary techniques. Many techniques have been proposed for for preparing the pps. These techniques include spatial averaging [51], temporal averaging [52], logical labelling [53] and the cat-state method [54].

2.2.3   Universal set of gates

All quantum computations are unitary evolutions. This means that a necessary criteria for a potential QIP is the ability for it to perform any unitary operation. The Solovay–Kitaev theorem [55] ensures that this can be done efficiently given that the QIP can implement

certain finite gate sets, known as *universal quantum gate sets*. The gates in these sets can be used to construct any unitary evolution. The single qubit rotations and the CNOT gate together form an example of such a gate set. Both the single qubit rotations and the CNOT gate can be implemented on an NMR QIP, and thus an NMR QIP can implement any unitary evolution.

We will first consider how the single qubit rotations can be implemented on an NMR QIP. To do so, we first consider the state of a single qubit using the Bloch sphere representation. The Bloch sphere is a geometrical representation of a two-level quantum system. This representation is a unit 2-sphere whose north and south poles correspond to the $|0\rangle$ and $|1\rangle$ vectors, respectively. Any pure state $|\psi\rangle$ can be written in the form of

$$|\psi\rangle = \cos(\theta/2)\,|0\rangle + e^{i\phi}\sin(\theta/2)\,|1\rangle \tag{2.14}$$

for $0 \le \theta \le \pi$ and $0 \le \phi \le 2\pi$. The parameters θ and ϕ can be re-interpreted in spherical coordinates as $\vec{v} = (\sin\theta\cos\phi, \sin\theta\sin\phi, \cos\theta)$. Thus any pure state can be uniquely represented as a point on the unit sphere. Furthermore this representation can be used to represent mixed states as points on the interior of the sphere. This is the Bloch sphere representation of a two-level quantum system.

In this representation a single qubit rotation is equivalent to a rotation around an axis of the sphere. Thus, implementing these gates on an NMR QIP requires a method for rotating the spins of the nuclei. Such rotations can be implemented by applying a radio-frequency (RF) pulse along the desired axis of rotation. This applied pulse will rotate the direction of the spins counter clock wise to the desired axis. Furthermore, the degree of this rotation can be controlled by adjusting the power and/or duration of the pulse. In practise, these RF pulses are only applied in the plane transversal to the magnetic field, *i.e.* the x-y plane. This is sufficient to implement any single qubit Pauli gate. Note though, that the implementation of this effect requires that the RF pulse be applied at a fixed angle to the nuclei. However, the nuclei themselves are precessing at a frequency of ω_n. Thus to achieve the desired rotation, the RF pulses must be applied at the same precession frequency of the target nuclei (see Fig. 2.4). This mechanism also explains how it is that the different nuclei in a sample can be targeted. If the RF pulse is applied out of phase with the precession frequency of the non-target nuclei then that nuclei will effectively feel the RF pulse from all directions and thus will experience no net rotation (see Fig. 2.4). If the frequency of the different nuclei in a sample are relatively close, *e.g.* two homo-nuclear spins with different chemical environments, the RF pulses need to be applied for longer durations and with less power. What this does is effectively give the RF pulse more time to fall out of phase with the non-target nuclei. Pulses implemented in this manor are known as *soft pulses*.
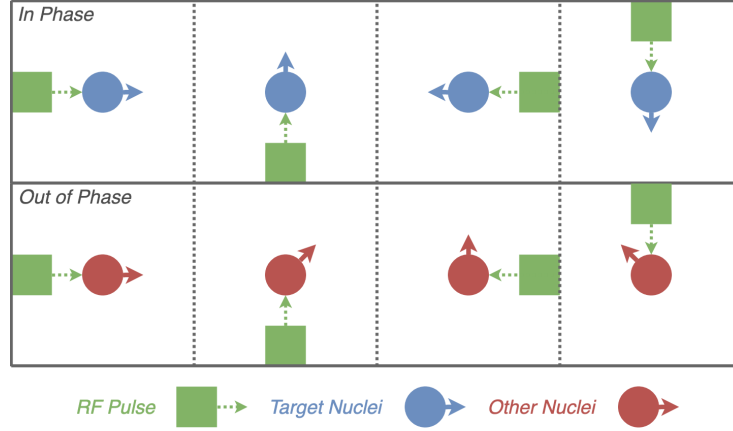
Figure 2.4: An RF pulse being applied to a two nuclei sample. The RF pulse is applied in phase to the target nuclei. This means that the target nuclei will experience the pulse at a fixed angle and thus its spin will be rotated. In this sample though there exists a second nuclei which is precessing at some different frequency. From the perspective of this other nuclei the RF pulse is being applied evenly from all angles and thus the spin of this other nuclei will not be rotated.

To complete our universal gate set we will also require a means for implementing the CNOT gate. The CNOT can be implemented through regulating the evolution caused by the J-coupling term of the samples Hamiltonian. For example, consider the two qubit Hamiltonian of ^{13}C-chloroform

$$H_{chloro} = -\frac{\omega_1}{2}ZI - \frac{\omega_2}{2}IZ + \frac{\pi J_{12}}{2}ZZ \tag{2.15}$$

If the first qubit is in the state $|0\rangle$ then the Hamiltonian for the second spin reduces to (ignoring scalar constants)

$$H_{chloro}^0 = (-\frac{\omega_2}{2} + \frac{\pi J_{12}}{2})Z \tag{2.16}$$

This new Hamiltonian is identical to the original Zeeman Hamiltonian of the second qubit except that the second qubit is now precessing faster. If the first qubit had been in the state $|1\rangle$ then the Hamiltonian would of reduced to

$$H_{chloro}^1 = (-\frac{\omega_2}{2} - \frac{\pi J_{12}}{2})Z \tag{2.17}$$

This new Hamiltonian is also identical to the original Zeeman Hamiltonian of the second qubit except that the second qubit is now precessing slower. The effective of the J-coupling
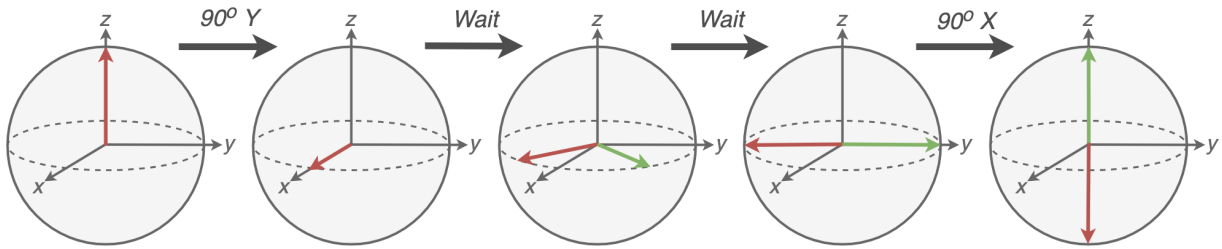
Figure 2.5: The step by step effect of the pulse sequence for implementing the CNOT gate. The Bloch sphere in this figure depicts the evolution on the second qubit of a two qubit system. The red arrow depicts the evolution of the second qubit when the first qubit is in the state $|1\rangle$ and the green arrow depicts the evolution of the second qubit when the first qubit is in the state $|0\rangle$. The total waiting time shown is $\frac{1}{2J}$ seconds. Note that the green arrow is below the red arrow for the first two images of the Bloch sphere.

can in a sense be thought of as a controlled frequency shift. This controlled frequency shift is what can be regulated, with the use of Pauli gates, to implement a CNOT. This process is depicted using the Bloch sphere representation in Fig. 2.5. The exact sequence of pulses for this evolution is [56]

$$U_{CNOT} = \sqrt{i}R_Z^1\left(\frac{\pi}{2}\right)R_Z^2\left(\frac{-\pi}{2}\right)R_X^2\left(\frac{\pi}{2}\right)U\left(\frac{1}{2J}\right)R_Y^2\left(\frac{\pi}{2}\right) \qquad (2.18)$$

where $R_A^n(m)$ is a rotation of m radians, along the A axis on qubit n and $U(t)$ is the evolution under the J-coupling for t seconds. The constant $\sqrt{i}$ is commonly included for mathematical equivalence, but is a global phase which can be ignored when applying the pulse sequence (when applying U_{CNOT} is conjugation $\sqrt{i}\sqrt{i}^\dagger = 1$). As well, in NMR experiments the single qubit Pauli Z rotations is not applied. In practise the pulse sequence can be designed using Pauli Z gates, but then commutation relations are used to move the application of all the Pauli Z gates to the beginning of the experiment after the pps is prepared. Since a Pauli Z gate has no effect on the pps it can then be effectively ignored.

Thus, the single qubit Pauli gates and the CNOT gate can be implemented on an NMR QIP. Since these gates form a universal quantum gate set, an NMR QIP can perform any unitary evolution and thus any quantum computation.

2.2.4   Measurement

The fourth criteria for a QIP is a qubit-specific measurement capability. As we briefly mentioned before, this is done by measuring the induced current from the changing magnetic field of the ensemble of spins. The ensemble of spins will have a net magnetic moment pointing along $\hat{z}$ when first placed in the spectrometer. This net magnetic moment is then rotated into the x-y plane where it proceeds to precess around $\hat{z}$. According to Faraday's law, this changing magnetic can induce a current. This current is detected by coils placed around the sample. The current is measured along the $\hat{x}$ axis to determine the magnetization $M_x(t)$ and along the $\hat{y}$ axis to determine the magnetization $M_y(t)$. These two signals are then combined into a complex function $M(t) = M_x(t) + iM_y(t)$ which is delivered to a classical computer.

As mentioned in section 2.2.1, the transversal magnetization is represented in the density matrix by the coherence terms. As the name may suggest, the coherence terms reflects the degree of alignment of the precessing spins. The greater this alignment is the greater will be the net magnetization. Zero coherence, for example, would mean that the transverse components of the spin are completely out of phase with one another. Algebraically the magnetizations are given as

$$M_x = 4\text{Re}(\rho_-)/\mathcal{B} \tag{2.19}$$
$$M_y = 4\text{Im}(\rho_-)/\mathcal{B} \tag{2.20}$$

The magnetization along the $\hat{z}$ can not be measured by the spectrometer but can be determined by the density matrix

$$M_z = 2(\rho_0 - \rho_1)/\mathcal{B} \tag{2.21}$$

However, these magnetizations are not static values. The offset frequency, Ω_l, is the difference between the precession frequency of the nuclei ω_l and the rotating frame of reference ω_{ref}. In the absence of any relaxation M_z will remain constant and M_x and M_y will vary with Ω_l. The magnetizations as functions of time are then given as

$$M_x(t) = M_x \cos(\Omega_l t) - M_y \sin(\Omega_l t) \tag{2.22}$$
$$M_y(t) = M_x \sin(\Omega_l t) + M_y \cos(\Omega_l t) \tag{2.23}$$
$$M_z(t) = M_z \tag{2.24}$$

in the absence of decoherence. However, due to fluctuations in the magnetic field the magnetizations will decohere with time, as we will discuss further in the proceeding subsection.

This decoherence is why the measured signal is not a continual sinusoid but one which dampens to zero with time. This decaying signal is known as the *free induction decay* (FID). The signal of the FID is difficult to interpret when viewed from the time domain since most FID will consist of multiple signals from different qubits. To interpret the data, the different frequencies are distinguished by taking the Fourier transform of the signal.

Determining the final state of the qubits is done through a process of tomography. Once an experiment is completed the signal is, as mentioned before, measured along the $\hat{x}$ and $\hat{y}$ axis. The information from this signal is sufficient to determine the Pauli X and Y components of a one qubit experiments, the Pauli XI, YI, XZ, YZ components of a two qubit experiment and so on and so forth for higher order experiments.[3] To determine the other components of the density matrix, the experiment must be repeated but with some additional pulses at the end of the experiment. These pulses will rotate other components of the signal into the detectable frame. For example to determine the ZI term in a two-qubit experiment, one would run the experiment and then apply a 90° rotation along the Y axis to rotate the ZI component into the XI component. Thus when now measuring the final signal, what is measured as the XI terms is in fact the desired ZI term from the experiment.

Determining expectation values of operators from raw data

We will consider an example of determining the expectation values of operators from the raw data to help illustrate the measurement process that was described. For this example, we will consider the process of measuring the pseudo-pure state for a two qubit heteronuclear sample (we choose to work with a heteronuclear sample so that the first and second qubits are observed separately). Recall that for a two-qubit sample the pps is given by

$$\rho_{pps} = \frac{1 - \epsilon}{4} II + \epsilon(ZI + IZ + ZZ) \tag{2.25}$$

Furthermore, we explained that the identity term is neither effected by the applied RF pulses nor does it produce a detectable signal and as such can be effectively ignored. It is this form of the density matrix, called the *reduced density matrix*, which we consider experimentally. For this example it is given by:

$$\rho_{pps}^{R} = ZI + IZ + ZZ \tag{2.26}$$

---

[3]Consider an n qubit experiments where the signal is being measured on the lth qubit. The Pauli matrix terms consisting of an X or Y on the lth qubit along with any other combination of I and Z on other qubits can be observed.
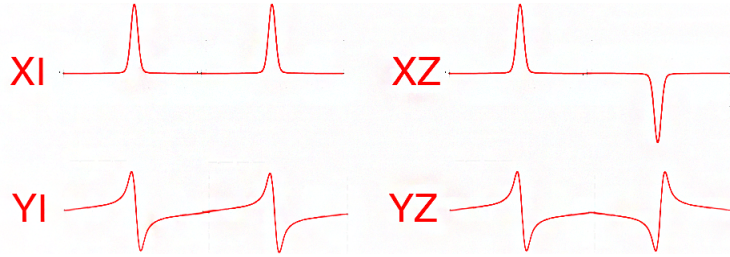
Figure 2.6: The NMR spectra for the XI, XZ, YI and YZ components of the signal. These four shapes provide a basis for all two-qubit NMR spectra.

For our example, we will assume that we have implemented a pulse sequence which we expect produces the state ρ^R_{pps} and would like to verify this. After we apply the pulse sequence, the NMR coils will detect the FID which will then undergo a Fourier transform to produce the NMR spectra we observe. This spectra will consist of two distinct peaks for this example. The peaks in NMR spectra are, ideally, in a Lorentzian shape, but will in practise have some Gaussian component due to the noise. We now need to interpret what reduced density matrix the peaks we observe correspond to.

Since it is only the magnetization in the $x - y$ plane that is measured, we will only see the XI, XZ, YI and YZ components of the signal if we are looking at the first channel (*i.e.* looking at the first qubit). These four components each have a distinct shape which is given in Figure 2.6. All other components of the reduced density matrix will produce no signal when the first qubit is being observed. These four spectra shapes form a basis for all two-qubit NMR spectra. Once an NMR spectra is taken from the spectrometer, it is then run through some software which fits the shape of the spectra to a linear combination of the shape of the XI, XZ, YI and YZ spectra. Two examples of this are provided in Figure 2.7. Since such a code can only provide relative values, a certain spectra must first be used as a reference in which to scale the outputs from all other spectra. This is most commonly done with the *pps* state.

To perform the full tomography, the experiment must be run multiples times with different components of the final signal being rotated into the $x - y$ plane in each run. For example we would run the sequence for the pps once and apply no final pulses and as such we would expect to see no signal. By fitting that spectra with our software we would return that the components $XI = 0$, $XZ = 0$, $YI = 0$ and $YZ = 0$. We could then run the sequence again, but apply a $Y(\pi/2)$ pulse at the end of the experiment to rotate the components $ZI \to XI$, $ZZ \to XZ$ and leave the YI and YZ components unchanged. We

Figure 2.7: An example of two spectra decomposed into linear combinations of the XI, YI, XZ ans YZ spectra. The first spectra is equal to $XI + XZ$ while the second spectra is equal to $\frac{1}{2}XZ + \frac{3}{4}YI$.

would then expect to our software to return the values of $XI = 1$, $XZ = 1$, $YI = 0$ and $YZ = 0$ (this is the first example given in Figure 2.7). We would then continue with this procedure until we have determined every one of the 16 two qubit Pauli matrices and thus recreated out full density matrix.

2.2.5   Decoherence

As soon as quantum system is initialized it will begin to lose quantum information to the environment. This process is called decoherence. The decoherence time needs to be sufficiently long so that meaningful computations can be performed before too much information is lost to the environment.

In an NMR experiment the quantum information is stored in the samples magnetization in the transversal plane. This magnetization gradually decreases due to the relaxation of the sample back to thermal equilibrium. As such the primary source of decoherence in NMR is the relaxation of the transversal magnetization. This relaxation occurs due to fluctuations in the magnetic field [57]. Fluctuations exist in the magnetic field for a number of reasons, including changes in temperature which effect the spectrometer, different magnetic impurities or the presence of other magnetic fields.

These fluctuations will cause two forms of relaxation. The first is longitudinal relaxation, which causes the magnetization of the ensemble of spins to gradually realign with $\hat{z}$ (see Fig. 2.8). The rate of this relaxation is known as the T_1 relaxation. The second
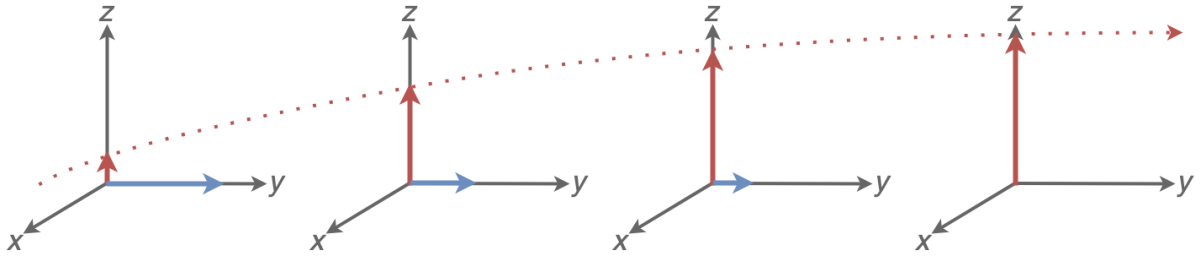
Figure 2.8: With time the magnetization of the sample will realign with the external magnetic field. As this realignment occurs the magnetization in the $x - y$ plane, and thus the signal, is lost.

form of relaxation is the transversal relaxation. Fluctuations in the magnetization along the z axis cause the individual nuclei to precess faster or slower in the $x - y$ plane. As such the spin of the individual nuclei become gradually out of phase with one another. As a result the net magnetization in the $x - y$ plane decreases (see Fig. 2.9). The rate of this relaxation is known as the T_2 relaxation.

The overall effect of T_1 and T_2 relaxation is a decrease of M_x and M_y and a corresponding increase of M_z. This is given mathematically as

$$M_x(t) = (M_x \cos(\Omega_0 t) - M_y \sin(\Omega_0 t))e^{-\tau/T_2} \tag{2.27}$$

$$M_y(t) = (M_x \sin(\Omega_0 t) + M_y \cos(\Omega_0 t))e^{-\tau/T_2} \tag{2.28}$$

$$M_z(t) = (M_z - 1)e^{-\tau/T_1} + 1 \tag{2.29}$$
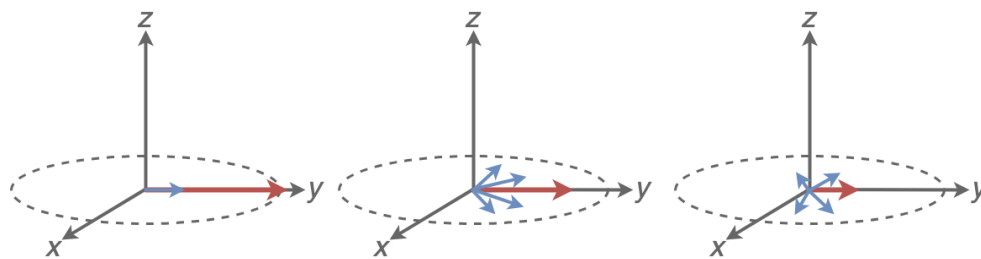
Figure 2.9: Fluctuation in the magnetic field will cause the spins of the individual nuclei to precess at different rates. As the individual nuclei gradually fall out of phase with one another the net magnetic moment will decrease and the signal will be lost.

Chapter 3

Violation of an augmented set of Leggett-Garg inequalities

3.1   The augmented set of Leggett-Garg inequalities

Despite years of experimental tests of the LGIs, the question of conditions for MR that are both necessary and sufficient has been addressed only recently [6, 7, 8, 9]. The LG framework was designed in close parallel to tests of local realism using the Bell and CHSH inequalities [21]. There, Fine's theorem [25] ensures that the Bell and CHSH inequalities are both necessary and sufficient conditions for local realism. The LG framework differs at this point since Fine's theorem does not immediately apply and as a consequence the usual three-time LGIs are only necessary conditions for MR and not sufficient ones. The difference arises from the fact that, for pairs of measurements acting sequentially in time, the so-called "no- signalling in time" (NSIT) conditions

$$p_j(s_j) = \sum_{s_i} p_{ij}(s_i, s_j) \tag{3.1}$$

do not hold in general. Here $p_{ij}(s_i, s_j)$, the *two-time probability*, is the probability of obtaining the results s_i and s_j when measurements are made at times t_i, t_j, respectively. As well, $p_j(s_j)$ is the single time probability for obtaining the result s_j at time t_j in which no earlier measurement is made. By contrast in Bell tests the analogous conditions to the NSIT ones are ensured by locality. As a consequence, pairwise probabilities of the form $p_{12}(s_1, s_2)$, for example, are not in general compatible with the probabilities $p_{23}(s_2, s_3)$ on

their overlap. This means that Fine's theorem, which seeks an underlying joint probability matching a *compatible* set of marginals, does not immediately apply.

In the current literature there are two different approaches to address this shortcoming. One involves a set of NSIT conditions of the form of Eq.(3.1) (and generalizations to three times) which simply restricts the parameter space to situations in which such conditions are satisfied [6, 7]. These are quite strong conditions which, in quantum mechanics, require zero interference. The other approach, which remains close to the original LG framework, adopts an indirect procedure for determining the two-time probabilities in which the averages $\langle Q_i \rangle$, $\langle Q_j \rangle$ and the correlation function C_{ij} are determined, non-invasively, in three separate experiments [8, 9]. They may then be assembled into a two-time probability if and only if the following two-time LGIs (LG2s) hold:

$$1 + s_i\langle Q_i \rangle + s_j\langle Q_j \rangle + s_is_jC_{ij} \geq 0 \tag{3.2}$$

for $i, j \in \{1, 2, 3\}, i \neq j$. For a derivation of the LG2s see [8, 9]. These twelve conditions are clearly much weaker than the NSIT conditions and in quantum mechanics require only suitable bounds on the degree of interference. The two-time probabilities themselves $p(s_i, s_j)$ are then given by the left-hand side of this expression, multiplied by $\frac{1}{4}$. The indirect measurement procedure ensures that different two-time probabilities determined in this way are then compatible with each other (and so satisfy NSIT in a formal sense, but this does not say anything about signaling) and Fine's theorem then applies. We thus obtain a set of necessary and sufficient conditions for MR consisting of the four original LG3s augmented with the twelve LG2s, Eq.(3.2). In this work, we experimentally test the definition of MR using these augmented LGIs.

3.1.1 Two regimes of interest

The augmented LGI framework consists of four regimes, depending on whether each of the LG2s and LG3s are, or are not, satisfied. It could be of interest to explore all four regimes but here we will consider the two most interesting cases. The first is the case in which the LG3s are satisfied but the LG2s are violated. This is a new regime compared to the original LG framework and detects MR violations which are not detected by the LG3s alone. The second is the case in which the LG2s are satisfied but the LG3s are violated. This is a natural parallel to the Bell case, in which the situation "looks classical" for the partial snapshots consisting of the pairwise measurements, but the violation of MR is only apparent when one looks for an underlying three-time probability.

Experiments	LG3s	LG2s	INM
Previous tests	✘		✔
First set	✔	✘	✔
Second set	✘	✔	✔

Table 3.1: An overview of the the sets of experiments described in Section 3.1.1. The checkmarks and crosses indicate whether the inequalities are satisfied or violated. All the experiments achieve non-invasiveness by implementing the INM protocol.

Experimental tests of the LGIs to date have consisted of finding violations of the LG3s. In this chapter we carry out two sets of experiments which explore the two aforementioned regimes of greatest interest. In both sets of experiments the non-invasiveness of the measurement is accomplished by using the current benchmark technique of ideal negative measurements. A comparison of the two sets of experiments which are performed in this chapter with the previously studied cases is provided in Table 3.1.

First set of experiments

As mentioned, the goal of the first set of experiments is to demonstrate a violation of the LG2s while the LG3s are satisfied. We will first consider the requirement of satisfying the LG3s. As was shown in Fig. 1.8, for the case of equidistant time intervals, the LG3s will only be satisfied for $\omega t = n\frac{\pi}{2}$ for $n \in \mathbb{Z}$. Furthermore, even for the case of non-equidistant time intervals, the LG3s will still only be satisfied for discrete values of ωt. Thus, to experimentally satisfy the LG3s we will require a means of widening the range of values of ωt in which the LG3s are satisfied.

As shown by Athalye et al [58], this may be accomplished by taking advantage of the small amount of decoherence naturally present in the system due to the unavoidable interactions with the surroundings. The decoherence dampens the magnitude of the correlation functions with time as shown in Fig. 3.1. This will in turn dampen the LG3s (Eq.(1.61) and (1.62)) as shown in Fig. 3.2. This gradual dampening leads to progressively larger ranges of ωt, centred around multiples of $\omega t = \frac{\pi}{2}$, in which the LG3s are satisfied (above the LGI bound). The next question is then – Does there exist parameters in these ranges of ωt in which the LG2s can still be violated even when accounting for the effect of the decoherence on the LG2s?
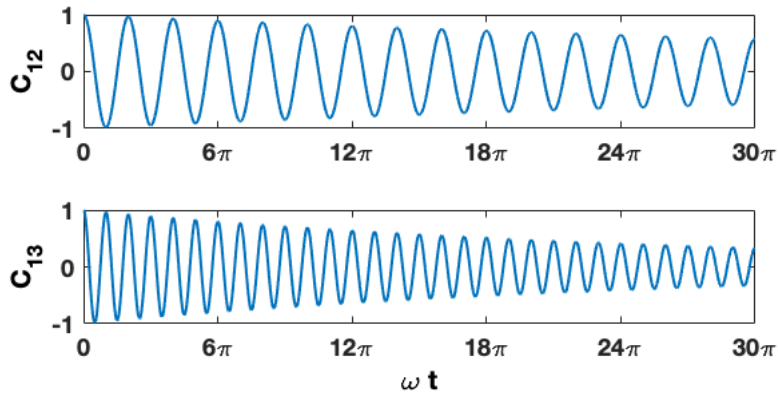
Figure 3.1: A simulation of the effect of the decoherence on the correlation functions as a function of ωt.
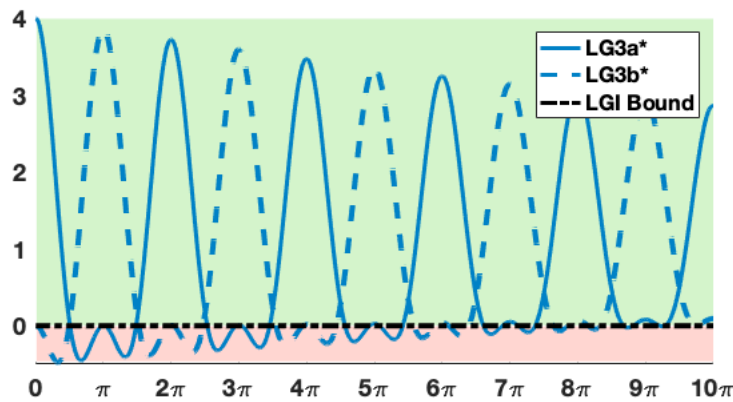
Figure 3.2: Eq.(1.61) and (1.62) are plotted with the dampening effect of the decoherence. As ωt increase the LG3s gradually have larger regions in which they exist above the LGI bound. The decoherence in this figure is exaggerated for clarity. The $*$ is to indicate that these are not the same as the LG3s defined earlier, since they also include the effect of the decoherence.
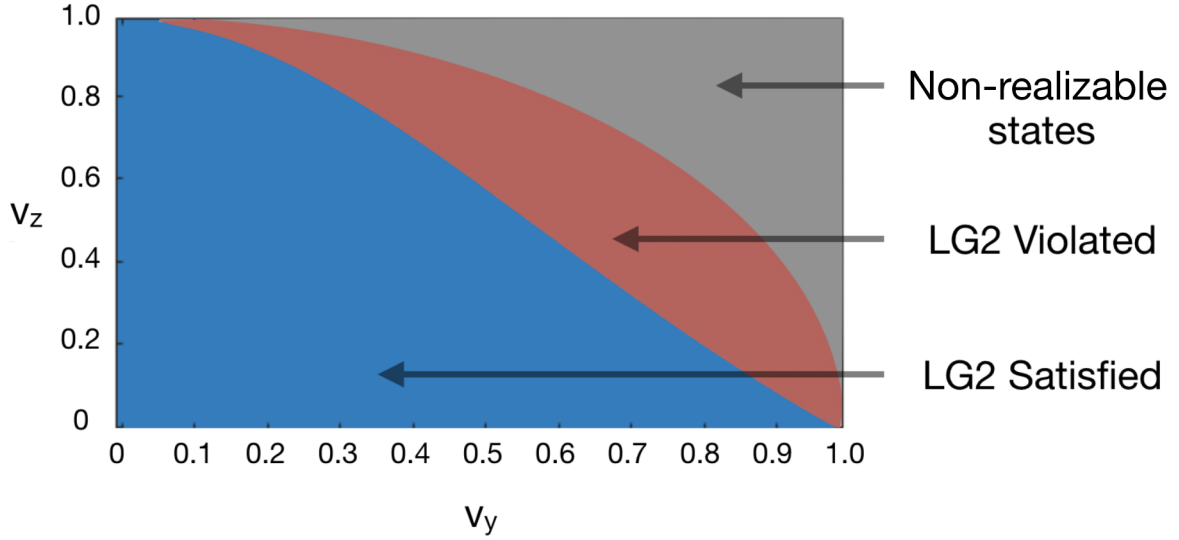
Figure 3.3: The results of a search over the values of v_y, v_z (from Eqn. 3.6) for which the LG2s are, or are not, satisfied for $\omega t = \pi/2$. Since the Pauli vector is bound by 1 ($v_y^2 + v_z^2 \leq 1$) there exists a region in the figure which represent non-realizable states.

Unlike the LG3s, the LG2s also depend on the initial state, $\rho = \frac{1}{2}(I + \vec{v} \cdot \vec{\sigma})$, in addition to the value of ωt. This is due to the LG2s (Eq.(3.2)) being functions of $\langle Q_i \rangle$. For our spin model the $\langle Q_i \rangle$ is equal to

$$\langle Q_i \rangle = \text{tr}\big[e^{iHt_i} Z e^{-iHt_i} \rho\big] \tag{3.3}$$

$$= \text{tr}\big[Z e^{-i\omega t_i X} \rho\big] \tag{3.4}$$

$$= \text{tr}\big[(\cos(\omega t_i)Z + \sin(\omega t_i)Y)\frac{1}{2}(I + \vec{v} \cdot \vec{\sigma})\big] \tag{3.5}$$

$$= v_z \cos(\omega t_i) + v_y \sin(\omega t_i) \tag{3.6}$$

Thus, for any choice of ωt one can search over all possible initial states to find parameters in which the LG2s are satisfied. The results of such a search for $\omega t = \pi/2$ are presented in Fig. 3.3. Of the possible initial states generated from such a search, we choose one which is experimentally simple to prepare. The state ρ_1 satisfied these criteria:

$$\rho_1 = \frac{1}{2}\Big(I + \frac{Y}{\sqrt{2}} + \frac{Z}{\sqrt{2}}\Big) \tag{3.7}$$

Having chosen an initial state ρ_1 and $\omega t = \pi/2$, the effect of the decoherence on the
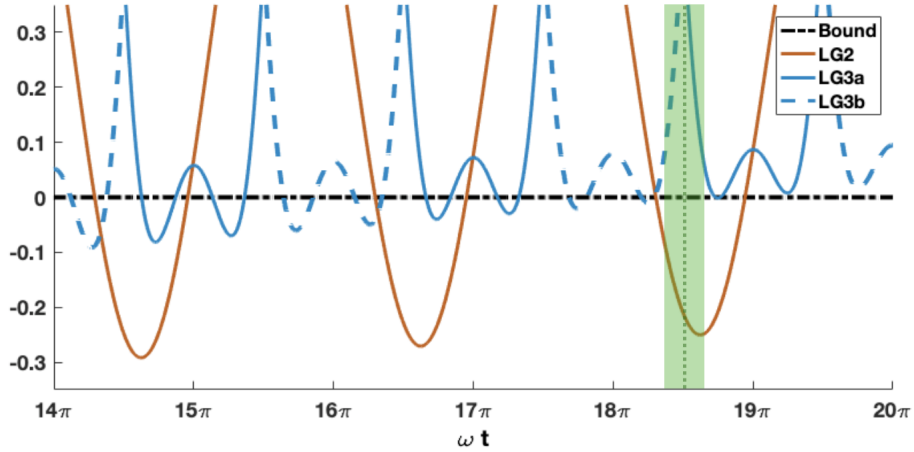
Figure 3.4: One of the twelve LG2s and the LG3s (Eq.(1.61) and (1.62)) are plotted as functions of ωt with the effect of the decoherence. The figure shows that there exists a region of ωt in which at least one of the LG2s is violated (exists below the bound) while the LG3s are satisfied (exist above the bound). This figure uses the same decoherence parameter as Fig. 3.2.

LG2s and the LG3s can be simulated [59]. A segment of the results of such a simulation are provided in Fig. 3.4. Fig. 3.4 depicts the existence of a regime in which the LG2s are violated (exist below the LGI bound) and the LG3s are satisfied (exist above the bound). In this work we use a delay of 0.1s between each measurement interval to achieve the desired dampening effect (which is approximately one eighth of the T_2 time of 0.76s). The details of how this is achieved is provided in Section 3.2.

Second set of experiments

The goal of the second set of experiments is to demonstrate a violation of the LG3s while the LG2s are satisfied. As discussed, the LG3s are always violated except for discrete choices of ωt. Of the possible values of ωt available to us we will choose $\omega t = 3\pi/10$. This value is chosen for reasons which will be made clear in Ch. 4. As was done for the previous set of experiments, a search is performed over the possible values of v_y, v_z to find the regions in which the LG2s are satisfied. Again, for experimental ease we will select one that can be prepared from the pseudo-pure state with a single pulse.

$$\rho_2 = \frac{1}{2}\Big(I + (0.951)X + (0.309)Z\Big) \tag{3.8}$$

54

This choice of initial state and ωt will provide a set of initial conditions which will violate the LG3s and satisfy the LG2s as desired.

3.2 Experimental design

All the experiments performed in this work are carried out at 298K on a Bruker DRX spectrometer with a nominal ^{1}H frequency of 700 MHZ. The NMR sample consisted of ^{13}C-chloforom dissolved in acetone to produce a heteronuclear two-spin system. The ^{1}H was used as the ancilla qubit and the ^{13} C was used as the primary qubit. Both spins were placed on resonance so that the Hamiltonian consisted of only the spin-spin coupling which has a value of 215.15 Hz. The measured relaxation times were $T_1 = 7.91$s and $T_2 = 0.76$s for ^1H and $T_1 = 8.51$s and $T_2 = 1.10$s for ^{13}C. An inter-scan delay of 90s was used to ensure that the spins began each experiment close to their thermal state.

3.2.1 Ideal negative measurements

In both sets of experiments the measurements are done by using the INM protocol. In the INM protocol the ancilla is coupled to only one of the two measurement outcomes. If an experiment is performed and the ancilla changes states, then those measurements are discarded. If the ancilla does not change states then it can be inferred that the system was in the orthogonal space and those results are kept. This entire procedure is then repeated with the ancilla being coupled to the other measurement outcome. This protocol thus provides a macroscopic argument for the system-ancilla interaction not being a potential source of invasiveness.

Before describing the full details of the INM, we first consider a general qubit that is evolving in time and is measured by Z at times t_i, t_j. This system begins in some initial state ρ at time 0 and evolves freely for time t_i. The state ρ at time t_i can be written generally as

$$\rho_i = \begin{bmatrix} a & b \\ b^* & 1\text{-}a \end{bmatrix} \tag{3.9}$$

where a is real, b is complex and $a^2 + |b|^2 \leq 1$ (with the equality for a pure state). At this time the first measurement of Z is conducted and the states $|0\rangle$ and $|1\rangle$ will be returned with probabilities a and $(1\text{-}a)$ respectively. Once the measurement is completed the state will update to $|0\rangle \langle 0|$ or $|1\rangle \langle 1|$ depending on the measured out come. The system then
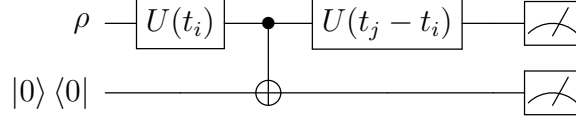
Figure 3.5: The quantum circuit used for implementing the INM protocol. The evolutions $U(t_i) = e^{-iHt_i}$ and $U(t_j - t_i) = e^{-iH(t_j-t_i)}$ behave exactly as defined in Section 3.2.1.

evolves freely again until time t_j. This second evolution can be written generally as the mapping between states

$$|0\rangle \langle 0| \to \begin{bmatrix} a' & b' \\ b'^* & 1\text{-}a' \end{bmatrix}, \quad |1\rangle \langle 1| \to \begin{bmatrix} a'' & b'' \\ b''^* & 1\text{-}a'' \end{bmatrix}$$

At this point the second measurement of Z is conducted. If the measurement outcome at t_i was $|0\rangle$ then the states $|0\rangle$ and $|1\rangle$ will be returned at t_j with probabilities a' and $(1\text{-}a')$ respectively. If the measurement outcome at t_i was $|1\rangle$ then the states $|0\rangle$ and $|1\rangle$ will be returned at t_j with probabilities a'' and $(1\text{-}a'')$ respectively. Thus the two-times probabilities $p_{12}(s_i, s_j)$ for all possible measurements are equal to

$$\begin{aligned} p_{12}(+,+) &= aa', & p_{12}(+,-) &= a(1\text{-}a') \\ p_{12}(-,+) &= (1\text{-}a)a'', & p_{12}(-,-) &= (1\text{-}a)(1\text{-}a'') \end{aligned}$$

and, using Eq.(1.41), the correlation function can be written as

$$C_{ij} = aa' - a(1\text{-}a') - (1\text{-}a)a'' + (1\text{-}a)(1\text{-}a'') \tag{3.10}$$

The diagonal entries of the final output of the circuit in Fig. 3.5 is precisely equal to $aa', a(1\text{-}a'), (1\text{-}a)a''$ and $(1\text{-}a)(1\text{-}a'')$. Thus a single measurement of these diagonal entries can be done to determine C_{ij}.

Proof. Begin with an initial system that is evolving in time, coupled to the ancilla which is in the state $|0\rangle \langle 0|$. After evolving for some time t_i this system is in the state

$$\rho_1 = U(t_i)\rho U(t_i)^\dagger \otimes |0\rangle \langle 0| \tag{3.11}$$

$$= \begin{bmatrix} a & b \\ b^* & (1-a) \end{bmatrix} \otimes |0\rangle \langle 0| \tag{3.12}$$

$$= \begin{bmatrix} a & 0 & b & 0 \\ 0 & 0 & 0 & 0 \\ b^* & 0 & 1-a & 0 \\ 0 & 0 & 0 & 0 \end{bmatrix} \tag{3.13}$$

the system then undergoes a CNOT

$$\rho_2 = \text{CNOT}\rho_1\text{CNOT}^\dagger \tag{3.14}$$

$$= \begin{bmatrix} a & 0 & 0 & b \\ 0 & 0 & 0 & 0 \\ 0 & 0 & 0 & 0 \\ b^* & 0 & 0 & 1-a \end{bmatrix} \tag{3.15}$$

before evolving again for time $t_j - t_i$. Written most generally this evolution maps

$$\begin{bmatrix} 1 & 0 \\ 0 & 0 \end{bmatrix} \to \begin{bmatrix} a' & b' \\ b'^* & (1-a') \end{bmatrix}, \quad \begin{bmatrix} 0 & 0 \\ 0 & 1 \end{bmatrix} \to \begin{bmatrix} a'' & b'' \\ b''^* & (1-a'') \end{bmatrix}$$

The evolution of the states $|0\rangle\langle 1|$ and $|1\rangle\langle 0|$ will not effect the outcome of the diagonal elements, so we will drop these terms here. The evolution $U(t_j - t_i)$ will thus map the diagonal elements of ρ_2 to ρ_3 as

$$\rho_2 = \begin{bmatrix} 1 & 0 \\ 0 & 0 \end{bmatrix} \otimes \begin{bmatrix} a & 0 \\ 0 & 0 \end{bmatrix} + \begin{bmatrix} 0 & 0 \\ 0 & 1 \end{bmatrix} \otimes \begin{bmatrix} 0 & 0 \\ 0 & (1-a) \end{bmatrix} \tag{3.16}$$

$$\rho_3 = \begin{bmatrix} a' & b' \\ b'^* & (1-a') \end{bmatrix} \otimes \begin{bmatrix} a & 0 \\ 0 & 0 \end{bmatrix} + \begin{bmatrix} a'' & b'' \\ b''^* & (1-a'') \end{bmatrix} \otimes \begin{bmatrix} 0 & 0 \\ 0 & (1-a) \end{bmatrix} \tag{3.17}$$

Which again, by considering just the diagonal terms becomes

$$\rho_3 = \begin{bmatrix} aa' & 0 & 0 & 0 \\ 0 & a(1-a') & 0 & 0 \\ 0 & 0 & (1-a)a'' & 0 \\ 0 & 0 & 0 & (1-a)(1-a'') \end{bmatrix} \tag{3.18}$$

Thus, the diagonal terms of the final state from Fig. 3.5 are equivalent to the two-time probabilities required to determine the correlations C_{ij}. $\square$

This procedure to measure C_{ij} can be modified to implement the INM protocol. From a macro-realistic perspective the primary system in Fig. 3.5 would be completely undisturbed before being measured, were it not for the potential interactions with the CNOT gate. However, from this perspective the ancilla does not interact with the CNOT gate if the primary system is in the state $|0\rangle$. Therefore, to implement a non-invasive protocol the experiment is run twice. Once the experiment is run with the CNOT gate and only the results in which the primary system was in the state $|0\rangle$ are kept ($p_{12}(+, +)$ and $p_{12}(+, -)$). Then the experiment is run again with an anti-CNOT gate and only the results where the primary system was in the state $|1\rangle$ are kept ($p_{12}(-, +)$ and $p_{12}(-, -)$). Together these two experiments provide all the information necessary to determine C_{ij}. The numerical result from this measurement procedure matches the theoretical result of $C_{ij} = \cos(\omega(t_j - t_i))$ for the simple spin model.

57

Proof. We again consider our simple spin model, where the primary system evolves according to $H = \omega X/2$ and so $U(t_i) = e^{-i\omega X t_i/2}$. We will first consider the CNOT circuit. At time t_i the system exists in the general state

$$\rho(t_i) \otimes \begin{bmatrix} 1 & 0 \\ 0 & 0 \end{bmatrix} = \begin{bmatrix} a & b \\ b^* & (1-a) \end{bmatrix} \otimes \begin{bmatrix} 1 & 0 \\ 0 & 0 \end{bmatrix} \tag{3.19}$$

the initial state then undergoes the CNOT evolution to arrive at the state.

$$\rho_2 = \text{CNOT}(\rho(t_i) \otimes \begin{bmatrix} 1 & 0 \\ 0 & 0 \end{bmatrix})\text{CNOT}^\dagger = \begin{bmatrix} a & 0 & 0 & b \\ 0 & 0 & 0 & 0 \\ 0 & 0 & 0 & 0 \\ b^* & 0 & 0 & 1-a \end{bmatrix} \tag{3.20}$$

the system then, from time $t_j - t_i \equiv t$, undergoes the evolution

$$U(t) \otimes I = e^{-i\omega X t/2} \otimes I \tag{3.21}$$

$$= \cos\left(\frac{\omega t}{2}\right) II - i\sin\left(\frac{\omega t}{2}\right) XI \tag{3.22}$$

to arrive at the state ρ_3 $(c \equiv \cos\left(\frac{\omega t}{2}\right),\ s \equiv \sin\left(\frac{\omega t}{2}\right))$

$$\rho_3 = \begin{bmatrix} c & 0 & -is & 0 \\ 0 & c & 0 & -is \\ -is & 0 & c & 0 \\ 0 & -is & 0 & c \end{bmatrix} \begin{bmatrix} a & 0 & 0 & b \\ 0 & 0 & 0 & 0 \\ 0 & 0 & 0 & 0 \\ b^* & 0 & 0 & 1-a \end{bmatrix} \begin{bmatrix} c & 0 & is & 0 \\ 0 & c & 0 & is \\ is & 0 & c & 0 \\ 0 & is & 0 & c \end{bmatrix} \tag{3.23}$$

$$= \begin{bmatrix} ac^2 & ibcs & iacs & bc^2 \\ -ib^*cs & -(a-1)s^2 & b^*s^2 & i(a-1)cs \\ -iacs & bs^2 & as^2 & -ibcs \\ b^*c^2 & -i(a-1)cs & ib^*cs & -(a-1)c^2 \end{bmatrix} \tag{3.24}$$

and by measuring the diagonal terms we find

$$p(+,+) = ac^2, \quad p(+,-) = (1-a)s^2$$
$$p(-,+) = as^2, \quad p(-,-) = (1-a)c^2$$

Since these values were determined using the CNOT circuit, to satisfy the INM protocol, only the $p(+,+)$ and $p(+,-)$ results can be kept. It is easy to show that these calculations can be repeated with the anti-CNOT circuit to find

$$\rho_3 = \begin{bmatrix} c & 0 & -is & 0 \\ 0 & c & 0 & -is \\ -is & 0 & c & 0 \\ 0 & -is & 0 & c \end{bmatrix} \begin{bmatrix} 0 & 0 & 0 & 0 \\ 0 & a & b & 0 \\ 0 & b^* & (1-a) & 0 \\ 0 & 0 & 0 & 0 \end{bmatrix} \begin{bmatrix} c & 0 & is & 0 \\ 0 & c & 0 & is \\ is & 0 & c & 0 \\ 0 & is & 0 & c \end{bmatrix} \tag{3.25}$$

$$= \begin{bmatrix} -(a-1)s^2 & -ib^*cs & i(a-1)cs & b^*s^2 \\ ibcs & ac^2 & bc^2 & iacs \\ -i(a-1)cs & b^*c^2 & -(a-1)c^2 & ib^*cs \\ bs^2 & -iacs & -ibcs & as^2 \end{bmatrix} \tag{3.26}$$

and by measuring the diagonal terms we find

$$p(+,+) = ac^2, \quad p(+,-) = (1-a)s^2$$
$$p(-,+) = as^2, \quad p(-,-) = (1-a)c^2$$

Since these values were determined using the anti-CNOT circuit, to satisfy the INM protocol, only the $p(-,+)$ and $p(-,-)$ results can be kept. Thus the correlation function is

$$C_{ij} = p(++) - p(+-) - p(-+) + p(--) \tag{3.27}$$
$$= ac^2 - (1-a)s^2 - as^2 + (1-a)c^2 \tag{3.28}$$
$$= c^2 - s^2 \tag{3.29}$$
$$= \cos\left(\frac{\omega t}{2}\right)^2 - \sin\left(\frac{\omega t}{2}\right)^2 \tag{3.30}$$
$$= \cos(\omega t) \tag{3.31}$$
$$= \cos(\omega(t_j - t_i)) \tag{3.32}$$

Thus providing the expected theoretical value for C_{ij}. $\qquad\qquad\blacksquare$

It may seem counter-intuitive that the correlations do not depend on the systems initial state, but the temporal correlations are essentially a measure of the likelihood of a system having changed states between the two measurements and thus the correlations do not require information on the systems exact state.

3.2.2 Pulse sequence components

In this subsection we will outline the pulse sequences for the two sets of experiments. In total, this will consist of sixteen different pulse sequences that are each composed of a combination of twenty to thirty different individual pulses, free evolutions and gradients. We will first group together different pulse sequences into components and label these components according to their function. We will then use these components to construct pulse sequences which are easier to interpret.

In all the pulse sequences in this work $X(n)$ and $Y(n)$ depict rotations of n radians around the X and Y axis ($X(n) = e^{-iX\frac{n}{2}}$ and $Y(n) = e^{-iY\frac{n}{2}}$). $ZZ(n)$ depicts the free evolution of the system that will provide an n radian rotation of ZZ ($ZZ(n) = e^{-iZZ\frac{n}{4}}$). For some experiments we will be implementing a free evolution for much longer periods of time for the purpose of increasing the decoherence experienced. We will use $D(\tau)$ to denote
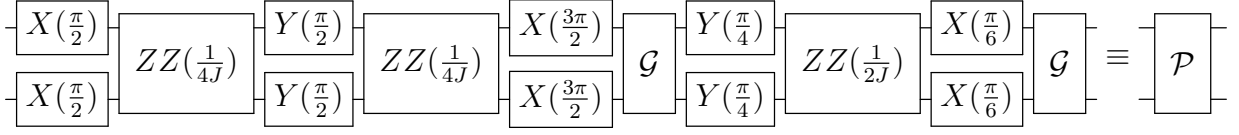
Figure 3.6: A pulse sequence for producing the pseudo-pure state. The full sequence will be defined as $\mathcal{P}$.

the implementation of these kinds of delays for times τ. Lastly, we use $\mathcal{G}$ to represent the application of a gradient.

The first component of each experiment will be a pulse sequence for preparing the pseudo-pure state (pps) [49, 50]. The pps is the analog of the $|0\rangle^{\otimes n}$ state for NMR experiments. The pulse sequence used to prepare the pps in this work is given in Fig. 3.6 and we define this component as $\mathcal{P}$.

Preparing the pps is the first step in preparing our desired initial states. Recall that the initial states for these experiments were chosen so that they could be prepared from the pps with a single pulse. Preparing the state ρ_1 (Eq.(3.7)), for the first set of experiments, requires preparing the pps and then performing a $X(\frac{-\pi}{4})$ rotation, we define this entire procedure as:

$$\mathcal{P}_1 \equiv (\mathcal{P})(X(\tfrac{-\pi}{4}) \otimes I) \tag{3.33}$$

Likewise, preparing the state ρ_2 (Eq.(3.8)), for the second set of experiments, requires preparing the pps and then performing a $Y(\frac{2\pi}{5})$, we define this entire procedure as:

$$\mathcal{P}_2 \equiv (\mathcal{P})(Y(\tfrac{2\pi}{5}) \otimes I) \tag{3.34}$$

Thus the components $\mathcal{P}_1$ and $\mathcal{P}_2$ represent the full preparation procedures for the first and second set of experiments respectively.

The implementation of the INM protocol itself broadly consists of two components. The first is the CNOT and anti-CNOT gates. The pulse sequence used to implement the CNOT in this work is given in Fig. 3.7 and we define this component as U_c. The anti-CNOT can be performed by implementing U_c with a preceding and succeeding $X(\pi)$ on the first qubit. We define this sequence for implementing the anti-CNOT as:

$$U_{ac} \equiv (X(\pi) \otimes I)(U_c)(X(\pi) \otimes I) \tag{3.35}$$

The second component for the INM protocol consists of the evolution of the system between measurements. For a system with a Hamiltonian $H = \omega X$ being measured at equidistant
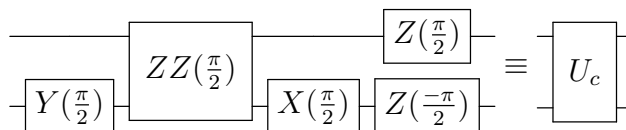
Figure 3.7: A pulse sequence for implementing the CNOT gate in NMR. The full sequence will be defined as U_c.
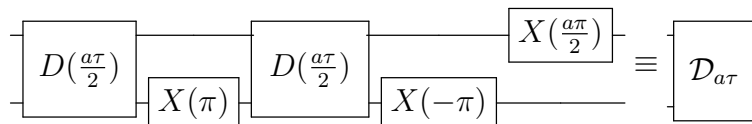
Figure 3.8: A pulse sequence for implementing the time delay while undoing the effect of the J-coupling. $D(\frac{a\tau}{2})$ depict waiting for time $\frac{a\tau}{2}$. The full sequence will be refereed to as $\mathcal{D}_{a\tau}$.

time intervals the system will undergo a $X(\omega t)$ or $X(2\omega t)$ evolution between measurements. These evolutions can be implemented with a single Pauli rotation and this is how these evolutions are implemented in the second set of experiments. However, in the first set of experiments we also require the system to experience the effect of the decoherence as well during the evolution between measurements. This is done by first implementing a time delay. During the time delay the system will also evolve according to its natural Hamiltonian. Since both spins are placed on resonance this natural Hamiltonian will consist of only the j-coupling term. We undo the effect of the j-coupling through the use of π-pulses. Once the decoherence is implemented, for a time τ, in this fashion then a Pauli rotation can be done to implement the $X(\omega t)$ or $X(2\omega t)$ evolution. This entire component is depicted in Fig. (3.8) and is labelled as $\mathcal{D}_{a\tau}$.

3.2.3 First set of experiments

The first set of experiments (which look for violations of LG2 with LG3s satisfied) consists of nine pulse sequences which are depicted in in Fig. 3.9. In experiments 1-3 the initial state is prepared and the system is evolved for different times before being measured. These measurements are used to determine $\langle Q_i \rangle$. The remaining experiments come in pairs, 4-5, 6-7 and 8-9. These experiments are used to determine the correlations. In each pair of experiments the measurement is done once with a CNOT gate and then once with an anti-CNOT gate. These measurements are done for the three different combinations of time
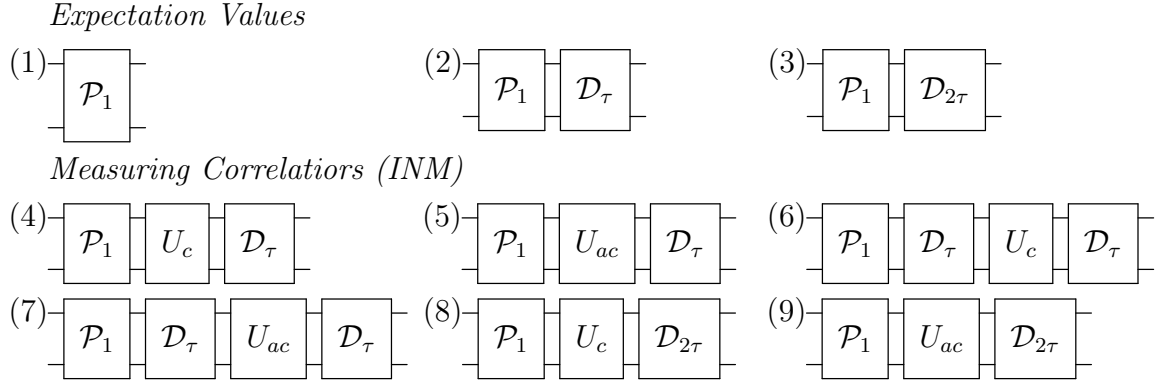
Figure 3.9: The first set of experiments. Experiments 1-3 are used to measure the values of $\langle Q_i \rangle$ and experiments 4-9 are used to measure the values of C_{ij} using the INM protocol. The pulse sequence components, as defined in Section 3.2.2, having the following functions, $\mathcal{P}_1$: preparing the state $\rho_1 = \frac{1}{2}(I + \frac{Y}{\sqrt{2}} + \frac{Z}{\sqrt{2}})$, $\mathcal{D}_{\alpha\tau}$: implementing a time delay for time $\alpha\tau$ ($\alpha \in \{1,2\}$, and $\tau = 0.1$s) followed by a rotation of $\alpha\pi/2$ around the X axis, U_C: implementing a CNOT gate, U_{ac}: implementing an anti-CNOT gate.

intervals. For these experiments both the system and the ancilla are measured. This two qubit measurement is used to determine C_{ij} as outlined in Section 3.2.1.

3.2.4 Second set of experiments

The second set of experiments (which looks for violations of LG3 with LG2s satisfied) consists of the nine pulse sequence depicted in Fig. 3.10. The logic for which experiments are used to determine $\langle Q_i \rangle$ and C_{ij} follows exactly from the first set of experiments.

3.3 Experimental results

The experimental data from the first and second sets of experiments is provided in Table 3.2. The results from these two tables is used to calculate the values of $\langle Q_i \rangle$ and C_{ij}, which are provided in Table 3.3. These tables also include two simulated values for comparison. The ideal simulations use ideal pulses, assume no natural decoherence, no noise and no imperfections. The noisy simulations account for the added effect of the systems Hamiltonian

Expectation Values

(10) $\boxed{\mathcal{P}_2}$

(11) $\boxed{\mathcal{P}_2}$ $\boxed{X(\frac{3\pi}{10})}$

(12) $\boxed{\mathcal{P}_2}$ $\boxed{X(\frac{6\pi}{10})}$

Measuring Correlatiors (INM)

(13) $\boxed{\mathcal{P}_2}$ $\boxed{U_c}$ $\boxed{X(\frac{3\pi}{10})}$

(14) $\boxed{\mathcal{P}_2}$ $\boxed{U_{ac}}$ $\boxed{X(\frac{3\pi}{10})}$

(15) $\boxed{\mathcal{P}_2}$ $\boxed{X(\frac{3\pi}{10})}$ $\boxed{U_c}$ $\boxed{X(\frac{3\pi}{10})}$

(16) $\boxed{\mathcal{P}_2}$ $\boxed{X(\frac{3\pi}{10})}$ $\boxed{U_{ac}}$ $\boxed{X(\frac{3\pi}{10})}$

(17) $\boxed{\mathcal{P}_2}$ $\boxed{U_c}$ $\boxed{X(\frac{6\pi}{10})}$

(18) $\boxed{\mathcal{P}_2}$ $\boxed{U_{ac}}$ $\boxed{X(\frac{6\pi}{10})}$
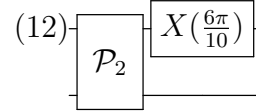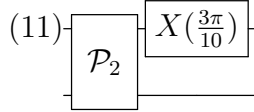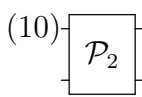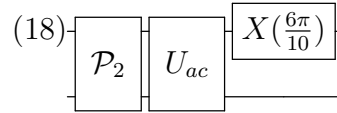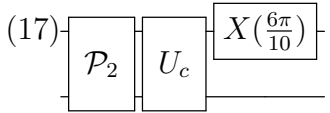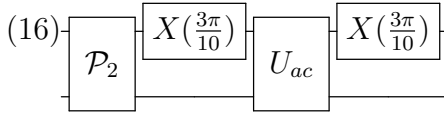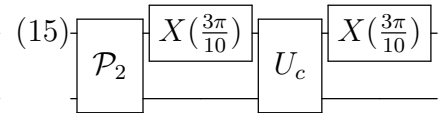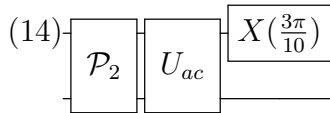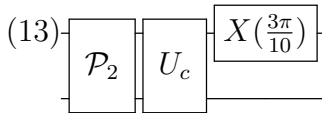
Figure 3.10: The second set of experiments. Experiments 10-12 are used to measure the values of $\langle Q_i \rangle$ and experiments 13-18 are used to measure the values of C_{ij} using the INM protocol. The pulse sequence components, as defined in Section 3.2.2, having the following functions, $\mathcal{P}_1$: preparing the state $\rho_1 = \frac{1}{2}(I + \frac{Y}{\sqrt{2}} + \frac{Z}{\sqrt{2}})$, X_θ: applying a rotation of θ around the X axis $(e^{-iX\frac{\theta}{2}})$, U_C: implementing a CNOT gate, U_{ac}: implementing an anti-CNOT gate.

	I	N	E		I	N	E
	First set of experiments				Second set of experiments		
(1)	0.8536	0.8494	0.8443 ± 0.01	(10)	0.6546	0.6527	0.6484 ± 0.01
	0.1464	0.1506	0.1557 ± 0.01		0.3455	0.3473	0.3516 ± 0.01
(2)	0.7267	0.7240	0.7144 ± 0.01	(11)	0.5908	0.5899	0.5892 ± 0.01
	0.2733	0.2760	0.2856 ± 0.01		0.4092	0.4101	0.4107 ± 0.01
(3)	0.1961	0.1997	0.2122 ± 0.01	(12)	0.4523	0.4558	0.4692 ± 0.01
	0.8039	0.8003	0.7878 ± 0.01		0.5477	0.5442	0.5307 ± 0.01
(4)	0.4149	0.4136	0.4326 ± 0.01	(13)	0.5196	0.5188	0.4828 ± 0.01
	0.0861	0.0896	0.0872 ± 0.01		0.0712	0.0708	0.0981 ± 0.01
	0.4139	0.4125	0.4025 ± 0.01		0.1349	0.1361	0.1771 ± 0.01
	0.0861	0.0844	0.0867 ± 0.01		0.2743	0.2742	0.2420 ± 0.01
(5)	0.0861	0.0869	0.0817 ± 0.01	(14)	0.0712	0.0708	0.1057 ± 0.01
	0.4139	0.4122	0.3906 ± 0.01		0.5196	0.5188	0.4560 ± 0.01
	0.0861	0.0868	0.0918 ± 0.01		0.2743	0.2743	0.3119 ± 0.01
	0.4139	0.4140	0.4359 ± 0.01		0.1349	0.1361	0.1264 ± 0.01
(6)	0.3551	0.3567	0.3840 ± 0.01	(15)	0.4690	0.1638	0.1875 ± 0.01
	0.1449	0.1460	0.1156 ± 0.01		0.0843	0.1655	0.1874 ± 0.01
	0.3551	0.3550	0.3892 ± 0.01		0.1218	0.0415	0.0562 ± 0.01
	0.1449	0.1423	0.1112 ± 0.01		0.3248	0.6292	0.5687 ± 0.01
(7)	0.1449	0.1468	0.1617 ± 0.01	(16)	0.0843	0.1655	0.2163 ± 0.01
	0.3551	0.3584	0.3267 ± 0.01		0.4690	0.1639	0.1431 ± 0.01
	0.1449	0.1411	0.1346 ± 0.01		0.3248	0.6292	0.6010 ± 0.01
	0.3551	0.3537	0.3770 ± 0.01		0.1218	0.0414	0.0395 ± 0.01
(8)	0.0351	0.0403	0.0157 ± 0.01	(17)	0.2261	0.2267	0.2199 ± 0.01
	0.1610	0.1589	0.1284 ± 0.01		0.2261	0.2260	0.2582 ± 0.01
	0.7687	0.7662	0.7761 ± 0.01		0.4284	0.4282	0.4021 ± 0.01
	0.0351	0.0336	0.0797 ± 0.01		0.1194	0.1191	0.1194 ± 0.01
(9)	0.1610	0.1633	0.1034 ± 0.01	(18)	0.2261	0.2260	0.2447 ± 0.01
	0.0351	0.0373	0.0416 ± 0.01		0.2261	0.2268	0.1802 ± 0.01
	0.0351	0.0303	0.0673 ± 0.01		0.1194	0.1191	0.1619 ± 0.01
	0.7687	0.7691	0.7877 ± 0.01		0.4284	0.4281	0.4133 ± 0.01

Table 3.2: The experimental data from the first and second set of experiments. The diagonal elements of the first qubits density matrix are recorded for experiments 1-3 and 10-12. The diagonal elements of the two qubit density matrix are recorded for experiments 4-9 and 13-18 (Ideal simulated (I), Noisy simulated (S) Experimentally determined (E)).

when pulses are being applied and also approximate the effect of the natural decoherence of the system.

For each experiment in Table 3.2 either two or four values are record. For the experiments which are used to determine the expectation values (experiments 1-3 and 10-12) only two values are recorded. These are the two diagonal elements of the first qubits density matrix. These values alone are sufficient for determining $\langle Q_i \rangle$. This can be seen by considering the expectation value for a general state $\rho(t_i) = \left[\begin{smallmatrix} a & b \\ b^* & (1-a) \end{smallmatrix} \right]$

$$\langle Q_i \rangle = \text{tr}(Z\rho(t_i)) \tag{3.36}$$

$$= \text{tr}(Z\left[\begin{smallmatrix} a & b \\ b^* & (1-a) \end{smallmatrix} \right]) \tag{3.37}$$

$$= 2a - 1 \tag{3.38}$$

On the other hand, four values were records for experiments 4-9 and 13-18. This is because these experiments were used to determine the values of the correlators. These four values are the diagonal elements of the full two-qubit density matrix. As was shown in Section 3.2.1, only these values are necessary for determining the correlators when using the INM protocol.

The measured values of $\langle Q_i \rangle$ and C_{ij} from Table 3.3 were then used to determined the LG2s and LG3s for the two sets of experiments. The numerical results for the LG2s and LG3s are provided for the first and second set of experiments in Tables 3.4 and 3.5, respectively. The LG2s and LG3s for the two sets of experiments are also plotted, side by side, in Fig. 3.11.

The key points of the experimental results are as follows: As seen in Table 3.4 and Fig. 3.11, in the first set of experiments the LG3s (labelled 3.1 - 3.4) were all satisfied and two of the LG2s (2.4 and 2.6) were violated. The violation of 2.4 is much more significant than that of 2.6 and since we only require one LG2 to be violated, we will focus on 2.4 as the violation of the LG2s. Furthermore, as seen in Table 3.5 and again in Fig. 3.11, for the seconds set of experiments the LG2s (labelled 2.1 - 2.12) were all satisfied and one of the LG3s (3.2) was violated.

3.3.1 Error bars

The error bars on the experimentally determined values for the experiments performed in this work were determined by considering two potential sources of error, the first source being from the calibration of the pulses. Note that the degree of rotation from an NMR pulse depends on the power of the pulse and the length of its duration. The calibration

	I	N	E
First Set of Experiments			
Expectation values			
$\langle Q_1 \rangle$	0.7071	0.6988	0.6886 ± 0.02
$\langle Q_2 \rangle$	0.4534	0.4480	0.4288 ± 0.02
$\langle Q_3 \rangle$	-0.6077	-0.6006	-0.5757 ± 0.02
Correlators (INM)			
C_{12}	0.0000	-0.0032	-0.0077 ± 0.02
C_{23}	0.0000	-0.0019	-0.0076 ± 0.02
C_{13}	-0.8595	-0.8582	-0.8331 ± 0.02
Second Set of Experiments			
Expectation values			
$\langle Q_1 \rangle$	0.3090	0.3054	0.2967 ± 0.02
$\langle Q_2 \rangle$	0.1816	0.1798	0.1787 ± 0.02
$\langle Q_3 \rangle$	-0.0955	-0.0884	-0.0615 ± 0.02
Correlators (INM)			
C_{12}	0.5878	0.5862	0.5703 ± 0.03
C_{23}	0.5878	0.5862	0.5615 ± 0.02
C_{13}	-0.3090	-0.3083	-0.2901 ± 0.02

Table 3.3: The values of $\langle Q_i \rangle$ and C_{ij} and calculated from the data from the first and second set of experiments (Table 3.2) as outlined in Section 3.3 (Ideal simulated (I), Noisy simulated (S) Experimentally determined (E)).

First Set of Experiments				
Label	Inequality	I	N	E
2.1	$1 + \langle Q_1 \rangle + \langle Q_2 \rangle + C_{12} \geq 0$	2.161	2.144	2.110 ± 0.03
2.2	$1 - \langle Q_1 \rangle + \langle Q_2 \rangle - C_{12} \geq 0$	0.746	0.752	0.748 ± 0.03
2.3	$1 + \langle Q_1 \rangle - \langle Q_2 \rangle - C_{12} \geq 0$	1.254	1.254	1.268 ± 0.03
2.4	$1 - \langle Q_1 \rangle - \langle Q_2 \rangle + C_{12} \geq 0$	-0.161	-0.150	-0.125 ± 0.03
2.5	$1 + \langle Q_2 \rangle + \langle Q_3 \rangle + C_{23} \geq 0$	0.846	0.846	0.846 ± 0.03
2.6	$1 - \langle Q_2 \rangle + \langle Q_3 \rangle - C_{23} \geq 0$	-0.061	-0.047	-0.003 ± 0.03
2.7	$1 + \langle Q_2 \rangle - \langle Q_3 \rangle - C_{23} \geq 0$	2.061	2.051	2.021 ± 0.03
2.8	$1 - \langle Q_2 \rangle - \langle Q_3 \rangle + C_{23} \geq 0$	1.154	1.151	1.139 ± 0.03
2.9	$1 + \langle Q_1 \rangle + \langle Q_3 \rangle + C_{13} \geq 0$	0.240	0.240	0.280 ± 0.03
2.10	$1 - \langle Q_1 \rangle + \langle Q_3 \rangle - C_{13} \geq 0$	0.545	0.559	0.569 ± 0.03
2.11	$1 + \langle Q_1 \rangle - \langle Q_3 \rangle - C_{13} \geq 0$	3.174	3.158	3.097 ± 0.03
2.12	$1 - \langle Q_1 \rangle - \langle Q_3 \rangle + C_{13} \geq 0$	0.041	0.044	0.054 ± 0.03
3.1	$1 + C_{12} + C_{23} + C_{13} \geq 0$	0.141	0.135	0.152 ± 0.04
3.2	$1 - C_{12} - C_{23} + C_{13} \geq 0$	0.141	0.148	0.182 ± 0.04
3.3	$1 + C_{12} - C_{23} - C_{13} \geq 0$	1.860	1.858	1.833 ± 0.04
3.4	$1 - C_{12} + C_{23} - C_{13} \geq 0$	1.860	1.858	1.833 ± 0.04

Table 3.4: The values of the LG2s and LG3s constructed from the first set of experiments. The labels in green highlight which inequalities were satisfied and the labels in red highlight which were violated. (Ideal simulated (I), Noisy simulated (S) Experimentally determined (E)).

Second Set of Experiments				
Label	Inequality	I	N	E
2.1	$1 + \langle Q_1 \rangle + \langle Q_2 \rangle + C_{12} \geq 0$	2.078	2.071	2.046 ± 0.04
2.2	$1 - \langle Q_1 \rangle + \langle Q_2 \rangle - C_{12} \geq 0$	0.285	0.288	0.312 ± 0.04
2.3	$1 + \langle Q_1 \rangle - \langle Q_2 \rangle - C_{12} \geq 0$	0.540	0.539	0.548 ± 0.04
2.4	$1 - \langle Q_1 \rangle - \langle Q_2 \rangle + C_{12} \geq 0$	1.097	1.101	1.095 ± 0.04
2.5	$1 + \langle Q_2 \rangle + \langle Q_3 \rangle + C_{23} \geq 0$	1.674	1.678	1.679 ± 0.03
2.6	$1 - \langle Q_2 \rangle + \langle Q_3 \rangle - C_{23} \geq 0$	0.135	0.146	0.198 ± 0.03
2.7	$1 + \langle Q_2 \rangle - \langle Q_3 \rangle - C_{23} \geq 0$	0.689	0.682	0.679 ± 0.03
2.8	$1 - \langle Q_2 \rangle - \langle Q_3 \rangle + C_{23} \geq 0$	1.502	1.495	1.444 ± 0.03
2.9	$1 + \langle Q_1 \rangle + \langle Q_3 \rangle + C_{13} \geq 0$	0.905	0.909	0.945 ± 0.03
2.10	$1 - \langle Q_1 \rangle + \langle Q_3 \rangle - C_{13} \geq 0$	0.905	0.915	0.932 ± 0.03
2.11	$1 + \langle Q_1 \rangle - \langle Q_3 \rangle - C_{13} \geq 0$	1.714	1.702	1.648 ± 0.03
2.12	$1 - \langle Q_1 \rangle - \langle Q_3 \rangle + C_{13} \geq 0$	0.478	0.475	0.475 ± 0.03
3.1	$1 + C_{12} + C_{23} + C_{13} \geq 0$	1.867	1.864	1.842 ± 0.04
3.2	$1 - C_{12} - C_{23} + C_{13} \geq 0$	-0.485	-0.481	-0.422 ± 0.04
3.3	$1 + C_{12} - C_{23} - C_{13} \geq 0$	1.309	1.308	1.299 ± 0.04
3.4	$1 - C_{12} + C_{23} - C_{13} \geq 0$	1.309	1.308	1.281 ± 0.04

Table 3.5: The values of the LG2s and LG3s constructed from the second set of experiments. The labels in green highlight which inequalities were satisfied and the labels in red highlight which were violated. (Ideal simulated (I), Noisy simulated (S) Experimentally determined (E)).
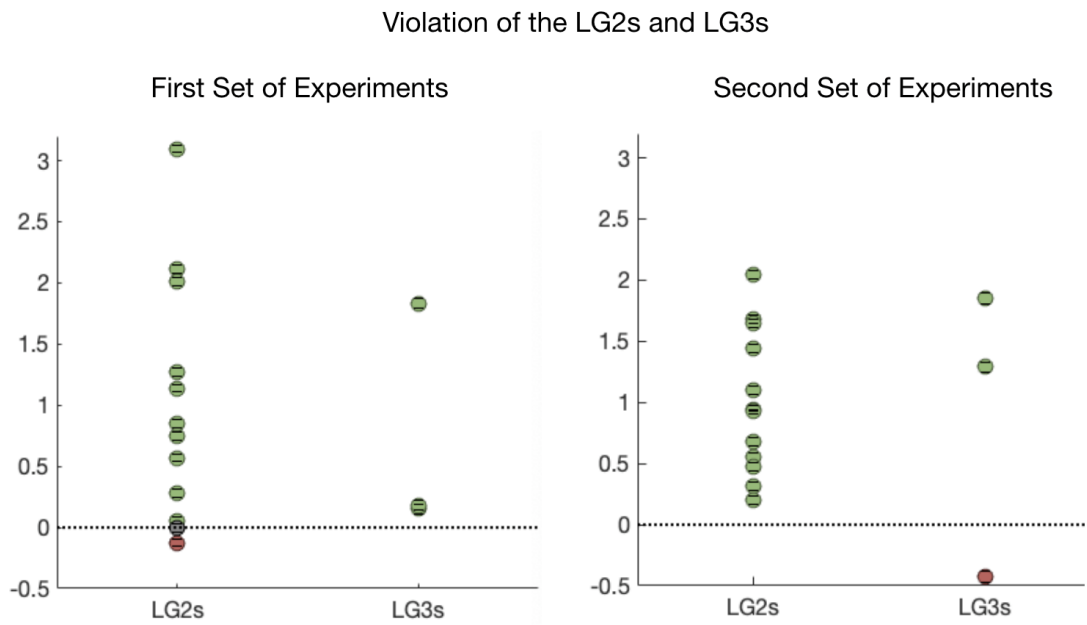
Figure 3.11: The values of the LG2s and LG3s constructed from the first and second set of experiments with their corresponding error bars. The labels in green highlight which inequalities were satisfied and the labels in red highlight which were violated.
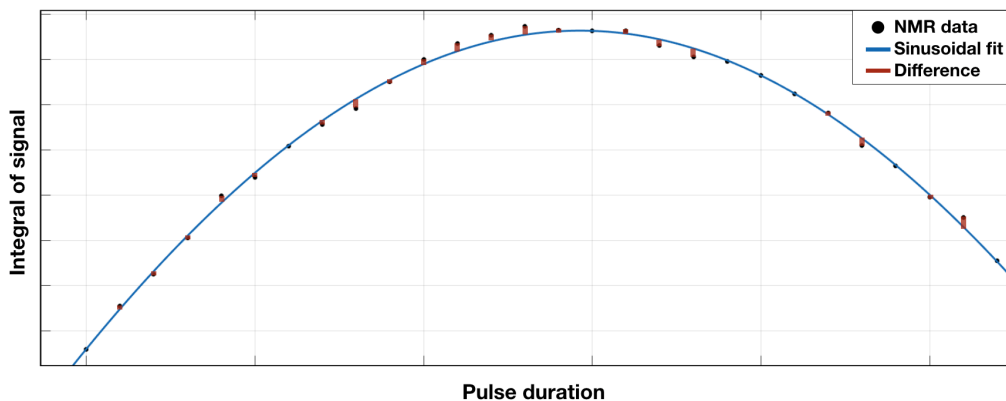
Figure 3.12: A visual aid for how the error on the calibration was determined. The strength of the signal from the NMR spectrometer is plotted as a function of the duration of the applied pulse, τ, and then fitted to the function $f(\tau) = a\cos(b\tau) + c$ to find the τ in which a π rotation occurrs. The difference between the experimental data and $f(\tau)$ is taken for each signal, this is depicted in red. These values were squared, summed and then square rooted to find the potential error from calibration.

procedure consisted of running forty experiments that each consisted of implementing two Y pulses on the thermal state. Each experiment used the same pulse power but varying pulse durations, τ, starting from $\tau = 0\mu s$. Furthermore, we note that the thermal state produces no signal, produces a maximum signal when rotated $\frac{\pi}{2}$ radians and produces again no signal when rotated π radians. Thus, as τ increases the signal reaches a maximum value before decreasing again to zero. The strength of the signal was plotted as a function of τ and then fitted to the function $f(\tau) = a\cos(b\tau) + c$ to find the τ in which a π rotation occurred (see blue fit in Figure 3.12). Since two pulses were implemented, this procedure provides a value of τ corresponding to a $\frac{\pi}{2}$ rotation. The difference between the experimental data and $f(\tau)$ was taken for each of the forty experiments (see the red bars in Figure 3.12). These values were squared, summed and then square rooted to find the potential error from calibration. The second source of error that was considered was from the noise of the signal. A band of data points which should ideally produce no signal were assessed. The square root of the sum of the squares of the data points in the band was calculated and divided by the total area of the signal to provide a percent error. This percent error was also incorporated into the error bars. The final source of error which was considered in this work was from the natural drift of the NMR spectrometers magnetic field through out consecutive experiments. Since the spectrometers magnetic field gradually drifts, periodic

70

breaks are taken between experiments to manually realign the magnetic field, a process known as *shimming*. To account for potential errors introduced from this the spectra for the pps state was taken between experiments to see the range of possible values the pps would take. This range of values was taken into account in the error bars on the data.

3.4 Conclusion

The purpose of this work in this chapter was to provide a more complete test of macroscopic realism using an augmented LG framework. To date, LGI experiments have tested a set of conditions for MR formulated entirely in terms of temporal correlation functions at three pairs of times. These conditions for MR are necessary but not sufficient. The augmented LG inequalities considered here include an additional set of two-time inequalities which also involve the averages, $\langle Q_i \rangle$, and lead to a set of conditions which are both necessary and sufficient. In this work we showed how these more decisive conditions for MR could be tested experimentally. We exhibited experimentally situations in which the LG2s were satisfied but the LG3s violated, a natural parallel to the Bell case. We also exhibited situations in which the LG3s were satisfied but the LG2s violated, the key case in which the original LG framework based solely on LG3s fails to pick up violations of MR.

Chapter 4

The implementation of a continuous in time velocity measurement

4.1 Continuous in time velocity measurements

A key requirement in all LGIs experiments is to adopt a macroscopically non-invasive measurement protocol. If the measurement protocol was deemed to be invasive it could then be argued that it was the effect of the measurement and not a failure of MR which caused the violation of the inequality [10, 11, 12]. The best one can hope to achieve in addressing this argument is to implement a measurement protocol whose argument for invasiveness would need to be so contrived that the alternative explanation of a violation of MR would be more likely. One strategy to treat this argument is to implement different measurement protocols that are constructed from different sets of assumptions. The agreement of the results from these different protocols will further strengthen either protocols argument for being non-invasive.

To advance this strategy we perform the first experimental implementation of the continuous in time velocity measurement (CTVM) protocol [13] and compare it with the current benchmark INM protocol. The CTVM and INM protocols are formulated on different sets of assumptions and thus provide different perspectives on non-invasiveness. The agreement on the outcome of the measured results from these two protocols will provide a much stronger argument for the non-invasiveness of either one. The implementation of CTVM protocol will thus be part of the third set of experiments done in this thesis. The comparison of these results will be made with the second set of experiments from Ch. 3. To be able to perform this comparison, we will use the same value of $\omega t = 3\pi/10$ and

Experiments	LG3s	LG2s	INM	CTVM
Previously tested	✘		✔	
Set 1	✔	✘	✔	
Set 2	✘	✔	✔	
Set 3	✘	✔		✔

Table 4.1: An overview of the goal of each set of experiments. The checkmarks indicate that the specified set of inequalities are all satisfied. The crosses indicate that the specified set of inequalities are violated. The checkmarks are also used to designate which measurement protocol is being implemented (either INM or CTVM).

the same initial state ρ_2 as was used in the second set of experiments. An overview of all experiments which have been discussed in this thesis are presented in Table 4.1.

4.1.1 Theoretical description

As mentioned, the CTVM protocol is constructed from a very different set of assumptions from those of the INM protocol. Common to most methods for measuring the correlation function is the need to conduct a pair of measurements at successive times. Such models carry the potential source of invasiveness from the earlier measurement affecting the later one. The CTVM protocol avoids this feature. It arose from the general observation that the correlation function depends only on whether Q takes the same sign or opposite signs at the initial and final times [60]. This in turn depends on how many sign changes $Q(t)$ makes during the given time interval. Of course it could change sign many times in general. However, we make the simplifying assumption that in the vast majority of histories, $Q(t)$ changes sign only once. This assumption may seem like a rather restrictive one, but it has been argued that there is in fact a regime in which this assumption is reasonable [13]. A single sign change can then be registered using a weakly coupled "waiting detector", which is designed to click if $Q(t)$ changes sign, but otherwise remains unchanged. Because this protocol involves just a single interaction at some (unknown) time during the given time interval, it is essentially non-invasive, since there are no later measurements to disturb. The only possible source of invasiveness is that the single interaction with the detector when Q changes sign may cause Q to change sign a second time and hence to interact with the detector a second time yielding a false detector result. However, as argued in Ref. [13],

for a weakly interacting detector, the probability for this happening is considerably smaller than the single click probability.

The waiting detector is readily modelled by assuming that the primary system may be assigned a velocity $v = \dot{Q}$ and then weakly coupling this to an ancilla with which it interacts continuously in time. It is readily shown that the ancilla then responds to the quantity

$$\int_{t_i}^{t_j} v(t)dt = Q_j - Q_i. \tag{4.1}$$

From this, the correlation function is then readily found from the formula,

$$\langle [Q_j - Q_i]^2 \rangle = 2(1 - C_{ij}) \tag{4.2}$$

The existence of a velocity is an assumption stronger than what is normally supposed in LG tests (which typically take a "black box" approach to the system and its dynamics as much as possible) but in practice LG tests are carried out on specific systems for which a velocity is readily identified. We will discuss the above two assumptions in more detail in what follows.

The quantum-mechanical implementation of such a protocol will require a Hamiltonian which reflects the characteristics outlined above. We consider the previously defined spin model with $\hat{H} = \omega X/2$ and operator $\hat{Q} = Z$. We also define a velocity operator $\dot{Q} = \omega Y$. The total system-detector Hamiltonian then for the system (S) and ancilla (A) is

$$H_D = \frac{\omega}{2} X_S \otimes I_A + \lambda \omega Y_S \otimes X_A \tag{4.3}$$

The first term represents the evolution under the desired Hamiltonian of the system, and the second term represents the coupling of the velocity operator with X on the second qubit, where λ corresponds to the strength of the coupling. The X gate acts as a flipping operator on the ancilla when the ancilla is in the Z basis. The ancilla will be initialized to the $+1$ eigenstate of Z ($|0\rangle$) that flips to the -1 eigenstate of Z ($|1\rangle$) when Q changes sign.

The value of C_{ij} can be extracted from the final value of the ancilla. First note that $H_D^2 = (\Omega^2/4)I$, where $\Omega = \omega\sqrt{1 + 4\lambda^2}$. From this it is easy to show that

$$e^{-iH_D t} = \cos\left(\frac{\Omega t}{2}\right)I - \frac{2i}{\Omega}\sin\left(\frac{\Omega t}{2}\right)H_D \tag{4.4}$$

The total state of the system at time t is then

$$|\Psi_t\rangle = e^{-iH_D t}(|\psi\rangle \otimes |0\rangle)$$

$$= \hat{A}_0(t)\,|+\rangle \otimes |0\rangle + \hat{A}_1(t)\,|+\rangle \otimes |1\rangle$$

for

$$\hat{A}_0(t) = \cos\left(\frac{\Omega t}{2}\right)I_S - \frac{i\omega}{\Omega}\sin\left(\frac{\Omega t}{2}\right)X_S \qquad (4.5)$$

$$\hat{A}_1(t) = -\frac{2i\lambda\omega}{\Omega}\sin\left(\frac{\Omega t}{2}\right)Y_S \qquad (4.6)$$

thus the probability of the ancilla being in the state $|1\rangle$ after a time t evolution is

$$p(1) = \langle+|\,\hat{A}_1(t)^\dagger \hat{A}_1(t)\,|+\rangle \qquad (4.7)$$

$$= \frac{2\lambda^2\omega^2}{\Omega^2}(1 - \cos(\Omega t)) \qquad (4.8)$$

For a sufficiently small λ

$$p(1) \approx 2\lambda^2(1 - \cos(\omega t)) \qquad (4.9)$$

$$= 2\lambda^2(1 - C_{12}) \qquad (4.10)$$

Thus, C_{ij} can be calculated with a single measurement that determines the probability of Q changing signs over the time interval $[t_i, t_j]$.

4.2 Experimental design

All the experiments performed in this chapter are carried out using the same experimental parameters described in Section 3.2.

4.2.1 Finding parameters

The successful implementation of the CTVM protocol will require selecting values of λ and ωt which satisfy these four criteria:

1. minimize the error from multiple sign changes of Q

2. justify the approximation made to determine C_{ij}

3. minimize the effect of the back action

4. produce a detectable signal

The first condition depends only on the choice of ωt, the second condition depends only on the choice of λ and the last two conditions will depend on both. Our objective in this section is to present a procedure which identifies initial conditions that suitably minimize the sources of error to faithfully implement the CTVM protocol.

Single sign change

Given that the LGIs are designed to rule out certain types of hidden variables models, we need to assess the assumption of a single sign change of Q from that perspective as well as from a quantum mechanical one. As shown in Ref. [13], in a simple hidden variable model, the value of $Q(t)$ is determined by the direction of a unit vector rotating around a single axis. Our system is evolving under the Hamiltonian $H = \omega X/2$, i.e. the vector representing the state is rotating with frequency ω around the x-axis. If the vector lies in the half of the hemisphere corresponding to $Q = +1$ then the vector can rotate into the opposite hemisphere but not come back out if the total time of the evolution is less than π/ω. Since the measurements are made at regular time intervals, t $(t_3 - t_2 = t_2 - t_1 = t)$, then the longest time which we require only one sign change to occur in is $2t$ (for when determining C_{13}). Thus in a simple hidden variable description of the system there will be a maximum of one sign change if $\omega t \leq \pi/2$.

Since we expect our system to conform to the laws of quantum mechanics, we can use a quantum model to determine the fraction of histories where Q will have two sign changes. By using $H = \omega X/2$, $Q = Z$ and defining the Z eigenstates by $|\pm\rangle$, the probability that Q takes values of $+1, -1, +1$ at times $0, t, 2t$ is

$$p_{123}(+, -, +) = |\langle +| e^{-iHt} |-\rangle|^2 |\langle -| e^{-iHt} |+\rangle|^2 \tag{4.11}$$

$$= \sin^4\left(\frac{\omega t}{2}\right) \tag{4.12}$$

and similarly the probability that Q takes the value of $+1$ at all times will be

$$p_{123}(+, +, +) = \cos^4\left(\frac{\omega t}{2}\right) \tag{4.13}$$

which gives the ratio of paths with two sign changes to those with none as

$$\frac{p_{123}(+, -, +)}{p_{123}(+, +, +)} = \tan^4\left(\frac{\omega t}{2}\right) \tag{4.14}$$

This probability is plotted as a function of ωt in Fig. 4.1.

76
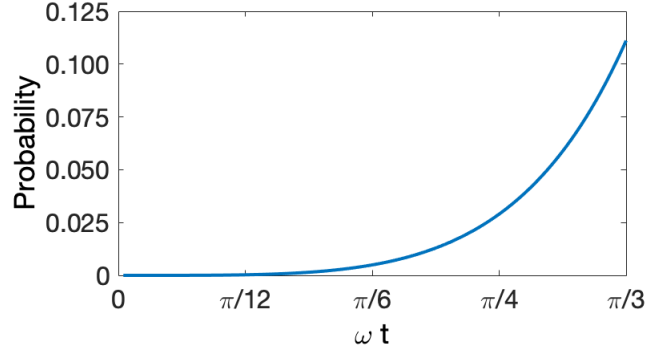
Figure 4.1: The probability of Q undergoing multiple sign changes as a function of ωt.

Justifying the C_{ij} approximation

In the derivation of the correlation functions an approxmation is necessarily made that

$$\sqrt{1 + 4\lambda^2} \approx 1 \tag{4.15}$$

The degree of the accuracy of this approximation can be considered as another probability of error. To stay true to the spirit of the CTVM protocol we will need to choose a λ for which this approximation is reasonable.

Minimizing back action

As mentioned before we must consider the potential effect of the back action from the ancilla on the system. Consider the probability that an experiment is conducted for time $2t$ where the expected result for the ancilla is $|1\rangle$ (*i.e.* one sign change) but due to the effect of back action the detected result is $|0\rangle$. The probability that the ancilla is in the state $|0\rangle \rightarrow |1\rangle \rightarrow |0\rangle$ at times $0, t, 2t$ follows from Eq.(4.5) to be

$$P_{|0\rangle \rightarrow |1\rangle \rightarrow |0\rangle} = \langle \psi | \, (\hat{A}_1(t)^\dagger \hat{A}_1(t))^2 \, |\psi\rangle \tag{4.16}$$

$$= 16\lambda^4 \sin^4\left(\frac{\omega t}{2}\right) \tag{4.17}$$

similarly the probability that the ancilla is in the state $|0\rangle \rightarrow |1\rangle \rightarrow |1\rangle$ at times $0, t, 2t$ is

$$P_{|0\rangle \rightarrow |1\rangle \rightarrow |1\rangle} = \langle \psi | \, (\hat{A}_0(t)^\dagger \hat{A}_1(t))^2 \, |\psi\rangle \tag{4.18}$$

77
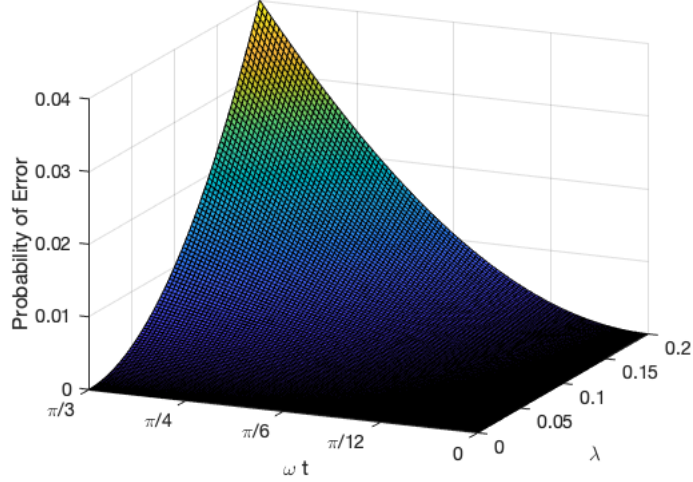
Figure 4.2: The probability of error from the back action of the ancilla on the system as a function of λ and ωt.

$$= 4\lambda^2 \sin^2\left(\frac{\omega t}{2}\right) \tag{4.19}$$

the ratio of these probabilities is

$$\frac{P_{|0\rangle \to |1\rangle \to |0\rangle}}{P_{|0\rangle \to |1\rangle \to |1\rangle}} = 4\lambda^2 \sin^2\left(\frac{\omega t}{2}\right) \tag{4.20}$$

This probability of error from the back action (Eq.(4.20)) is plotted as a function of λ and ωt in Fig. 4.2.

Producing a detectable signal

For the last two conditions that we considered it was most favourable to minimize λ to the furthest degree possible. Unfortunately, as λ decreases so to will the probability of measuring the value of $p(1)$ that is required for determining C_{ij}. If $p(1)$ is too small then it can not be accurately measured. The error on the measurement occurs on the third decimal place, so we will restrict $p(1) \geq 0.01$. Since experiments are conducted at both time t and $2t$ we need to consider two values of $p(1)$

$$p(1)_t = \langle 1|\left(\text{Tr}_1(e^{-iHt}\rho e^{iHt})\right)|1\rangle \tag{4.21}$$

78
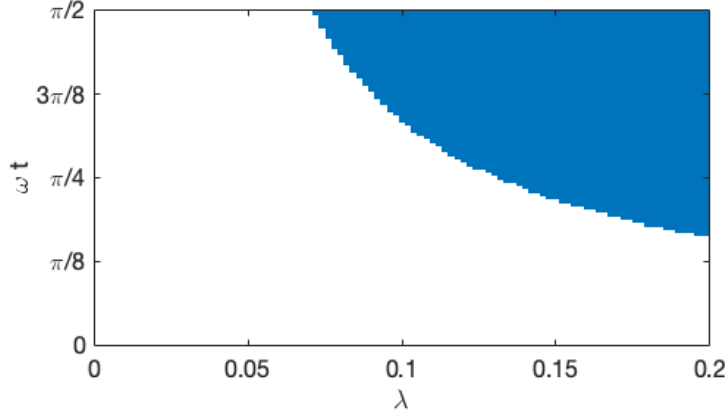
Figure 4.3: The values of λ and ωt for which the value of $p(1)$ from Eq.(4.21) is greater than 0.01 are highlighted in blue.

$$p(1)_{2t} = \langle 1| \left(\mathrm{Tr}_1(e^{-i2Ht} \rho e^{i2Ht}) \right) |1\rangle \tag{4.22}$$

It is easy to check algebraically that Eq.(4.21) is strictly less than Eq.(4.22). Intuitively this is also straightforward, since a longer time of coupling between the system and the ancilla can only lead to a greater probability of flipping the ancilla. Thus we only need to consider the lower bound on Eq.(4.21). The values of λ and ωt in which Eq.(4.21) is greater than zero are plotted in Fig. 4.3.

Chosen parameters

Our approach in addressing these different conditions was to first prioritize justifying the approximation from Eq.(4.15) to stay true to the spirit of the initial CTVM proposal. As shown in Fig. 4.3 as our choice of λ decreases our choice of ωt must subsequently increase to maintain having a detectable signal. Subsequently, as depicted in Fig. 4.1 our value of ωt can only increase so much before the error of multiple sign changes becomes too large. Lastly, as was mentioned the probability of error from the back action remains significantly smaller than the other sources of error for the range of ωt and λ which are feasible. With these considerations in mind we choose a $\lambda = 0.11$ and $\omega t = 3\pi/10$. This provides a probability of error from multiple sign changes of ≈ 0.067, a probability of error from the back action of ≈ 0.01, the approximation of $\sqrt{1 + 4\lambda^2} = 1$ being satisfied to with in .02 and the production of a detectable signal.

79

Figure 4.4: The effect of different values of λ on the LG3s.

4.2.2 Bounds on the violation
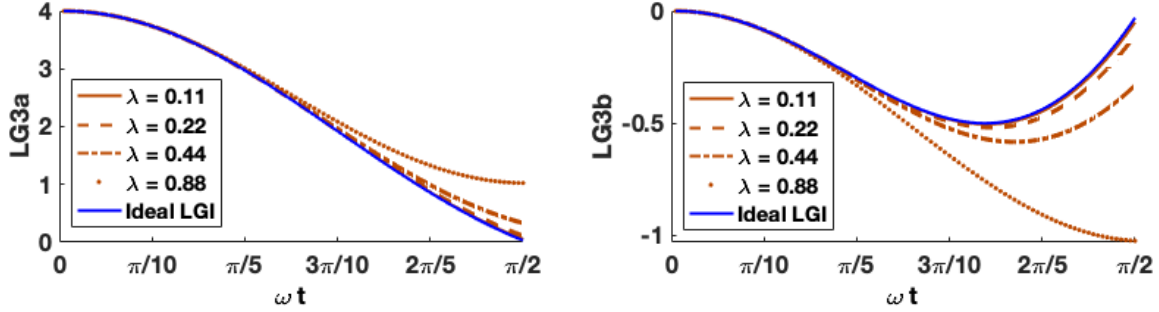
A final consideration that we must take is the effect of our choice of initial conditions on the LG3 violation. As noted, the derivation of the correlation functions with the CTVM protocol requires the approximation $\sqrt{1 + 4\lambda^2} \approx 1$. If this approximation does not hold exactly, then the theoretical values for C_{ij} from the CTVM protocol will differ to some extent from the ideal values of $C_{ij} = \cos(\omega t)$. The larger this difference is the greater of a violation of the LG3s we must have for the source of this violation to not be caused by the approximation. Fig. 4.4 compares the LG3s constructed using the ideal C_{ij} with those constructed using the theoretical correlation functions of the CTVM protocol for different choices of λ. For the first LG3 in Fig. 4.4 the greater values of λ create larger violations of the inequality but for the second LG3 the opposite is true. Thus, we only need to worry about potential violations coming from non-zero λ for the first case. For our choice of $\lambda = 0.11$ and $\omega t = 3\pi/10$ the LG3 is 0.0028 less than the ideal value. So to have a violation of the LG3s we will need to use a bound of -0.0028 instead of 0.

4.2.3 Pulse sequence components

As was done in the previous chapter, we will first group together different pulse sequences into components and label these components according to their function. We will then use these components to construct pulse sequences which are easier to interpret. In this chapter we will use the same notation defined in Section 3.2.2 for all of the individual pulses and gradients ($X(n)$, $Y(n)$, $ZZ(n)$, $\mathcal{G}$ and $\mathcal{D}$).

The CTVM protocol will require one of the components that was defined in the previous
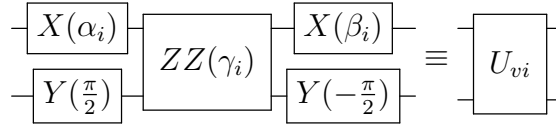
Figure 4.5: The pulse sequence used to implement the system-detector evolution. The parameters $\alpha_1 = 4.9751$, $\beta_1 = 1.8335$ and $\gamma_1 = 0.1035$ are used for implementing U_{v1} and the parameters $\alpha_2 = 5.2433$, $\beta_2 = 2.1018$ and $\gamma_2 = 0.1998$ are used for implementing U_{v2}.

x

set of experiments. Namely, it will require the state preparation procedure $\mathcal{P}_2$, for preparing the initial state ρ_2. Recall that $\mathcal{P}_2$ consists of the full pulse sequence that takes the thermal state to the initial state ρ_2.

In addition to this, the pulse sequence for implementing the CTVM protocol will also require a component for implementing the system-detector set up for times t and $2t$. The Hamiltonian for the system-detector evolution was given in Eq.(4.3) as H_D. Thus, implementing the system-detector evolution requires constructing a pulse sequence whose full evolution is equal to $U_{v1} = e^{-iH_D t}$ for the coupling of time t and another whose evolution is equal to $U_{v2} = e^{-iH_D 2t}$ for the coupling of time $2t$. The pulse sequences for implementing U_{v1} and U_{v2} are both provided in Fig. 4.5. It is readily shown that the full evolution of these systems is equal to $e^{-iH_D t}$ and $e^{-iH_D 2t}$ respectively.

4.2.4   Third set of experiments

The third set of experiments will consist of six pulse sequences which are depicted in Fig. 4.6. The CTVM and INM protocols are used to measure the correlators and not the expectation values. As such, experiments (19-21), used for determining the values $\langle Q_i \rangle$ in the third set of experiments, are identical to experiments (10-12), used for the same purpose in the second set of experiments. In experiments (22-24) the initial state is prepared and is then coupled to the ancilla through the system-detector component for different time intervals. The ancilla qubit is then measured to determine C_{ij} as outlined in Section 4.1.

4.3   Experimental results

The experimental data from the third sets of experiments is provided in Table 4.2. The results from this table are used to calculate the values of $\langle Q_i \rangle$ and C_{ij}, which are provided

Expectation Values

(19) $\boxed{\mathcal{P}_2}$

(20) $\boxed{\mathcal{P}_2}$ $\boxed{X\left(\frac{3\pi}{10}\right)}$

(21) $\boxed{\mathcal{P}_2}$ $\boxed{X\left(\frac{6\pi}{10}\right)}$

Measuring Correlatiors (CTVM)

(22) $\boxed{\mathcal{P}_2}$ $\boxed{U_{v1}}$

(23) $\boxed{\mathcal{P}_2}$ $\boxed{X\left(\frac{3\pi}{10}\right)}$ $\boxed{U_{v1}}$
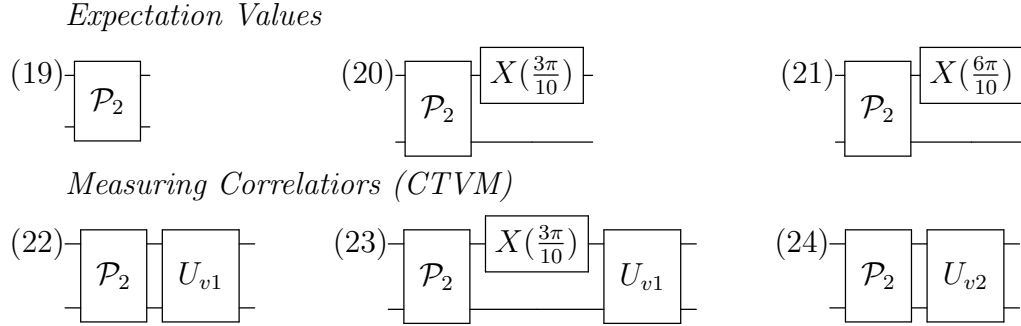
(24) $\boxed{\mathcal{P}_2}$ $\boxed{U_{v2}}$

Figure 4.6: The pulse sequences for the third set of experiments. Experiments 19-21 are used to measure the values of $\langle Q_i \rangle$ and experiments 22-24 are used to measure C_{ij}.

in Table 4.3. These tables also include two simulated values for comparison. The ideal simulations use ideal pulses and assume no natural decoherence. The noisy simulations account for the added effect of the systems Hamiltonian when pulses are being applied and also approximate the effect of the natural decoherence of the system.

Two values are provided for the result of each of the experiments. For experiments 19-21 these are the two diagonal elements of the first qubits density matrix. As shown in Section 3.3, these values are sufficient for determining $\langle Q_i \rangle$. For experiments 22-24 these are the two diagonal elements of the second qubits density matrix. Unlike the INM protocol, the CTVM protocol only requires two values to determine C_{ij}. As shown from Eq.(4.10) the value of C_{ij} for some general state $\rho(t_i) = \begin{bmatrix} a & b \\ b^* & (1-a) \end{bmatrix}$ can be determined from only the diagonal entries of the ancilla qubit.

$$C_{ij} = 1 - \frac{p(1)}{2\lambda^2} \tag{4.23}$$

$$= 1 - \frac{(1-a)}{2\lambda^2} \tag{4.24}$$

The measured values of $\langle Q_i \rangle$ and C_{ij} from Table 4.3 were then used to determined the LG2s and LG3s for the third set of experiments. The numerical results for the LG2s and LG3s are provided for the third set of experiments in Table 4.4. Table 4.4 also contains the experimental values from the second set of experiments for comparison. The LG2s and LG3s for the second and third set of experiments are also plotted, side by side, in Fig. 4.7.

The key points of the experimental results are as follows: As seen in Table 4.4 and Fig. 4.7, the second and third set of experiments give comparable results for the values

82

	I	N	E
	Third set of experiments		
(19)	0.6546	0.6527	0.6484 ± 0.01
	0.3455	0.3473	0.3516 ± 0.01
(20)	0.5908	0.5913	0.5892 ± 0.01
	0.4092	0.4087	0.4107 ± 0.01
(21)	0.4523	0.4558	0.4692 ± 0.01
	0.5477	0.5442	0.5307 ± 0.01
(22)	0.9901	0.9889	0.9883 ± 0.01
	0.0990	0.0111	0.0117 ± 0.01
(23)	0.9901	0.9889	0.9885 ± 0.01
	0.0990	0.0111	0.0115 ± 0.01
(24)	0.9688	0.9691	0.9704 ± 0.01
	0.0312	0.0309	0.0296 ± 0.01

Table 4.2: The experimental data from the third set of experiments. The diagonal elements of the first qubits density matrix are recorded for experiments 19 to 21. The diagonal elements of the second qubits density matrix are recorded for experiments 22 to 24 (Experiment number (Exp. #), Ideal simulated (I), Noisy simulated (S) Experimentally determined (E)).

of C_{ij} while also provide the same violation and satisfaction of the LG2s and LG3s. As calculated in Section 4.2.1, the LG3 violation for the CTVM protocol must violate the LGI bound by an extra value of 0.0028 for the violation to not be a result of the strength of the coupling constant, which they do.

4.4 Conclusion

The purpose of this work in this chapter was to implement a new type of non-invasive measurement protocol and compare it to the standard ideal negative measurement protocol. To achieve this we performed the first implementation of the continuous in time velocity measurement protocol for determining correlation functions, a non-invasive technique very different to the usual ideal negative measurement protocol and with the advantage that it involves a different set of assumptions. First, it assumes that enough is known about the

	I	N	E
Second Set of Experiments			
Expectation values			
$\langle Q_1 \rangle$	0.3090	0.3054	0.2967 ± 0.02
$\langle Q_2 \rangle$	0.1816	0.1798	0.1787 ± 0.02
$\langle Q_3 \rangle$	-0.0955	-0.0884	-0.0615 ± 0.02
Correlators (INM)			
C_{12}	0.5878	0.5862	0.5703 ± 0.03
C_{23}	0.5878	0.5862	0.5615 ± 0.02
C_{13}	-0.3090	-0.3083	-0.2901 ± 0.02
Third Set of Experiments			
Expectation values			
$\langle Q_1 \rangle$	0.3090	0.3054	0.2967 ± 0.02
$\langle Q_2 \rangle$	0.1816	0.1798	0.1787 ± 0.02
$\langle Q_3 \rangle$	-0.0955	-0.0884	-0.0615 ± 0.02
Correlators (CTVM)			
C_{12}	0.5890	0.5422	0.5248 ± 0.07
C_{23}	0.5890	0.5421	0.5149 ± 0.08
C_{13}	-0.2897	-0.2769	-0.2376 ± 0.08

Table 4.3: The values of $\langle Q_i \rangle$ and C_{ij} and calculated from the second and third set of experiments (Ideal simulated (I), Noisy simulated (S) Experimentally determined (E)). Note that the second and third set of experiments use the same protocol for measuring $\langle Q_i \rangle$ and thus as expected return the same measured results.

Label	Inequality	INM	CTVM		
		E	I	N	E
2.1	$1 + \langle Q_1 \rangle + \langle Q_2 \rangle + C_{12} \geq 0$	2.046 ± 0.04	2.080	2.030	2.012 ± 0.08
2.2	$1 - \langle Q_1 \rangle + \langle Q_2 \rangle - C_{12} \geq 0$	0.312 ± 0.04	0.284	0.335	0.352 ± 0.08
2.3	$1 + \langle Q_1 \rangle - \langle Q_2 \rangle - C_{12} \geq 0$	0.548 ± 0.04	0.538	0.581	0.598 ± 0.08
2.4	$1 - \langle Q_1 \rangle - \langle Q_2 \rangle + C_{12} \geq 0$	1.095 ± 0.04	1.098	1.054	1.037 ± 0.08
2.5	$1 + \langle Q_2 \rangle + \langle Q_3 \rangle + C_{23} \geq 0$	1.679 ± 0.03	1.675	1.636	1.609 ± 0.09
2.6	$1 - \langle Q_2 \rangle + \langle Q_3 \rangle - C_{23} \geq 0$	0.198 ± 0.03	0.134	0.187	0.214 ± 0.09
2.7	$1 + \langle Q_2 \rangle - \langle Q_3 \rangle - C_{23} \geq 0$	0.679 ± 0.03	0.688	0.729	0.756 ± 0.09
2.8	$1 - \langle Q_2 \rangle - \langle Q_3 \rangle + C_{23} \geq 0$	1.444 ± 0.03	1.503	1.448	1.421 ± 0.09
2.9	$1 + \langle Q_1 \rangle + \langle Q_3 \rangle + C_{13} \geq 0$	0.945 ± 0.03	0.924	0.940	0.979 ± 0.08
2.10	$1 - \langle Q_1 \rangle + \langle Q_3 \rangle - C_{13} \geq 0$	0.932 ± 0.03	0.885	0.883	0.844 ± 0.08
2.11	$1 + \langle Q_1 \rangle - \langle Q_3 \rangle - C_{13} \geq 0$	1.648 ± 0.03	1.694	1.671	1.632 ± 0.08
2.12	$1 - \langle Q_1 \rangle - \langle Q_3 \rangle + C_{13} \geq 0$	0.475 ± 0.03	0.497	0.506	0.546 ± 0.08
3.1	$1 + C_{12} + C_{23} + C_{13} \geq 0$	1.842 ± 0.04	1.888	1.807	1.802 ± 0.1
3.2	$1 - C_{12} - C_{23} + C_{13} \geq 0$	-0.422 ± 0.04	-0.468	-0.361	-0.277 ± 0.1
3.3	$1 + C_{12} - C_{23} - C_{13} \geq 0$	1.299 ± 0.04	1.290	1.277	1.248 ± 0.1
3.4	$1 - C_{12} + C_{23} - C_{13} \geq 0$	1.281 ± 0.04	1.290	1.277	1.228 ± 0.1

Table 4.4: The values of the LG2s and LG3s constructed from the third set of experiments. The labels in green highlight which inequalities were satisfied and the labels in red highlight which were violated (Ideal simulated (I), Noisy simulated (S) Experimentally determined (E)).
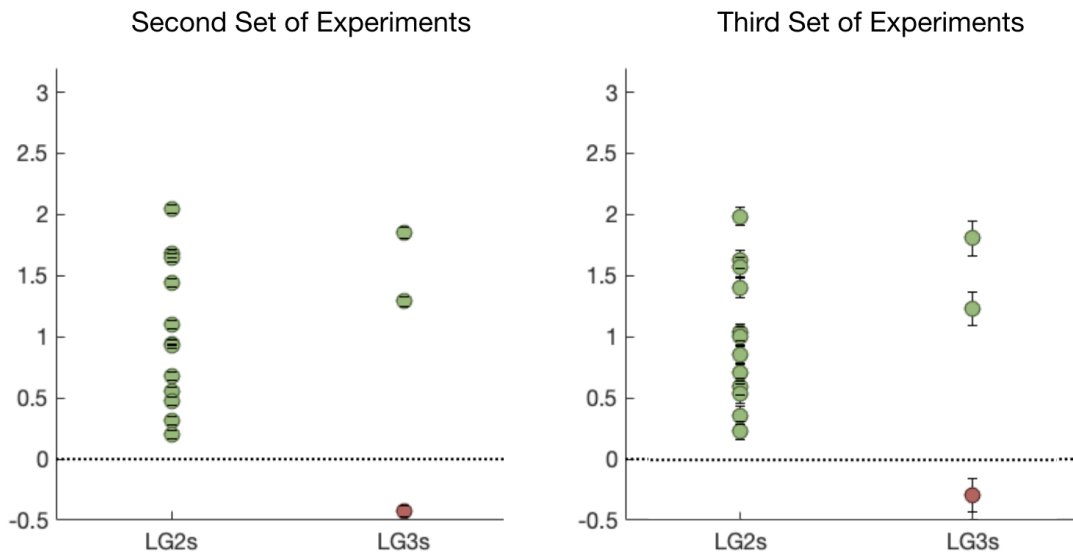
Figure 4.7: The values of the LG2s and LG3s constructed from the second and third set of experiments with their corresponding error bars. The labels in green highlight which inequalities were satisfied and the labels in red highlight which were violated.

system to be able to identify the velocity corresponding to Q. Second, it assumes that the time intervals involved are sufficiently short so that, to a high probability, Q will change sign only once. Lastly, it assumes that the coupling between the primary system and detector is sufficiently small that the back reaction of the detector on the future system dynamics is negligible. We argued that these three assumptions are easy to justify in the system we studied. In particular there is a regime in which they are satisfied in which there are also significant violations of the LG inequalities. Furthermore, we also found that in its domain of validity, the CTVM protocol agreed with the ideal negative measurement protocol.

A natural improvement of the CTVM protocol would be to use a detector with more than the two states used here. This would decrease the probability of error from multiple sign changes. This may be explored in future works.

Chapter 5

Conclusion and discussion

We conclude this thesis with an overview of the conclusions that were outlined in Sections 3.4 and 4.4 and a broader discussion on the content of this thesis.

5.1   Review of Ch. 3 and Ch. 4 conclusions

The purpose of the experiments in this work were twofold: to provide a more complete test of macroscopic realism using an augmented LG framework; to implement a new type of non-invasive measurement protocol and compare it to the standard ideal negative measurement protocol. To date, LGI experiments have tested a set of conditions for MR formulated entirely in terms of temporal correlation functions at three pairs of times. These conditions for MR are necessary but not sufficient. The augmented LG inequalities considered here include an additional set of two-time inequalities which also involve the averages, $\langle Q_i \rangle$, and lead to a set of conditions which are both necessary and sufficient. In this work we showed how these conditions for MR could be tested experimentally. We exhibited experimentally situations in which the LG2s were satisfied but the LG3s violated, a natural parallel to the Bell case. We also exhibited situations in which the LG3s were satisfied but the LG2s violated, the key case in which the original LG framework based solely on LG3s fails to pick up violations of MR.

In this work we also performed the first implementation of the continuous in time velocity measurement protocol for determining correlation functions, a non-invasive technique very different to the usual ideal negative measurement protocol and with the advantage that it involves a different set of assumptions. First, it assumes that enough is known

about the system to be able to identify the velocity corresponding to Q. Second, it assumes that the time intervals involved are sufficiently short so that, to a high probability, Q will change sign only once. Lastly, it assumes that the coupling between the primary system and detector is sufficiently small that the back reaction of the detector on the future system dynamics is negligible. We argued that these three assumptions are easy to justify in the system we studied. In particular there is a regime in which they are satisfied in which there are also significant violations of the LG inequalities. Furthermore, we also found that in its domain of validity, the CTVM protocol agreed with the ideal negative measurement protocol.

A natural improvement of the CTVM protocol would be to use a detector with more than the two states used here. This would decrease the probability of error from multiple sign changes. This will be explored in future works.

5.2   Discussion

There are three pertinent matters to address in this closing section.

Firstly, the testing of violations of the Leggett-Garg inequalities is only a technique for determining whether a system is behaving in accordance with the assumptions of macroscopic realism. It was not the purpose of this work to provide a "decisive" violation of macroscopic realism. The purpose of this work was to further *refine* the Leggett-Garg technique by addressing two of its contemporary challenges, discussed above. The first aim of this paper (the testing of sufficient conditions for macroscopic realism) is only related to and not entirely parallel with the aim of finding a decisive test. A decisive test, in theory, would only require a violation of any one of the LG2s or LG3s. What exploring this augmented framework does is show that one must be cautious of false positive results which could occur from tests involving only the original LG3 framework. On the other hand, the second aim of this paper is in a more direct way related to the aim of a "decisive" test. As more macroscopically non-invasive measurement protocols which are formulated on differing assumptions are developed, tested and shown to agree, the argument for the clumsiness loophole applying to all of them in the same manor becomes a much weaker argument. This strategy can be thought of as a way of asymptotically closing out the clumsiness loophole, and not as one for creating a definitive closure to it.

Secondly, it is not true that a system which violates the Leggett-Garg inequalities, and thus macroscopic realism, is behaving quantum mechanically. The Leggett-Garg inequalities *have* been used in this fashion, but there is nothing that rules out the possibility of an

object not obeying macroscopic realism but also not necessarily being quantum mechanical. An argument can likely be made that a system which violates the Leggett-Garg inequalities is more *likely* to be behaving quantum mechanically than one which does not, but again, it is not a conclusive test, nor was it designed to be. There are many assumptions which are made of the macroscopic world and there are also many assumptions which are made of the quantum world. Testing combinations of these differing assumptions can only lead to greater insights into the nature of these worlds and their potential relationships.

Lastly, the question of violating realism still is an exciting area of research at different levels. Firstly, it remains interesting at a highly theoretical level. In this work we reviewed how John Bell, Anthony Leggett and Anupam Garg were able to create testable conditions for the notion of realism by enjoining realism with other assumptions. This leaves one to wonder what other assumptions could be tied to realism to formulate other testable conditions. Furthermore, it would be fascinating to see if any parallels exist between these enjoined assumptions (the two so far being locality and the non-invasiveness of measurements). At a less philosophical and more mathematical level, it would be interesting to compare the different conditions for violating realism using some common mathematical notation. The pseudo-density matrix formalism is one potential candidate for a space in which the the Leggett-Garg inequalities and the no-signalling in time conditions (another test of macroscopic realism mentioned in this work) could be compared. One could go one step further and use this formulation to find insights into the similarities and differences between the Leggett-Garg and Bell inequalities. For example, is their some difference that can be found in their representation as pseudo-density matrices which reflects the lack of Fine's theorem in the Leggett-Garg model. Lastly, at an experimental level there are still questions which could be explored. The criticisms of certain measurement protocols and their associated challenges with their implementations signal that it may be of interest to develop other protocols. Lastly, testing the Leggett-Garg inequalities in higher dimensions (LG4s, LG5s etc...) would also be of interest to explore.

References

[1] M. Mohseni, P. Read, H. Neven, S. Boixo, V. Denchev, R. Babbush, A. Fowler, V. Smelyanskiy, and J. Martinis. Commercialize quantum technologies in five years. *Nature News*, 543(7644):171, 2017.

[2] H Bennett Ch and G Brassard. Quantum cryptography: public key distribution and coin tossing int. In *Conf. on Computers, Systems and Signal Processing (Dec. 1984)*, pages 175–9, 1984.

[3] P. Shor. Algorithms for quantum computation: Discrete logarithms and factoring. In *Foundations of Computer Science, 1994, 35th Annual Symposium on*, pages 124–134. Ieee, 1994.

[4] Anthony J Leggett and Anupam Garg. Quantum mechanics versus macroscopic realism: Is the flux there when nobody looks? *Physical Review Letters*, 54(9):857, 1985.

[5] Anthony J Leggett. Realism and the physical world. *Reports on Progress in Physics*, 71(2):022001, 2008.

[6] J. Kofler and Č. Brukner. Condition for macroscopic realism beyond the Leggett-Garg inequalities. *Physical Review A*, 87(5):052115, 2013.

[7] Lucas Clemente and Johannes Kofler. Necessary and sufficient conditions for macroscopic realism from quantum mechanics. *Physical Review A*, 91(6):062103, 2015.

[8] JJ Halliwell. Leggett-Garg inequalities and no-signaling in time: A quasiprobability approach. *Physical Review A*, 93(2):022123, 2016.

[9] JJ Halliwell. Comparing conditions for macrorealism: Leggett-Garg inequalities versus no-signaling in time. *Physical Review A*, 96(1):012121, 2017.

[10] Alberto Montina. Dynamics of a qubit as a classical stochastic process with time-correlated noise: minimal measurement invasiveness. *Physical Review Letters*, 108(16):160501, 2012.

[11] JM Yearsley. The Leggett-Garg inequalities and non-invasive measurability. *arXiv preprint arXiv:1310.2149*, 2013.

[12] Otfried Gühne, Matthias Kleinmann, Adán Cabello, Jan-Åke Larsson, Gerhard Kirchmair, Florian Zähringer, Rene Gerritsma, and Christian F Roos. Compatibility and noncontextuality for sequential measurements. *Physical Review A*, 81(2):022121, 2010.

[13] JJ Halliwell. Leggett-Garg correlation functions from a noninvasive velocity measurement continuous in time. *Physical Review A*, 94(5):052114, 2016.

[14] G. Knee. Violation of a Leggett–Garg inequality with ideal non-invasive measurements. *Nature communications*, 3:606, 2012.

[15] Carsten Robens, Wolfgang Alt, Dieter Meschede, Clive Emary, and Andrea Alberti. Ideal negative measurements in quantum walks disprove theories based on classical trajectories. *Physical Review X*, 5(1):011003, 2015.

[16] Hemant Katiyar, Aharon Brodutch, Dawei Lu, and Raymond Laflamme. Experimental violation of the leggett–garg inequality in a three-level system. *New Journal of Physics*, 19(2):023033, 2017.

[17] Manjit Kumar. *Quantum: Einstein, Bohr, and the great debate about the nature of reality*. WW Norton & Company, 2008.

[18] Niels Bohr et al. *The quantum postulate and the recent development of atomic theory*, volume 3. Printed in Great Britain by R. & R. Clarke, Limited, 1928.

[19] Ramin Skibba. Einstein, Bohr and the war over quantum theory. *Nature*, 555(7698):582–584, 2018.

[20] Albert Einstein, Boris Podolsky, and Nathan Rosen. Can quantum-mechanical description of physical reality be considered complete? *Physical Review*, 47(10):777, 1935.

[21] John S Bell. On the Einstein Podolsky Rosen paradox. *Physics Physique Fizika*, 1(3):195, 1964.

[22] John F Clauser, Michael A Horne, Abner Shimony, and Richard A Holt. Proposed experiment to test local hidden-variable theories. *Physical Review Letters*, 23(15):880, 1969.

[23] John Preskill. Lecture notes for physics 229: Quantum information and computation. *California Institute of Technology*, 16, 1998.

[24] Alain Aspect, Jean Dalibard, and Gérard Roger. Experimental test of Bell's inequalities using time-varying analyzers. *Physical Review Letters*, 49(25):1804, 1982.

[25] Arthur Fine. Hidden variables, joint probability, and the Bell inequalities. *Physical Review Letters*, 48(5):291, 1982.

[26] David Bohm. A suggested interpretation of the quantum theory in terms of "hidden" variables. i. *Physical Review*, 85(2):166, 1952.

[27] Albert Einstein and Nathan Rosen. The particle problem in the general theory of relativity. *Physical Review*, 48(1):73, 1935.

[28] John Gribbin. *Erwin Schrödinger and the quantum revolution*. Random House, 2012.

[29] Hugh Everett III. Relative state formulation of quantum mechanics. *Reviews of modern physics*, 29(3):454, 1957.

[30] H Everett. The theory of the universal wave function the many-worlds hypothesis of quantum mechanics, 1973.

[31] Bryce S DeWitt. Quantum mechanics and reality. *Physics today*, 23(9):30–35, 1970.

[32] John F Clauser and Michael A Horne. Experimental consequences of objective local theories. *Physical review D*, 10(2):526, 1974.

[33] Asher Peres. Quantum limitations on measurement of magnetic flux. *Physical Review Letters*, 61(18):2019, 1988.

[34] OJE. Maroney and C. Timpson. Quantum-vs. macro-realism: What does the Leggett-Garg inequality actually test? *arXiv preprint arXiv:1412.6139*, 2014.

[35] C. Emary, N. Lambert, and F. Nori. Leggett-Garg inequalities. *Reports on Progress in Physics*, 77(1):016001, 2013.

[36] Anthony J Leggett. Testing the limits of quantum mechanics: motivation, state of play, prospects. *Journal of Physics: Condensed Matter*, 14(15):R415, 2002.

[37] L. Clemente. Necessary and sufficient conditions for macroscopic realism from quantum mechanics. *Phys. Rev. A*, 91:062103, 2015.

[38] Andreas Schmitt. Introduction to superfluidity. *Lect. Notes Phys*, 888(1), 2015.

[39] Michael Tinkham. *Introduction to superconductivity*. Courier Corporation, 2004.

[40] Agustin Palacios-Laloy. *Superconducting qubit in a resonator: test of the Legget-Garg inequality and single-shot readout*. PhD thesis, Université Pierre et Marie Curie-Paris VI, 2010.

[41] Neill Lambert, Clive Emary, Yueh-Nan Chen, and Franco Nori. Distinguishing quantum and classical transport through nanostructures. *Physical Review Letters*, 105(17):176801, 2010.

[42] Neill Lambert, Robert Johansson, and Franco Nori. Macrorealism inequality for optoelectromechanical systems. *Physical Review B*, 84(24):245421, 2011.

[43] Fumiaki Morikoshi. Information-theoretic temporal Bell inequality and quantum computation. *Physical Review A*, 73(5):052308, 2006.

[44] Juan Pablo Paz and Günter Mahler. Proposed test for temporal Bell inequalities. *Physical Review Letters*, 71(20):3235, 1993.

[45] Rusko Ruskov, Alexander N Korotkov, and Ari Mizel. Signatures of quantum behavior in single-qubit weak measurements. *Physical Review Letters*, 96(20):200404, 2006.

[46] Agustin Palacios-Laloy, François Mallet, François Nguyen, Patrice Bertet, Denis Vion, Daniel Esteve, and Alexander N Korotkov. Experimental violation of a Bell's inequality in time with weak measurement. *Nature Physics*, 6(6):442, 2010.

[47] Raymond Laflamme, Emanuel Knill, David G Cory, Evan M Fortunato, Timothy F Havel, Cesar Miquel, Rudy Martinez, Camille J Negrevergne, Gerardo Ortiz, Marco A Pravia, et al. NMR and quantum information processing. *Los Alamos Science*, 27:226–259, 2002.

[48] David P DiVincenzo. The physical implementation of quantum computation. *Fortschritte der Physik: Progress of Physics*, 48(9-11):771–783, 2000.

[49] David G Cory, Amr F Fahmy, and Timothy F Havel. Ensemble quantum computing by NMR spectroscopy. *Proceedings of the National Academy of Sciences*, 94(5):1634–1639, 1997.

[50] Neil Gershenfeld and Isaac L Chuang. Quantum computing with molecules. *Scientific American*, 278(6):66–71, 1998.

[51] David G Cory, Mark D Price, and Timothy F Havel. Nuclear magnetic resonance spectroscopy: An experimentally accessible paradigm for quantum computing. *Physica D: Nonlinear Phenomena*, 120(1-2):82–101, 1998.

[52] Emanuel Knill, Isaac Chuang, and Raymond Laflamme. Effective pure states for bulk quantum computation. *Physical Review A*, 57(5):3348, 1998.

[53] Lieven MK Vandersypen, Costantino S Yannoni, Mark H Sherwood, and Isaac L Chuang. Realization of logically labeled effective pure states for bulk quantum computation. *Physical Review Letters*, 83(15):3085, 1999.

[54] Emanuel Knill, R Laflamme, R Martinez, and C-H Tseng. An algorithmic benchmark for quantum information processing. *Nature*, 404(6776):368, 2000.

[55] Christopher M Dawson and Michael A Nielsen. The solovay-kitaev algorithm. *arXiv preprint quant-ph/0505030*, 2005.

[56] Dawei Lu, Aharon Brodutch, Jihyun Park, Hemant Katiyar, Tomas Jochym-O'Connor, and Raymond Laflamme. NMR quantum information processing. In *Electron Spin Resonance (ESR) Based Quantum Computing*, pages 193–226. Springer, 2016.

[57] N Bloembergen and LO Morgan. Proton relaxation times in paramagnetic solutions. effects of electron spin relaxation. *The Journal of Chemical Physics*, 34(3):842–850, 1961.

[58] V. Athalye, S. Roy, and TS Mahesh. Investigation of the Leggett-Garg inequality for precessing nuclear spins. *Physical Review Letters*, 107(13):130402, 2011.

[59] Martin Laforest. Error characterization and quantum control benchmarking in liquid state NMR using quantum information processing techniques. *PhD Thesis. University of Waterloo*, 2008.

[60] JJ Halliwell. Decoherent histories and measurement of temporal correlation functions for Leggett-Garg inequalities. *Physical Review A*, 94(5):052131, 2016.

[61] S. Popescu and D. Rohrlich. Quantum nonlocality as an axiom. *Foundations of Physics*, 24(3):379–385, 1994.

[62] S. Freedman and J. Clauser. Experimental test of local hidden-variable theories. *Physical Review Letters*, 28(14):938, 1972.

[63] G Waldherr, P Neumann, SF Huelga, F Jelezko, and J Wrachtrup. Violation of a temporal Bell inequality for single spins in a diamond defect center. *Physical Review Letters*, 107(9):090401, 2011.

[64] ME et al. Goggin. Violation of the Leggett–Garg inequality with weak measurements of photons. *Proceedings of the National Academy of Sciences*, 108(4):1256–1261, 2011.

[65] Z. Zhou, S. Huelga, C. Li, and G. Guo. Experimental violation of a Leggett-Garg inequality with macroscopic crystals. *arXiv preprint arXiv:1209.2176*, 2012.

[66] A. Kofman, S. Ashhab, and F. Nori. Nonperturbative theory of weak pre-and post-selected measurements. *Physics Reports*, 520(2):43–133, 2012.

[67] MS Wang. Multitime measurements in quantum mechanics. *Physical Review A*, 65(2):022103, 2002.

[68] RH Dicke. Interaction-free quantum measurements: A paradox? *American Journal of Physics*, 49(10):925–930, 1981.

[69] M. Wilde and A. Mizel. Addressing the clumsiness loophole in a Leggett-Garg test of macrorealism. *Foundations of Physics*, 42(2):256–265, 2012.

[70] John S Bell. On the problem of hidden variables in quantum mechanics. In *John S Bell On The Foundations Of Quantum Mechanics*, pages 1–6. World Scientific, 2001.

[71] Charles H Bennett and Gilles Brassard. Quantum cryptography: Public key distribution and coin tossing. *Theor. Comput. Sci.*, 560(P1):7–11, 2014.

[72] Peter W Shor. Polynomial-time algorithms for prime factorization and discrete logarithms on a quantum computer. *SIAM review*, 41(2):303–332, 1999.

[73] JP Groen, D Ristè, Lars Tornberg, J Cramer, Pieter C De Groot, T Picot, Göran Johansson, and L DiCarlo. Partial-measurement backaction and nonclassical weak values in a superconducting circuit. *Physical Review Letters*, 111(9):090506, 2013.

[74] Richard E George, Lucio M Robledo, Owen JE Maroney, Machiel S Blok, Hannes Bernien, Matthew L Markham, Daniel J Twitchen, John JL Morton, G Andrew D Briggs, and Ronald Hanson. Opening up three quantum boxes causes classically undetectable wavefunction collapse. *Proceedings of the National Academy of Sciences*, 110(10):3777–3781, 2013.

[75] AM Souza, IS Oliveira, and RS Sarthour. A scattering quantum circuit for measuring Bell's time inequality: a nuclear magnetic resonance demonstration using maximally mixed states. *New Journal of Physics*, 13(5):053023, 2011.

[76] Hemant Katiyar, Abhishek Shukla, K Rama Koteswara Rao, and TS Mahesh. Violation of entropic Leggett-Garg inequality in nuclear spins. *Physical Review A*, 87(5):052102, 2013.

[77] Justin Dressel, CJ Broadbent, JC Howell, and Andrew N Jordan. Experimental violation of two-party Leggett-Garg inequalities with semiweak measurements. *Physical Review Letters*, 106(4):040402, 2011.

[78] Yutaro Suzuki, Masataka Iinuma, and Holger F Hofmann. Violation of leggett–garg inequalities in quantum measurements with variable resolution and back-action. *New Journal of Physics*, 14(10):103022, 2012.

[79] Jin-Shi Xu, Chuan-Feng Li, Xu-Bo Zou, and Guang-Can Guo. Experimental violation of the Leggett-Garg inequality under decoherence. *Scientific reports*, 1:101, 2011.

[80] JJ Halliwell. Necessary and sufficient conditions for macrorealism using two and three-time Leggett-Garg inequalities. *arXiv preprint arXiv:1811.10408*, 2018.

[81] Anthony Leggett. Realism versus quantum mechanics: Implications of some recent experiments. Conference on 90 Years of Quantum Mechanics, Institute of Advanced Studies, 2017.

[82] David Cory and Todd Heinrichs. Nuclear magnetic resonance approaches to quantum information processing and quantum computing. *A Quantum Information Science and Technology Roadmap, v2. 0*, 2004.

[83] Lucas Clemente and Johannes Kofler. No fine theorem for macrorealism: Limitations of the Leggett-Garg inequality. *Physical Review Letters*, 116(15):150401, 2016.

[84] DN Klyshko. The Bell theorem and the problem of moments. *Physics Letters A*, 218(3-6):119–127, 1996.

[85] Kunkun Wang, Clive Emary, Xiang Zhan, Zhihao Bian, Jian Li, and Peng Xue. Enhanced violations of Leggett-Garg inequalities in an experimental three-level system. *Optics express*, 25(25):31462–31470, 2017.

[86] Neil A Gershenfeld and Isaac L Chuang. Bulk spin-resonance quantum computation. *science*, 275(5298):350–356, 1997.

[87] David G Cory, Mark D Price, Amr F Fahmy, and Timothy F Havel. Nuclear magnetic resonance spectroscopy: an experimentally accessible paradigm for quantum computing. In *In Proceedings of the Fourth Workshop on Physics and Computation. New England Complex Systems Institute*. Citeseer, 1996.

[88] Jonathan A Jones. NMR quantum computation. *arXiv preprint quant-ph/0009002*, 2000.

[89] Anatole Abragam and Anatole Abragam. *The principles of nuclear magnetism*. Oxford university press, 1961.

[90] J McConnell. The theory of NMR spin relaxation in liquids, 1987.

[91] Frank Holger Försterling. Spin dynamics: basics of nuclear magnetic resonance. *Medical Physics*, 37(1):406–407, 2010.

[92] John Cavanagh, Wayne J Fairbrother, Arthur G Palmer III, and Nicholas J Skelton. *Protein NMR spectroscopy: principles and practice*. Elsevier, 1995.

[93] Rutger Vrijen, Eli Yablonovitch, Kang Wang, Hong Wen Jiang, Alex Balandin, Vwani Roychowdhury, Tal Mor, and David DiVincenzo. Electron-spin-resonance transistors for quantum computing in silicon-germanium heterostructures. *Physical Review A*, 62(1):012306, 2000.

[94] Warren S Warren. The usefulness of NMR quantum computing. *Science*, 277(5332):1688–1690, 1997.

[95] Arzhang Ardavan, Olivier Rival, John JL Morton, Stephen J Blundell, Alexei M Tyryshkin, Grigore A Timco, and Richard EP Winpenny. Will spin-relaxation times in molecular magnets permit quantum information processing? *Physical Review Letters*, 98(5):057201, 2007.

[96] Tôru Moriya. The effect of electron-electron interaction on the nuclear spin relaxation in metals. *Journal of the Physical Society of Japan*, 18(4):516–520, 1963.

[97] TD Ladd, D Maryenko, Y Yamamoto, E Abe, and KM Itoh. Coherence time of decoupled nuclear spins in silicon. *Physical Review B*, 71(1):014401, 2005.

[98] RL Vold, JS Waugh, M Pv Klein, and DE Phelps. Measurement of spin relaxation in complex systems. *The Journal of Chemical Physics*, 48(8):3831–3832, 1968.

[99] Arthur G Palmer III. Relaxation and dynamic processes. *Columbia University, USA*, pages 1–14, 1996.

[100] James Keeler. *Understanding NMR spectroscopy*. John Wiley & Sons, 2011.

[101] Lieven MK Vandersypen and Isaac L Chuang. NMR techniques for quantum control and computation. *Reviews of modern physics*, 76(4):1037, 2005.

[102] JH Van Vleck. The dipolar broadening of magnetic resonance lines in crystals. *Physical Review*, 74(9):1168, 1948.

[103] Erwin L Hahn. Spin echoes. *Physical Review*, 80(4):580, 1950.

[104] Herman Y Carr and Edward M Purcell. Effects of diffusion on free precession in nuclear magnetic resonance experiments. *Physical Review*, 94(3):630, 1954.

[105] Saul Meiboom and David Gill. Modified spin-echo method for measuring nuclear relaxation times. *Review of scientific instruments*, 29(8):688–691, 1958.

[106] JA Jones and E Knill. Efficient refocusing of one-spin and two-spin interactions for NMR quantum computation. *Journal of Magnetic Resonance*, 141(2):322–325, 1999.

[107] AA Maudsley. Modified Carr-Purcell-Meiboom-Gill sequence for NMR fourier imaging applications. *Journal of Magnetic Resonance (1969)*, 69(3):488–491, 1986.

[108] J Patrick Loria, Mark Rance, and Arthur G Palmer. A relaxation-compensated carr- purcell- meiboom- gill sequence for characterizing chemical exchange by NMR spectroscopy. *Journal of the American Chemical Society*, 121(10):2331–2332, 1999.

[109] Jozef Kowalewski and Lena Maler. *Nuclear spin relaxation in liquids: theory, experiments, and applications*. CRC press, 2017.

[110] Lorenzo Maccone. A simple proof of Bell's inequality. *American Journal of Physics*, 81(11):854–859, 2013.

[111] Michael A Nielsen and Isaac L Chuang. Quantum information and quantum computation. *Cambridge: Cambridge University Press*, 2(8):23, 2000.

[112] Tobias Fritz. Quantum correlations in the temporal Clauser–Horne–Shimony–Holt (CHSH) scenario. *New Journal of Physics*, 12(8):083055, 2010.

[113] R Vijay, MH Devoret, and I Siddiqi. Invited review article: The josephson bifurcation amplifier. *Review of Scientific Instruments*, 80(11):111101, 2009.

[114] JJ Halliwell. Two proofs of fine's theorem. *Physics Letters A*, 378(40):2945–2950, 2014.